Glacier response to climate change: modeling the effects of weather and debris-cover

by

Leif S. Anderson

B.S., Montana State University, 2007

A thesis submitted to the

Faculty of the Graduate School of the

University of Colorado in partial fulfillment

of the requirement for the degree of

Doctor of Philosophy

Department of Geological Sciences

This thesis entitled:
Glacier response to climate change: modeling the effects of weather and debris-cover

written by Leif Stefan Anderson
has been approved for the Department of Geological Sciences

_____

Professor Robert S. Anderson

_____

Professor Gerard H. Roe

_____

Professor Peter H. Molnar

_____

Professor Gregory E. Tucker

_____

Professor Harihar Rajaram

Date _____

The final copy of this thesis has been examined by the signatories, and we find that both the content and the form meet acceptable presentation standards of scholarly work in the above mentioned discipline

Abstract

Anderson, Leif Stefan (Ph.D., Geological Sciences)

Glacier response to climate change: modeling the effects of weather and debris-cover.

Thesis directed by Doctor Robert Anderson

Glaciers change length in response to fluctuations in climate. In addition, atmospheric and geomorphic processes modulate glacier response to climate change. These factors must be explored in detail to understand glacier response. I engage two factors modulating glacier response: 1) the effect of year-to-year weather variability on glacier length and 2) the effect of debris cover on glacier dynamics. I use case studies from the Last Glacial Maximum (LGM) in Colorado in addition to modern glaciers in the Nepalese Himalaya and Alaska to address these issues.

The effect of interannual variability on the moraine record

Multi-decadal, kilometer-scale fluctuations in glacier length occur in response to stochastic, year-to-year variability in mass balance. I address the effect of weather variability on our interpretation of the moraine record using glacier models in the Colorado Front Range during the LGM. My analyses suggest that (1) glacial standstills longer than 50 years were unlikely; (2) mean glacier lengths are ~10%–15% up-valley from maximum glacier lengths; and (3) individual LGM terminal moraines were formed by a combination of a climate change and interannual variability–forced advances.

Numerical modeling of debris-covered glaciers

Debris cover can significantly affect the length and dynamics of valley glaciers. I developed a 2D vertical plane long-valley numerical glacier model with which we explore the feedbacks between debris and ice dynamics. Debris input to the glacier in the accumulation zone emerges

in the ablation zone, and is then advected along the glacier surface, damping melt rate. Debris cover reduces ice surface slopes, ice thickness gradients, ice discharge gradients, and englacial velocities in the ablation zone.

Ice cliffs on debris-covered glaciers

Debris cover suppresses ice melt on glaciers. However, the retreat of debris-free ice cliffs within otherwise debris-covered glaciers counters the insulating effects of debris. I provide a theoretical framework for the production and removal of ice cliffs and glacier surface topography on the Kennicott Glacier, Wrangell Mountains, Alaska. Mean debris thickness exerts primary control on glacier surface relief and ice cliff concentration. Approximately 30% of net mass loss from the study area is due to the retreat of ice cliffs.

Acknowledgements

I am grateful to the wide arc of supporters that made this dissertation possible. Thank you to all the administrative staff, technical workers, and logisticians for supporting me at CU. My peers kindly allowed me to help with their fieldwork in a number of wonderful places: William Armstrong, Sarah Crump, Ulyana Horodyskyj, Ben Hudson and Francis Rengers. I learned so much from our interactions and experiences together. Thank you Dr. Andrew Wickert for inspiring me to ask big questions and work efficiently. We were fortunate to have you at CU! Thank you Kali Abel, Katy Barnhart, Maureen Berlin, Melissa Foster, Ben Hudson, Dylan Ward, Ethan Welty, and Eric Winchell for your support through the years.

Thank you to my advisor Robert Anderson for his support, advice, and flexibility. His broad interests allowed me to explore many fields within surface processes, which ultimately allowed me to work on glaciers. Your passion for your work is inspiring. I am proud of what we have achieved together and, yes, there is still more to do!

Thank you to Professor Gerard Roe for his willingness to work with me and support me over the last few years. Prof. Roe introduced me to a new level of rigor that I hope to carry with me throughout my career. I have very much appreciated our direct interactions and I have benefited greatly from your acute intellect and generous mentorship. I very much wished our opportunity to work together at UW would have worked out, but your support opened other opportunities. I am deeply grateful for your efforts.

And thank you to Professor Peter Molnar for instilling a desire to find strong research questions. I am grateful that he challenged and pushed me to be a better researcher as well. Prof. Molnar also kindly invited me to a Tectonics and Climate summer school where I first met Prof. Gerard Roe. I am fortunate to have your support. I am grateful to Prof. Harihar Rajaram and

Prof. Greg Tucker for their clear and exceptional teaching of numerical modeling. Thank you so much. Thank you to Prof. Lang Farmer for his steady support of graduate students. I have learned much from our interactions. Your leadership inspires me. Also, thank you to Prof. Bill Locke at Montana State University for honing my field observation skills and your generous mentorship.

I am grateful to my parents for instilling a love of the outdoors and exposing me to the mountains and glaciers. Their stories of the Himalaya, the high mountains, and debris-covered glaciers inspired this work. My parents also helped with fieldwork in the Wind River Range, Wyoming and on the Kennicott Glacier in Alaska. Thank you for your unwavering support of my efforts. Thank you also to Ian MacMurdie for his company and assistance in the field. Thank you to my siblings for years of love and support. Most of all, thank you, Meekyung, for supporting me over the last five years. Even from a distance you helped me through much adversity. I am so fortunate to have you in my life. Thank you.

The projects presented below and others tackled during my time at the University of Colorado were supported by National Science Foundation (NSF) grant DGE-1144083 (GRFP), a 2014 University of Colorado-Boulder Graduate School Summer Fellowship, The Dudley and Marion Bolyard Scholarship from the Rocky Mountain Association of Geologists, a David Love Geology Fellowship, a Tobacco Root Geological Society Scholarship, A Geological Society of America research grant, two University of Colorado Department of Geological Sciences student research grants, an Alaska National Parks Murie Science and Learning Center Fellowship, and a Neal B. Kiding fellowship from the Colorado Mountain Club. I am also grateful to the department of Geological Sciences and Prof. Robert Anderson for teaching assistantships and funding. Thank you!

Table of Contents

List of Tables

List of Figures

Chapter 1 Introduction

Glaciers change length in response to fluctuations in climate. While this is true, a number of atmospheric, geomorphic, and solid earth processes modulate glacier response to climate change. These complicating factors must be explored in detail to understand past, modern, and future glacier response. I engage three broad factors modulating glacier response: 1) the effect of year-to-year weather variability on glacier length; 2) the effect of debris cover on glacier length and dynamics; and 3) the effect of flexural-isostatic depression on glacier response. I use case studies from the Last Glacial Maximum (LGM) in Colorado, New Zealand, and the Greater Yellowstone region, in addition to case studies from modern glaciers in the Nepalese Himalaya and Alaska to address these issues. Summaries of each chapter are provided below.

Chapter 2: The effect of interannual climate variability on the moraine record

Valley glacier moraines are commonly used to infer past mean annual precipitation and mean melt-season temperature. However, recent research has demonstrated that, even in steady climates, multi-decadal, kilometer-scale fluctuations in glacier length occur in response to stochastic, year-to-year variability in mass balance. When interpreting moraine sequences it is important to include the effect of interannual weather variability on glacier length; moraines record advances that are forced either by interannual variability or by a combination of climate change and interannual variability. We address this issue for the Last Glacial Maximum (LGM) glaciers of the Colorado Front Range, United States. Using a linear glacier model that allows thorough exploration of parameter uncertainties, supplemented by a shallow-ice flowline model, our analyses suggest that (1) glacial standstills longer than 50 years were unlikely; (2) mean glacier lengths are ~10%–15% up-valley from maximum glacier lengths; and (3) individual

LGM terminal moraines were formed by a combination of a climate change and interannual variability forced advances.

Chapter 3: Numerical modeling of debris-covered glaciers: transient effects of debris on the length and dynamics of valley glaciers

Debris cover can significantly affect the length and dynamics of valley glaciers. However, the difficulty in measuring relevant variables such as ice thickness and sub-debris mass balance at the decadal scale limits documentation of the dynamic response of glaciers to debris cover. As a result, there is considerable uncertainty about how debris cover on glaciers will affect water resources in high relief settings and sea level rise. It is imperative that we create a conceptual framework that honors the effect of debris on ice dynamics. We developed a 2D long-valley shallow-ice approximation numerical glacier model modified with longitudinal coupling. The model allows transient feedbacks between englacial debris, surface debris, sub-debris melt, and ice dynamics. In our model simulations, we varied debris input from headwall sources while maintaining a steady climate, using parameters loosely designed to replicate Khumbu, Nepal, debris-covered glaciers. Model results replicate debris-cover surface velocity and debris thickness patterns from a range of Central Asian debris-covered glaciers.

Debris deposited on the glacier surface in the accumulation zone travels through the glacier to emerge in the ablation zone. Once on the glacier surface, debris is advected down glacier, and increases in thickness through the ablation zone. Debris reduces melt, leading to elongated glaciers. Even in steady state, debris reduces ice surface slopes, ice thickness gradients, ice discharge gradients, and englacial velocities in the ablation zone. We show that debris thickness is dependent on debris emergence rates and the surface velocity field, while also providing a means to interpret debris thickness patterns on modern glaciers. Steady state glacier

length is nonlinearly related to debris deposition rates. Glacier surfaces can become saturated with debris, at which point adding more debris to the glacier leads to insignificant changes in glacier length. Surface debris emerging near the terminus suppresses glacier-wide net melt more than debris emerging near the ELA. Ice thickness perturbations caused by emerging debris are diffused up the glacier leading to lower ice surface slopes and larger ice thicknesses up glacier of the debris covered reach.

Chapter 4: Surface relief and ice cliffs on debris-covered glaciers: A case study from the Kennicott Glacier, Alaska, USA

Debris cover suppresses ice melt on glaciers. However, the retreat of debris-free ice cliffs within otherwise debris-covered glaciers counters the insulating effect of debris. Glacier surface processes (e.g., differential melt under debris, supraglacial stream erosion, englacial conduit collapse, etc.) control spatial distribution of ice cliffs. We provide a theoretical framework for the production and removal of ice cliffs and glacier surface topography on debris-covered glaciers. We apply this framework to assess the causes of cliff distribution and the mass loss due to ice cliff backwasting on the Kennicott Glacier, Wrangell Mountains, Alaska. Throughout the study area we measured ice cliff backwasting, ice cliff geometry and orientation, sub-debris melt rates, and debris thicknesses. Using Worldview 1 imagery we documented the spatial distribution of ice cliffs, lakes, and supraglacial streams, in addition to calculating ice surface velocities and glacier surface relief at 10^4 m^2 scale. Linear ice-cliff concentration, defined as the concentration of long-axis ice cliff length per area, increases and then decreases through the debris-covered portion of the glacier. Mean debris thickness appears to be the primary control on glacier surface relief and ice cliff concentration. Thin mean debris thicknesses lead to the largest relief and ice cliff concentration increases. Supraglacial streams increase in sinuosity within the debris-covered

portion of the glacier, potentially leading to a positive feedback between supraglacial streams, relief production and ice cliff formation. Approximately 30% of net mass loss from the study area is due to the backwasting of ice cliffs. In some elevation bands approximately 55% of the total melt is due to ice cliff backwasting. Our results highlight the importance of ice cliff backwasting and the processes that control their distribution on debris-covered glacier surface mass loss.

Chapter 2 The effect of interannual climate variability on the moraine record

Leif S. Anderson[1], Gerard H. Roe[2], and Robert S. Anderson[1]

[1]Institute of Arctic and Alpine Research, and Department of Geological Sciences, University of Colorado, Campus Box 450, Boulder, Colorado 80309, USA

[2]Department of Earth and Space Sciences, University of Washington, 4000 15th Avenue NE, Seattle, Washington 98195, USA

2.1 Abstract

Valley glacier moraines are commonly used to infer past mean annual precipitation and mean melt-season temperature. However, recent research has demonstrated that, even in steady climates, multi-decadal, kilometer-scale fluctuations in glacier length occur in response to stochastic, year-to-year variability in mass balance. When interpreting moraine sequences it is important to include the effect of interannual weather variability on glacier length; moraines record advances that are forced either by interannual variability or by a combination of climate change and interannual variability. We address this issue for the Last Glacial Maximum (LGM) glaciers of the Colorado Front Range, United States. Using a linear glacier model that allows thorough exploration of parameter uncertainties, supplemented by a shallow-ice flowline model, our analyses suggest that (1) glacial standstills longer than 50 years were unlikely; (2) mean glacier lengths are ~10%–15% up-valley from maximum glacier lengths; and (3) individual LGM terminal moraines were formed by a combination of a climate change and interannual variability forced advances.

2.2 Introduction

Glacial to interglacial changes in the long-term averages of annual precipitation (P) and mean melt-season temperature (T) are sufficient, in many places, to force significant changes in glacier length (tens of kilometers). But even in steady climates, year-to-year (interannual) variations in P and T have also been shown to force multi-decadal, kilometer-scale length fluctuations in valley glaciers, due solely to the random alignment of years of negative and positive mass balance (e.g., Reichert et al., 2002; section 2.9.8). A steady climate implies constant long-term averages ($\equiv \overline{P}, \overline{T}$) and, importantly, constant standard deviations ($\equiv \sigma_P, \sigma_T$). All climates, steady or transient, include interannual variability. It is often incorrectly assumed that glaciers average away all interannual climate variability, and respond only to more persistent climate fluctuations. However, glaciers act as low-pass filters, producing multi-decadal (for the glaciers discussed in this paper) length fluctuations even if the climate forcing it is not correlated from year-to-year (white noise), which is almost always the case (Fig. 2.1B; Burke and Roe, 2013). Interannual variability is a result of the stochastic fluctuations of weather (climate noise) and the internal modes of variability in the climate system, such as the North Atlantic, the Pacific/North American, and the El Niño-Southern Oscillations (see section 2.9.8 also). The amplitude of interannual variability varies with location and climate state, but it is always present. To constrain the values of past $\overline{T}$ and $\overline{P}$ using glacier moraines and to correctly interpret the moraine record we must understand the effects of year-to-year weather variability on glacier length and moraine emplacement.

To illustrate the problem, consider two glaciers: (a) a glacier subject to constant $\overline{T}$ and $\overline{P}$ forms a steady ice-surface profile that terminates at a steady, mean length, $\overline{L}$ (Fig. 2.1A); and

(b) a glacier subject to a climate with the same $\overline{T}$ and $\overline{P}$ that also includes interannual variability. The glacier of case (b) will produce a terminus history that will fluctuate on multi-

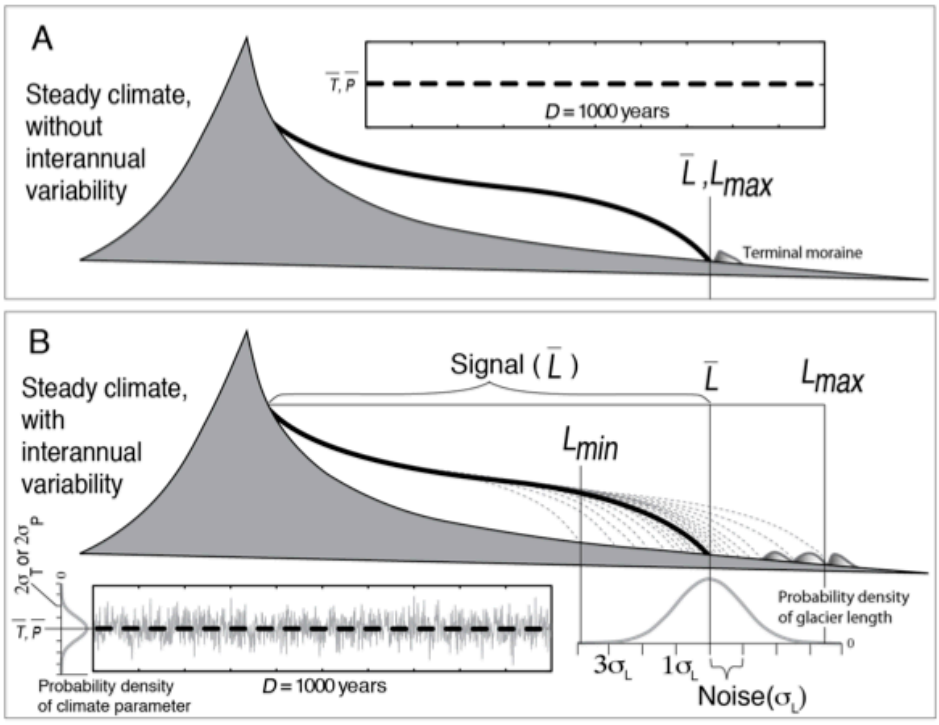

Figure 2.1 A: A glacier forced only by long-term average annual precipitation and mean melt-season temperature, $\bar{P}$ and $\bar{T}$ (bold dashed line), over time period, D, leads to a steady ice profile (bold black line) at mean length $\bar{L}$. The maximum terminal moraine forms at $\bar{L}$. B: A glacier forced by the same $\bar{P}$ and $\bar{T}$ as in A but with interannual variability included (gray white noise in the inset panel, which fills a normal distribution centered at $\bar{P}$ or $\bar{T}$) results in a terminus position that fluctuates around $\bar{L}$ and is shown by the gray dashed ice profiles. Given enough time, the terminus position fills a normal distribution centered at $\bar{L}$ (the signal; Equation 2.3) and is characterized by σ_L (the noise; Equation 2.2), the standard deviation of glacier length perturbations around $\bar{L}$. A change in $\bar{L}$ would occur with a change in $\bar{P}$ or $\bar{T}$ but not a change in σ_P or σ_T.

decadal scales (red noise) around the same $\bar{L}$ as glacier (a) (Figs. 2.1B and 2.2C). However, for glacier (b) $\bar{L}$ is a theoretical length with no expression in the landscape, and is the location around which the terminus fluctuates. If we assume that: (1) terminal moraines up to 40 m in height can be formed on time scales less than 50 yr, (2) moraines do not significantly impede subsequent advances, and (3) all moraines that are overrun by subsequent advances are removed, then the maximum excursion from $\bar{L}$ will form the furthest terminal moraines. Assumption 1 is supported by a compilation of 45 terminal moraine formation timescales and moraine heights, which shows that 25 m ice contact/dump moraines as well as 50 m push/glaciotectonic moraines form in less than 50 yr (section 2.9.3). Assumption 2 is primarily a concern when latero-frontal dump moraines >50 m in height are present; these are common in tectonically active regions such as the Himalaya, Andes, or Southern Alps (e.g., Benn and Evans, 1998; section 2.9.3). Estimates of average climate (i.e., $\bar{P}, \bar{T}$) should be based on $\bar{L}$ rather than L_{max} (Fig. 2.1B). Thus, we face the challenge of estimating the mean length $\bar{L}$ while knowing only the glacier geometry preserved by the maximum advance, $L_{\max}$, and recognizing the substantial uncertainties in physical parameters.

We focus on the Last Glacial Maximum (LGM) moraine record in the Colorado Front Range, United States, to establish the effect of interannual variability on the moraine record. We use a shallow-ice-approximation flowline model (using standard techniques; section 2.9.6) to confirm, in accordance with prior work in modern maritime, Alpine, and continental settings, that interannual variability can force significant multi-decadal length fluctuations. Oerlemans, 2001). We primarily focus on constraining the effect of parameter uncertainty on the magnitude of length fluctuations forced by interannual variability using a linearized glacier model for the 11-modeled glaciers.

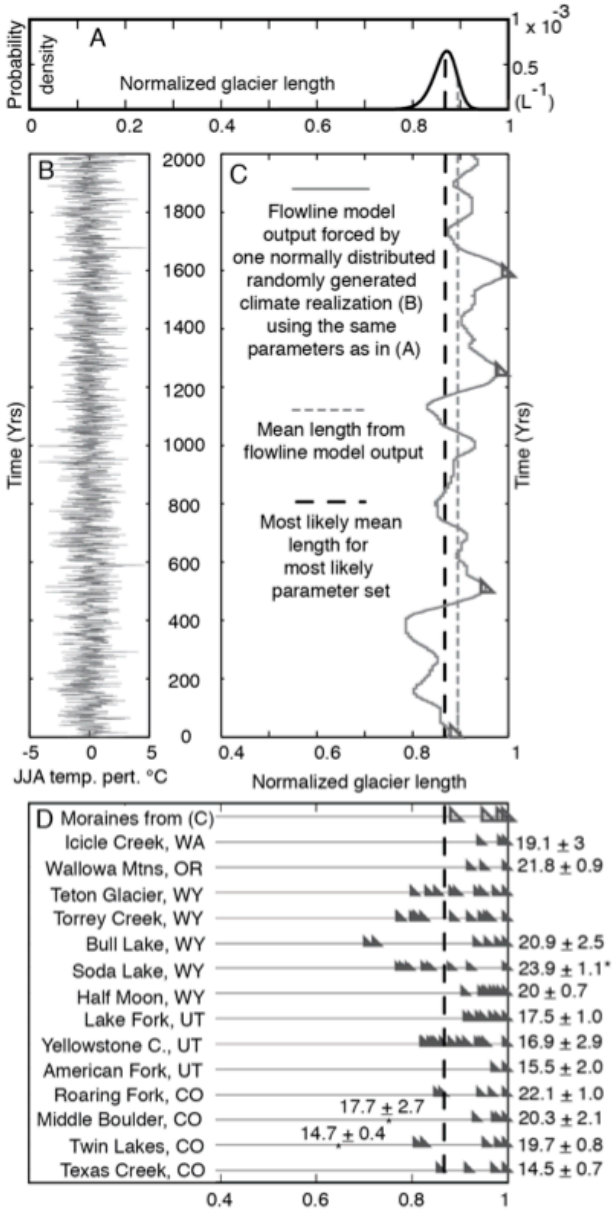
A
Probability density
Normalized glacier length
1 x 10^-3
0.5
(L^-1)
0
0.2
0.4
0.6
0.8
1
B
C
2000
1800
1600
1400
1200
1000
800
600
400
200
0
Time (Yrs)
-5
0
5
JJA temp. pert. °C
Flowline model output forced by one normally distributed randomly generated climate realization (B) using the same parameters as in (A)
Mean length from flowline model output
Most likely mean length for most likely parameter set
0.4
0.6
0.8
1
Normalized glacier length
Time (Yrs)
D Moraines from (C)
Icicle Creek, WA
19.1 ± 3
Wallowa Mtns, OR
21.8 ± 0.9
Teton Glacier, WY
Torrey Creek, WY
Bull Lake, WY
20.9 ± 2.5
Soda Lake, WY
23.9 ± 1.1*
Half Moon, WY
20 ± 0.7
Lake Fork, UT
17.5 ± 1.0
Yellowstone C., UT
16.9 ± 2.9
American Fork, UT
15.5 ± 2.0
Roaring Fork, CO
22.1 ± 1.0
17.7 ± 2.7
Middle Boulder, CO
20.3 ± 2.1
14.7 ± 0.4*
Twin Lakes, CO
19.7 ± 0.8
Texas Creek, CO
14.5 ± 0.7
0.4
0.6
0.8
1

Figure 2.2 An illustration of the relationship between the mean glacier length and moraine formation. A: The probability density function (pdf) of possible mean lengths derived from the most likely parameter set normalized by the maximum extent of the glacier. Equation 2.3 gives the most likely mean length $\bar{L}$ from this pdf. B: An example melt-season white-noise climatology, which is used to produce the example glacier terminus history in C. C: An example terminus history with potential moraine-forming locations indicated by triangles. D: Glacier length normalized to the LGM maximum terminal moraine with terminal moraines in-board from the maximum extent shown as triangles for western United States LGM valleys. Note the scatter in LGM maximum terminal moraines ages (ka) shown on the right.

2.3 Model Description

2.3.1 Linearized model

The linear model considers glacier length variations, L', as departures from a mean length $\bar{L}$ that are small enough that the equations are linear. Linear models use simplified glacier geometries to improve efficiency while still honoring the essence of glacier length change. They have been applied to a variety of glaciological problems (e.g., Jóhanneson et al., 1989; Oerlemans, 2001). Its use in this study is essential for efficient uncertainty analysis. Roe and O'Neal (2009) present a complete model description. If time is discretized into increments of Δt = 1 yr, then

$$L'_{t+\Delta t} = L'_t\left(1 - \frac{\Delta t}{\tau}\right) + \beta P'_t + \alpha T'_t \quad . \tag{2.1}$$

The first term on the right-hand side represents the glacier's dependence on its previous state. The last two terms are the forcing due to a given year's anomaly in precipitation, P', and melt-season temperature, T', for which we use white noise with standard deviations of σ_P and σ_T. The coefficients α and β are functions of glacier geometry: $\alpha = -\mu A_{T>0}\Delta t/(wH)$, $\beta = A_{tot}\Delta t/(wH)$, $A_{T>0} = A_{abl} + \bar{P}w/\mu\Gamma\tan\varphi$, and τ is the characteristic time scale (also response time) over which the glacier responds to past forcing: $\tau = wH/(\mu\Gamma\tan\varphi A_{abl})$ (see Table 2.1 for definitions).

Table 2.1 LINEAR MODEL PARAMETERS AND GEOMETRY INPUTS

Name	Units	Description	Min.	Mean	Max.
μ	(m $^{\circ}C^{-1}$ yr^{-1})	Melt factor	0.5	0.7	0.9
Γ	($^{\circ}C$ km^{-1})	On-ice near-surface lapse rate	3.5	5	6.5
AAR		Accumulation-area ratio	0.5	.65	0.8
$\overline{P}$	(m)	Mean annual precipitation	0.6	1.2	2.4
σ_T	($^{\circ}C$)	Std. of summertime temp.	1	1.3	1.6
σ_P	(m yr^{-1})	Std. of annual precipitation	0.11	0.22	0.44
D	(yr)	Duration of climate change	500	4000	7500
Geometry Inputs					
A_{tot}		Total area of the glacier			
A_{abl}		Ablation area of the glacier			
$tan\phi$		Slope of the glacier bed			
w		Width of the ablation zone			
H		Thickness of the glacier			

2.3.2 Climate data and parameter selection

Meteorological data were extracted from the longest-running high-elevation weather station in North America on Niwot Ridge, Colorado (Fig. 2.3B; Station D1; 1952–2010; 3743 m a.s.l. [above sea level]). Assuming that the melt season runs from June to September, we determined that melt-season temperature ($\overline{T}$, σ_T) is (6.3,1.3) °C and annual precipitation ($\overline{P}$, σ_P) is (1.2, 0.22) m yr^{-1}. Data were linearly detrended. We consider a range of near-surface lapse rates based on a global compilation of summer on-ice, near-surface lapse rates which for valley glaciers has a mean of 4.0 ± 2.1 °C km^{-1} (1σ) (Table 2.1; section 2.9.1). We constrain the melt-factor, μ (i.e., ablation rate per 1 °C change in *T*), based on a global compilation of μ for snow (4.5 ± 1.7 mm day^{-1} $°C^{-1}$) and ice (7.7 ± 3.2 mm day^{-1} $°C^{-1}$; section 2.9.2). We also consider a relatively broad range of accumulation-area ratios (*AAR*), the ratio of the accumulation area to the total glacier area, from 0.5 to 0.8 (Meier and Post, 1962).

Table 2.2 GLACIER GEOMETRY INPUTS, MEAN LENGTHS, AND SIGNAL-TO-NOISE RATIOS

Glacier name	Area (km^2)	Slope	Width (km)	Height (km)	L_{max} (km)	$\bar{L}_{min}$ % to L_{max}	$\bar{L}_{mean}$ % to L_{max}	$\bar{L}_{max}$ % to L_{max}	Mean Signal-to-Noise*	Response time (τ)
1. Middle Boulder	56.62	0.031	1.30	0.22	18.55	97	86	62	16.68	133.44
2. North Saint Vrain	45.89	0.050	1.16	0.19	15.25	97	88	68	19.63	77.95
3. Bear Lake	31.19	0.055	1.56	0.16	12.61	97	87	63	17.70	118.99
4. North Boulder	26.00	0.091	1.32	0.11	12.47	97	89	71	22.94	50.10
5. Fall Creek	14.57	0.078	0.58	0.14	10.55	96	86	65	17.86	57.75
6. Hunter's Creek	6.25	0.138	0.81	0.09	6.19	96	85	59	16.12	69.00
7. Mill Creek	5.80	0.089	0.52	0.11	5.94	95	79	41	10.27	91.33
8. Roaring Fork	4.11	0.178	0.51	0.08	5.72	96	86	63	17.69	45.59
9. Silver Creek	1.67	0.131	0.45	0.04	2.07	83	28	-119	1.11	67.22
10. Rainbow Creek	1.42	0.120	0.44	0.04	2.92	87	43	-77	2.11	83.50
11. Horseshoe Creek	1.41	0.137	0.35	0.05	2.86	90	57	-30	3.64	73.85

*Signal-to-noise ratio $\equiv \bar{L}/\sigma_L$

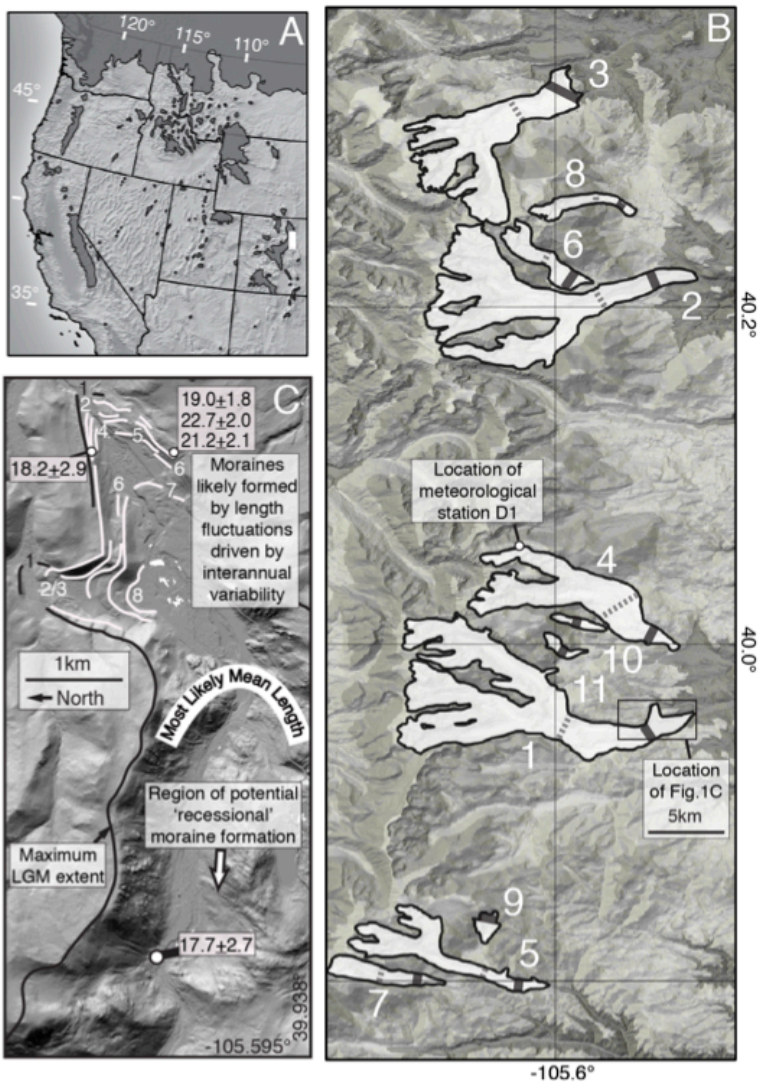
A
120°
115°
110°
45°
35°
B
3
8
6
2
40.2°
Location of meteorological station D1
4
10
11
1
40.0°
Location of Fig.1C
5km
9
5
7
-105.6°
C
19.0±1.8
22.7±2.0
21.2±2.1
18.2±2.9
Moraines likely formed by length fluctuations driven by interannual variability
1km
North
Most Likely Mean Length
Region of potential 'recessional' moraine formation
Maximum LGM extent
17.7±2.7
39.938°
-105.595°

Figure 2.3 A: Map of western U.S. glaciers during the LGM with generalized glacier outlines, after Young et al. (2011). (B) Shaded relief map showing the aerial extent of the 11 modeled glaciers (Table 2) and the location of the weather station used in this study. $\bar{L}_{mean}$*, the most likely estimate of mean length, and* $\bar{L}_{max}$*, the maximum possible mean length, are shown for each modeled glacier. C: Lidar-derived hillshade of the terminal region of the LGM Middle Boulder Creek (Colorado) glacier. Cosmogenic radionuclide dates are in ka (see the Data Repository [see footnote 1] for citations). Note that two distinct LGM advances could have been dated leading to the spread of CRN ages. Numbers near moraines denote the number of distinct ice advances recorded in the pro-*$\bar{L}$ *area. D: Lidar hillshade of Glacier Gulch, Wyoming, LGM terminal moraine complex. The 14 ice marginal features preserved support the mobile termini of Western US LGM glaciers. Note that ice marginal feature 4 was formed by a re-advance that crosscut advances 1–3.*

2.4 Impact of Interannual Variability on Mean Glacier Length

The flowline model (section 2.9.6) was integrated with mid-range parameters (Table 2.1) for the basal slope and length of a mid-sized LGM Front Range glacier (Fall Creek glacier; Table 2.2; Fig. 2.2C). The most likely parameter set generated a standard deviation of length fluctuations (σ_L) of 370 m. For the linear model σ_L can be solved exactly:

$$\sigma_L = \sqrt{\frac{\tau \Delta t}{2}} \sqrt{\alpha^2 \sigma_T^2 + \beta^2 \sigma_P^2} \, . \tag{2.2}$$

For the same parameters as the flowline model, the linear model suggests σ_L = 415 m, consistent with the ~15% overestimate of the flowline model results described by Roe (2011). This inter-model difference is much smaller than the parameter uncertainty (Table 2.1). The outer bounds of the linear model σ_L are 180 and 800 m. A high sensitivity to *T* or *P* (i.e., large α or β), or a long response time leads to a large σ_L.

We use excursion statistics for glaciers driven by climate variability (after Roe, 2011; Reichert et al. 2002). In any given time interval *D*, the mean glacier length, $\overline{L}$, cannot be known exactly, but it is described by a probability distribution (Fig. 2.2A). Roe (2011) showed that the most likely $\overline{L}$ can be related to the maximum glacial length, $L_{\max}$, by

$$\overline{L} = L_{\max} - \sigma_L \sqrt{2 \ln\left(\frac{D \dot{\sigma}_L}{2\pi \sigma_L \ln(2)} \right)}, \tag{2.3}$$

where $\dot{\sigma}_L$ is the standard deviation of the time rate of change of glacier length (see Roe, 2011, his Equations 9 and A8) with p = 0.5. Equation 2.3 is quite general, and holds provided the probability distribution of glacier fluctuations is normally distributed (Fig. 2.1B). It has been shown to govern the variability of terminus position in flowline glacier models (Reichert et al., 2002; section 2.9.7). Roe (2011) further demonstrated that setting $\sigma_{\dot{L}} = \sigma_L \sqrt{2/\psi \tau \Delta t}$ emulated

the behavior of a standard numerical flowline model, where ψ (≈10) is a factor introduced because high frequencies are damped more strongly in a numerical flowline model than is predicted by the linear model. The effect of varying ψ is minimal: doubling or halving of ψ results in a ± 0.6% change in $\bar{L}$ when *D* is larger than the glacier response time, τ. We consider a broad range of *D* (the duration of the climate of interest) values between 500 and 7500 yr, the upper limit being the duration of the LGM sea-level low stand (Clark et al., 2009). Alternatively, a natural choice for *D* is the time interval separating two dated moraines we wish to attribute to either climate change or interannual weather variability.

2.4.1 Mean length and signal-to-noise results

For glaciers with areas between 56 and 4 km^2, the most likely mean glacier length is 10%–15% up valley from L_{max} (Table 2.2, column 8). Bounds on the potential location of the mean length—3% to 50% up valley from L_{max}— represent cases in which all parameters are simultaneously given their extreme values (Table 2.2, columns 7 and 9). As this is unlikely, this range should be considered an outer bound on $\bar{L}$. Interpreting the cause of glacier length changes requires that we discern the competing influences of a signal (a change in $\bar{P}$ or $\bar{T}$ leading to a change in $\bar{L}$; Fig. 2.1B; Equation 2.3) and a noise component (climate noise σ_P, σ_T driving length fluctuations, σ_L; Equation 2.2). Glaciers with area less than 2 km^2 have a σ_L comparable to their $\bar{L}$ (Table 2.2), and so perhaps flickered in-and-out of existence or hung on as small stagnant ice bodies during periods of the local LGM.

Table 2.3 HISTORICAL EXAMPLES OF MORAINES FORMED BY INTERANNUAL VARIABILITY FORCED ADVANCES

Glacier	Time	Relief	Citation*
Engabreen, NO	<20 yr	15 m	Worsely and Alexander, 1976
Nigardsbreen, NO	<10 yr	<10 m	Nussbaumer et al., 2011
Six glaciers, NO	<10 yr	<3 m	Winkler and Matthews, 2010
Upper Grindelwald, CH	<10 yr	10 m	Zumbühl et al., 2008
Des Bossons, FR	~10 yr	20 m	Nussbaumer and Zumbühl,
Mer de Glace, FR	~10yr	<10m	Zumbühl et al., 2008

Note: NO—Norway; CH—Switzerland; FR—France.
*Citations are given in the Data Repository (see text footnote 1).

2.5 Discussion

Historical records of advance and retreat show that 1–20 m moraines can form from interannual variability forced advances (Table 2.3; see the references in the Data Repository). They also support the notion that valley glaciers fluctuate on multi-decadal timescales in response to interannual variability. It is often assumed that long glacial standstills (century scale) were required to form large LGM terminal moraines (often >10 m in height). Our results suggest that century-scale glacial standstills (terminus within 50 m of the same location) did not occur for the Colorado Front Range glaciers we modeled. Rather, our numerical model shows that the longest standstills lasted ~50 yr (glaciers with longer response times have a propensity for longer standstills) (Fig. 2.2C; section 2.9.4; Johnson and Gillam, 1995).

Glacier length fluctuations forced by interannual variability can be viewed as a smaller-scale example of the moraine survival problem (e.g., Gibbons et al., 1984). Broad LGM terminal moraine complexes (Fig. 2.3D), which are often conglomerates of many moraines formed by different advances, may represent cycles of kilometer-scale retreat and re-advance that are independent of true climate change. The glacier likely formed one moraine, then left the terminal moraine complex and returned, forming a second moraine (Figs. 2.2C and 2.3D). Terminal moraines between $\bar{L}$ and L_{max} are therefore not necessarily 'recessional' moraines in the classic sense.

Because maximum moraines reflect advances formed sometime after the glacier reached $\bar{L}$, dating the maximum moraine provides a minimum estimate of when a climate change initiated. Constraining the timing of retreat from $\bar{L}$ provides an estimate of when $\bar{P}$ and $\bar{T}$ changed (e.g., Young et al., 2011; Fig. 2.1B). The sampling of boulders deposited by multiple advances could explain the variation of cosmogenic radionuclide exposure (CRN) ages from

some LGM terminal deposits assumed to be formed by a single advance (Fig. 2.3). Sampling the highest ridge in a moraine complex may not provide dates from the oldest advance (Fig. 2.3D). The potential for sporadic exposure of bedrock between L_{max} and L_{min} could also impact the interpretation of CRN concentrations in bedrock for either exposure ages or production rates.

Incoherent patterns of interannual variability from region-to-region (coherence can be expected over an ~500 km length scale; Letréguilly and Reynaud, 1989) could have resulted in glacier advances and retreats at different times around the western United States during the regional LGM. This effect could potentially explain the spread of ages derived from LGM maximum terminal moraines across the western United States (e.g., Young et al., 2011), and even globally (Schäfer et al., 2006).

Moraines reflect maximum advances, and our results suggest that climate noise (weather) is likely to force kilometer-scale advances beyond what the mean climate conditions support. Climate estimates derived from maximum glacier geometries do not represent the local LGM-mean climate. Rather, they have a one-sided bias due to glacial length excursions down valley from $\overline{L}$. Equilibrium-line-altitudes (ELAs) and climate change estimates derived from glacier models directly reconstructed from maximum moraines will therefore overestimate the climate change. In our setting, the central parameter range suggests this is a 10%–15% effect for LGM moraines.

2.6 Conclusions

Interannual variability is present in all climates and results in decadal-scale glacial length fluctuations around a mean length. We should therefore expect it to play an important role in kilometer-scale length fluctuations and moraine formation in the past and present as well as in maritime, Alpine, and continental settings (e.g., Oerlemans, 2001). Glacier response times and

the magnitude of σ_P and σ_T will determine the expected timescale and magnitude of length fluctuation. Several modeling efforts, historical glacier extent records, and documentation of modern moraine formation support our conclusions. Glacier length fluctuations due to year-to-year climate variability should therefore be included in the interpretation of the moraine record.

2.7 Acknowledgements

We thank the Niwot Ridge Long Term Ecological Research for weather station data. L. Anderson acknowledges support from National Science Foundation (NSF) grant DGE-1144083 (GRFP). R. Anderson acknowledges support of NSF grant EAR-1239281 (Boulder Creek CZO) and grant EAR-1123855.

2.8 References Cited

Benn, D.I., and Evans, D.J.A., 1998, Glaciers and Glaciation: Arnold, London. 734 p.

Burke, E.E., and Roe, G.H., 2013, The absence of memory in the climatic forcing of glaciers: Climate Dynamics, p. 1–12, doi:10.1007/s00382-013-1758-0.

Clark, P.U., Dyke, A.S., Shakun, J.D., Carlson, A.E., Clark, J., Wohlfarth, B., Mitrovica, J.X., Hostetler, S.W., and McCabe, A.M., 2009, The Last Glacial Maximum: Science, v. 325, no. 5941, p. 710–714, doi:10.1126/science.1172873.

Gibbons, A.B., Megeath, J.D., and Pierce, K.L., 1984, Probability of moraine survival in a succession of glacial advances: Geology, v. 12, p. 327–330, doi:10.1130/0091-7613(1984)12<327:POMSIA>2.0.CO;2.

Jóhannesson, T., Raymond, C.F., and Waddington, E.D., 1989, Time-scale for adjustment of glaciers to changes in mass balance: Journal of Glaciology, v. 35, no. 121, p. 355–369.

Johnson, M.D., and Gillam, M.L., 1995, Composition and construction of late Pleistocene end moraines, Durango, Colorado: Geological Society of America Bulletin, v. 107, no. 10, p. 1241–1253, doi:10.1130/0016-7606(1995)107<1241:CACOLP>2.3.CO;2.

Letréguilly, A., and Reynaud, L., 1989, Spatial patterns of mass-balance fluctuations of North American glaciers: Journal of Glaciology, v. 35, no. 120, p. 163–168.

Meier, M.F., and Post, A.S., 1962, Recent variations in mass net budgets of glaciers in western North America, International Association of Hydrological Sciences Publication, No. 58, p. 63–77.

Oerlemans, J., 2001, Glaciers and Climate Change: Lisse, NL, Swets and Zeitlinger, 160 p.

Reichert, B.K., Bengtsson, L., and Oerlemans, J., 2002, Recent glacier retreat exceeds internal variability: Journal of Climate, v. 15, no. 21, p. 3069–3081, doi:10.1175/1520-0442(2002)015<3069:RGREIV>2.0.CO;2.

Roe, G.H., 2011, What do glaciers tell us about climate variability and climate change?: Journal of Glaciology, v. 57, no. 203, p. 567–578, doi:10.3189/002214311796905640.

Roe, G.H., and O'Neal, M.A., 2009, The response of glaciers to intrinsic climate variability: observations and models of late-Holocene variations in the Pacific Northwest: Journal of Glaciology, v. 55, p. 839–854, doi:10.3189/002214309790152438.

Schäfer, J.M., Denton, G.H., Barrell, D.J., Ivy-Ochs, S., Kubik, P.W., Andersen, B.G., Phillips, F.M., Lowell, T.V., and Schlüchter, C., 2006, Near-synchronous interhemispheric termination of the last glacial maximum in mid-latitudes: Science, v. 312, no. 5779, p. 1510–1513, doi:10.1126/science.1122872.

Young, N.E., Briner, J.P., Leonard, E.M., Licciardi, J.M., and Lee, K., 2011, Assessing climatic and nonclimatic forcing of Pinedale glaciation and deglaciation in the western United States: Geology, v. 39, no. 2, p. 171–174, doi:10.1130/G31527.1.

2.9 Supplemental Material

2.9.1 *On-ice near surface lapse rates*

The selection of the lapse rate, Γ, for glaciological purposes must be made with care because reported summertime on-ice (≡ measurements only on glacier surface), near-surface (≡ measurements made 2 m above the surface) lapse rates vary by nearly a factor of eight (Table 2.4). Since Γ governs how ablation changes with elevation, much of the uncertainty in the results arises from this parameter. We argue that observed on-ice, summertime lapse rates provide a better approximation of the relevant paleo lapse rates than either the standard moist adiabatic lapse rate, observed free atmospheric lapse rates, or observed off-ice (measurements made off-glacier) near-surface lapse rates— even in those in the Front Range.

Lapse rates in the free atmosphere are determined by atmospheric vertical mixing and moisture. However, surface lapse rates are controlled surface radiative transfer and by the near

surface environment (surface albedo, roughness, topographic aspect, and local meteorological effects, e.g., Marshall and Sharp, 2007). While the use of modern summer near-surface temperature lapse rates from the Front Range is likely more appropriate than the often-used 6.5 °C km^{-1} moist adiabatic lapse rate, modern environmental conditions obviously differ greatly from likely summer conditions on an LGM glacier (presence of ice, reduced roughness, different elevation and topography due to the presence of the glacier). We therefore used modern on-ice near-surface temperature lapse rates to guide our uncertainty analysis. Table A shows that the most likely mean summer on-ice near surface lapse rate is 4.9 °C km^{-1} with a 1σ value of 1.7 °C km^{-1} . Extreme mean values are 1.1 °C km^{-1} (Pasterze Glacier, Austria) and 7.9 °C km^{-1} (Greenland Ice Sheet).

Table 2.4 COMPILATION OF ON-ICE NEAR SURFACE LAPSE RATES

Valley Glaciers

Location	Classification	Latitude	Lapse Rate °C km^{-1}	Period of Averaging	Reference
Pasterze Glacier, Austria	Valley	47°N	1.1	June, July	Greuell and Smeets, 2001
John Evans Glacier, Canada	Valley	80°N	1.1	Summer	Arendt and Sharp, 1999
Pasterze Glacier, Austria	Valley	47°N	1.4	June, July	Greuell and Smeets, 2001
Haut Glacier, Switzerland	Valley	45.97°N	2.0	Summer	Strasser et al., 2004
John Evans Glacier, Canada	Valley	80°N	3.1	Summer	Gardner et al., 2009
Pasterze Glacier, Austria	Valley	47°N	3.5	June, August	Denby and Greuell, 2000
Franz Josef Glacier, New Zealand	Valley	43.49°N	4.8	Annual	Anderson et al., 2006
Keqicar Glacier, Tien Shan	Valley	41.75°N	5.0	July	Li et al, 2011
South Glacier, Yukon	Valley	60.8°N	5.3	Annual	MacDougall and Flowers, 2011
Storglaciären, Sweden	Valley	67.9°N	5.5	Annual	Hock and Holmgren, 2005
North Glacier, Yukon	Valley	60.8°N	6.0	Annual	MacDougall and Flowers, 2011
Keqicar Baqi, Tien Shan, China*	Valley	41.75°N	6.0	Summer	Zhang et al., 2007*
South Cascade Glacier, WA	Valley	48.35°N	6.5	Summer	Anslow et al., 2008
Juncal Norte, Chile	Valley	32.6°S	6.5	Summer	Petersen and Pellicciotti, 2011
Miage glacier, Italy*	Valley	45.5°N	6.7	Summer	Brock et al., 2010*
Baltoro Glacier, Pakistan*	Valley	35.7°N	7.5	Summer	Mihalcea et al., 2006*
Miage glacier, Italy*	Valley	45.5°N	8.0	Summer	Brock et al., 2010*
	Valley Glacier Mean:		*4.7±2.2*	*w/ debris-cover*	
			4.0±2.1	*w/o debris-cover*	

Ice Sheet and Ice Cap

Location	Classification	Latitude	Lapse Rate °C km^{-1}	Period of Averaging	Reference
Vatnajökull, Iceland	Ice Cap	64.1°N	3.6	Summer	Oerlemans et al., 1999
Prince of Whales Icefield, Canada	Ice Cap	78°N	3.7	JJA	Marshall et al., 2007
Prince of Whales Icefield, Canada	Ice Cap	78°N	4.3	Summer	Marshall et al., 2007
Prince of Wales Ice Field, Canada	Ice Cap	78°N	4.4	Summer	Marshall and Sharp, 2009
Prince of Whales Icefield, Canada	Ice Cap	78°N	4.6	Summer	Gardner et al., 2009
Devon Ice Cap, Canada	Ice Cap	75.2°N	4.8	Summer	Mair et al. 2005
Prince of Whales Icefield, Canada	Ice Cap	78°N	4.8	JJA	Marshall et al., 2007
Devon Ice Cap, Canada	Ice Cap	75.2°N	4.9	Summer	Gardner et al., 2009
Prince of Whales Icefield, Canada	Ice Cap	78°N	5.3	JJA	Marshall et al., 2007
Langjökull, Iceland	Ice Cap	64.5°N	5.6	JJA	Gudmundsson, et al, 2003
Vestari Hagafellsjökull, Iceland	Ice Cap	64.5°N	5.7	Summer	Hodgkins et al., 2012
King George Island, Antarctica	Ice Cap	62.3°S	6	Summer	Braun and Hock, 2004
Aggasiz Ice Cap, Canada	Ice Cap	80.2°N	6.4	Summer	Gardner et al., 2009
Greenland Ice Sheet (>1000m a.s.l)	Ice Sheet	~67°N	2.4	Summer	Oerlemans and Vugts, 1993
Greenland Ice Sheet	Ice Sheet	60-	4	June	Steffen and Box, 2001
NE Greenland Ice Sheet	Ice Sheet	70-	4	June, August	Boggild et al., 1994
Greenland Ice Sheet (<1000m a.s.l.)	Ice Sheet	60-	4.3	Summer	Hanna et al., 2005
Greenland Ice Sheet	Ice Sheet	60-	5	June, July	Box and Rinke, 2003
Greenland Ice Sheet (<1000m a.s.l.)	Ice Sheet	~67°N	5	Summer	Oerlemans and Vugts, 1993
West Greenland Ice Sheet	Ice Sheet	~67°N	5.8	Mean	van den Broeke et al., 2011
Greenland Ice Sheet (<1000m a.s.l.)	Ice Sheet	~67°N	6.3	Summer	Oerlemans and Vugts, 1993
West Greenland Ice Sheet	Ice Sheet	~67°N	7.4	Mean	van den Broeke et al., 2011
Greenland Ice Sheet (>1000m a.s.l.)	Ice Sheet	60-	7.9	Summer	Hanna et al., 2005
	Ice Sheet and Ice Cap Mean:		*5.1±1.2*		

* Debris-covered glacier	Mean of all cited lapse rates:	*4.9±1.7*	*w/ debris-cover*
	Mean of all cited lapse rates:	*4.7±1.6*	*w/o debris-cover*

2.9.2 Melt-factors

The melt factor, μ, employed in our ablation parameterization is a simplified form of the often used positive-degree-day model that relates mean summer temperatures to vertical surface mass loss. The melt factor μ is converted from published positive-degree-day factors by assuming a melt season covering the months of June, July, and August (Table 2.5). The selection of μ must be made with care as positive degree-day factors for snow can vary by nearly a factor of ten, and for ice by a factor of six. We combine and supplement several previous compilations of snow and ice melt-factors for modern glaciers and mountainous regions. Table 2.5 shows that the most likely positive degree day factor for ice: is 7.7 mm day^{-1} $°C^{-1}$ with a 1σ value of 3.2 mm day^{-1} $°C^{-1}$ with extreme values of 20 mm day^{-1} $°C^{-1}$; Van de Wal (1992) and 2.6 mm day^{-1} $°C^{-1}$; Zhang et al. (2006); and the most likely positive degree day factor for snow is 4.5 m $°C^{-1}$ a^{-1} with a 1σ value of 1.7 mm day^{-1} $°C^{-1}$ with extreme values of 11.6 mm $day^{-1}°C^{-1}$; Kayastha et al. (2000) and 1.4 mm day^{-1} $°C^{-1}$ Howat et al. (2007). It is important to note that our parameter combinations produce mass balance values that are reasonable for continental climates.

Table 2.5 GLOBAL COMPILATION OF POSITIVE DEGREE-DAY MELT FACTORS (mm ° day^{-1} C^{-1})

Greenland							
Location	Snow	Ice	Elevation	Latitude	Duration	Reference	Cited in
Thule Ramp, Greenland		12	570	76°25'N	1 Jul - 31 Jul 1954	Schytt, 1955	Hock, 2003
Thule Ramp, Greenland		7	570		1 Aug-31 Aug 1954	Schytt, 1955	Hock, 2003
Camp IV-EGIG, Greenland		18.6	1013	69°40'N	Melt season 1959	Ambach, 1988a	Hock, 2003
GIMEX profile, Greenland		8.7	341	67°06'N	10 Jun-31 Jul 1991	Van de Wal, 1992	Hock, 2003
GIMEX profile, Greenland		9.2	519	67°06'N	15 Jun-6 Aug 1991	Van de Wal, 1992	Hock, 2003
GIMEX profile, Greenland		***20***	1028	67°04'N	15 Jun-6 Aug 1991	Van de Wal, 1992	Hock, 2003
Qamanârssûp sermia, Greenland	2.8	7.3	370-1410	64°28'N	1979-1987	Johannesson et al., 1995	Hock, 2003
Qamanârssûp sermia, Greenland	2.9	8.2	790	64°28'N	512 days (1980-86)	Braithwaite, 1995	Hock, 2003
Nordboglacier, Greenland	3.7	7.5	880	61°28'N	415 days (1979-83)	Braithwaite, 1995	Hock, 2003
Kronprins Christian Land, Greenland		9.8	380	79°54'N	8 Jul - 27 Jul 1999	Braithwaite et al., 1998	Hock, 2003
Hans Tausen Ice Cap, Greenland		5.9	540	82°49'N	2 Jul-5 Aug 1994	Braithwaite et al., 1998	Hock, 2003
Qamanârssûp sermia, Greenland	2.5	7.7	~800	64°28'N	Summer	Braithwaite, 1989	Braithwaite and Zhang, 2000
Qamanârssûp sermia, Greenland		7.9	790	64°28'N	May-Sep 1980-1986	Braithwaite, 1993	Braithwaite and Zhang, 2000
Greenland means:	*3.0±0.5*	*10.0±4.4*					
Europe/Americas/NZ							
Location	Snow	Ice	Elevation	Latitude	Duration	Reference	Cited in
Aletshgletscher, Switzerland		11.7	2220	46°270' N	2 Aug - 27 Aug,1965	Lang, 1986	Hock, 2003
Ålfotbreen, Norway	4.5	6	850-1400	61°45'N	1961-1990	Laumann and Reeh, 1993	Hock, 2003
Ålfotbreen, Norway	3.5	5.5	1450-2200	61°34'N	1961-1990	Laumann and Reeh, 1993	Hock, 2003
Ålfotbreen, Norway	4	5.5	300-2000	61°41'N	1961-1990	Laumann and Reeh, 1993	Hock, 2003
Nigardsbreen, Norway	4.4	6.4	300-2000	61°41'N	1964-1990	Johannesson et al., 1995	Hock, 2003
Storglaciären, Sweden	3.2		1550	67°55'N	5 Jul-7 Sep 1993	Hock, 1999	Hock, 2003
Storglaciären, Sweden		6	1370	67°55'N	5 Aug - 12 Aug 1993	Hock, 1999	Hock, 2003
Storglaciären, Sweden		6.4	1370	67°55'N	19 Jul-27 Aug 1994	Hock, 1999	Hock, 2003
Storglaciären, Sweden		5.4	1250	67°55'N	9 Jul-4 Sep 1994	Hock, 1999	Hock, 2003
Vestfonna, Spitzbergen		13.8	310-410	~80°N	26 Jun - 5 Aug 1958	Schytt, 1964	Hock, 2003
Satujökull, Iceland	5.6	7.7	800-1800	~65°N	1987-1992	Johannesson et al., 1995	Hock, 2003
Aletshgletscher, Switzerland	5.3		3366	46°270' N	3 Aug-19 Aug, 1973	Lang, 1986	Hock, 2003
John Evans Glacier, Canada	5.5		260	79°40' N	27 Jun-29 Jun 1996	Arendt and Sharp, 1999	Hock, 2003
John Evans Glacier, Canada	4.1		820	79°40' N	19 Jun - 14 Jul 1996	Arendt and Sharp, 1999	Hock, 2003
John Evans Glacier, Canada	3.9		820	79°40' N	23 May - 1 Jul 1998	Arendt and Sharp, 1999	Hock, 2003
John Evans Glacier, Canada	3.9		1180	79°40' N	25 Jun-19 Jul 1996	Arendt and Sharp, 1999	Hock, 2003
John Evans Glacier, Canada	2.7		1180	79°40' N	31 May - 19 Jul 1996	Arendt and Sharp, 1999	Hock, 2003
John Evans Glacier, Canada		7.6	260	79°40' N	4 Jul - 16 Jul 1996	Arendt and Sharp, 1999	Hock, 2003
John Evans Glacier, Canada		8.1	820	79°40' N	15 Jul - 19 Jul 1996	Arendt and Sharp, 1999	Hock, 2003
John Evans Glacier, Canada		5.5	820	79°40' N	2 Jul -19 Jul 1998	Arendt and Sharp, 1999	Hock, 2003
Weissfluhjoch, Switzerland	4.2		2540	46°48'N	28 year record	de Quervain, 1979	Braithwaite and Zhang, 2000
Franz Josef Glacier, New Zealand	3	6	122	43°28'N	Summer	Woo and Fitzharris, 1992	Braithwaite and Zhang, 2000
Saint Supphellebreen, Norway		6.3		61°30'N	Summer	Orheim, 1970	Braithwaite and Zhang, 2000
Glacier de Sarennes, France	3.8	6.2	~3000	45°10'N	Summer	Vincent and Vallon, 1997	Braithwaite and Zhang, 2000
Griesgletscher, Switzerland		8.9	2287	46°39'N	112 summer days	Braithwaite, 2000	Braithwaite and Zhang, 2000
Australian Alps	2.9		1250	36°30'S	1966-1985	Whetton, et al., 1996	Brugger, 2010
Blöndujökull, Kv ıslajökull, Iceland	4.5	5	115	64°50'N	Summer	Johennesson, 1997	Brugger, 2010
Illvirajökull, Iceland	5.6	7.6	115	64°50'N	Summer	Johennesson, 1997	Brugger, 2010
Glacier Upsala, Patagonia		7.1	350	49°58S	Summer 1993-1994	Naruse et al., 1997	Brugger, 2010
South Cascade Glacier, USA		6.2	1980	48°21'N	Summer	Tangborn,1999	Brugger, 2010
Rabots Glacier, Sweden	4.7	6.8	~1300	67°55'N	Summer	Refsnider, 2001	Brugger, 2010
Sverdrup Glacier, Canada		4	300	75°N	Summer 1963	Braithwaite, 1981	

Andrews Glacier, USA	4.3				Summer	Outcalt and MacPhail, 1965	Lauman & Reeh, 1993
Storsteinsfjellbreen, Norway	5,6	7.5		68°15'N	Summer	Pytte and Liestol, 1966	Lauman & Reeh, 1993
Storbreen, Norway		5.5		61°34'N	Summer 1949-1965	Liestol, 1967	Lauman & Reeh, 1993
White Glacier, Canada		4.9	210	79°N	Summer 1960-1962	Braithwaite, 1981	
Alfotbreen, Norway	5.3	7.5		61°45'N	Summer 1965	NVE, 1965	Lauman & Reeh, 1993
Various Swiss glaciers		6		~46°30'N	Summer	Kasser, 1959	Braithwaite and Zhang, 2000
Fillefjell, Norway	3.9			61°10'N	Summer 1967-1964	Furmyr and Tollan, 1975	Lauman & Reeh, 1993
Moreno glacier, Argentina		7	330	50°28'S	1993 -1994	Takeuchi et al., 1996	Hock, 2003
Martial Este Glacier, Argentina	4.7	9.4	990	54°47'S	Dec 2005 - Feb 2006	Buttstadt et al., 2009	
Haut Glacier d'Arolla, Switzerland	7.7	10.8	~2900	45°58'N	May - Sep 2001	Pellicciotti et al., 2005	
Mount Shasta, Cascade Range, USA	1.6	6.9	2600	41°12'N	May - Nov 2002	Howat et al., 2007	
Mount Shasta, Cascade Range, USA	***1.4***	5.5	3000	41°12'N	May - Nov 2002	Howat et al., 2007	
Hansbreen, Svalbard	6	8.3	180	77°05'N	JJA, 2008	Grabiec et al., 2012	
Franz Josef Glacier, New Zealand	4.6	7.1		43°28'N	Summer	Anderson, 2004	
Hansbreen, Svalbard		6.8	316	77°05'N	1994-1995	Szafraniec, 2002	
Gran Campo Nevado Ice Cap, Chile		7.6	450	53°S	Feb - Apr 2000	Schneider et al., 2007	
Tasman Glacier, New Zealand		4.5	1360	43°37'S	1985-1986	Kirkbride, 1995	
Tasman Glacier, New Zealand		5	1360	43°37'S	1986-1987	Kirkbride, 1995	
Tasman Glacier, New Zealand		3.9	960	43°37'S	1985-1986	Kirkbride, 1995	
Tasman Glacier, New Zealand		3.6	960	43°37'S	1986-1987	Kirkbride, 1995	
Glacier de Saint-Sorlin, France	4	6.4	2760	45°N	21 Jul- 31 Jul 2006	Six et al., 2009	
Koryto Glacier, Kamchatk, Russia	4.7	7	810	54°50'N	7 Aug-12 S. 2000	Konya et al., 2004	
Europe/America/NZ means:	*4.3±1.3*	*6.8±2.0*					

Central Asia

Location	Snow	Ice	Elevation	Latitude	Duration	Reference	Cited in
Urumqi glacier,Tien Shan, China	6.3	8.5	3831-3945	~42°N	1986-1993	Liu et al., 1996	Zhang_etal 2006
Urumqui glacier,Tien Shan, China		7.3	3754-3898	~42°N	1986-1988	Liu et al., 1996	Zhang_etal 2006
Urumqui glacier,Tien Shan, China	3.1		4048	~42°N	1986-1993	Liu et al., 1996	Zhang_etal 2006
Keqicar Baqi, Tien Shan, China		4.5	3347	~42°N	28 Jun- 12 Sep 2003	Zhang et al., 2005	Zhang_etal 2006
Keqicar Baqi, Tien Shan, China		7	4216	~42°N	11 Jul-13 Sep 2003	Zhang et al., 2005	Zhang_etal 2006
Qiongtailan glacier, Tien Shan, China		4.5	3675	~42°N	17 Jun- 14 Aug 1978	Zhang et al., 2006	
Qiongtailan glacier, Tien Shan, China		7.3	4100	~42°N	25 Jun-14 Aug 1978	Zhang et al., 2006	
Qiongtailan glacier, Tien Shan, China		8.6	4200	~42°N	21 Jun-31 Jul 1978	Zhang et al., 2006	
Qiongtailan glacier, Tien Shan, China	3.4		4400	~42°N	21 Jun- 11 Aug 1978	Zhang et al., 2006	
Hailuogou, Hengduan mtns, China		5	3301	~30°N	Aug 1982- Aug 1983	Zhang et al., 2006	
Baishuihe Hengduan mtns, China		13.3	4600	~30°N	23 Jun- 30 Aug 1982	Zhang et al., 2006	
Baishuihe,Hengduan mtns, China	5.9		4800	~30°N	26 Jun- 11 Jul 1982	Zhang et al., 2006	
Dagongba glacier, Hengduan, China		13.2	4540	~30°N	Sep 1982- Sep 1983	Zhang et al., 2006	
Xiaogongba glacier, China		12	4550	~30°N	Jul 1982- Jul 1983	Zhang et al., 2006	
Batura, Karakoram, China		3.4	2780	~36°N	Jun-Aug 1975	Zhang et al., 2006	
Teram Kangri, Karakoram, China		5.9	4630	~36°N	25 Jun- 7 Sep 1987	Zhang et al., 2006	
Teram Kangri, Karakoram, China		6.4	4650	~36°N	24 Jun- 7 Sep 1987	Zhang et al., 2006	
Qirbulake, Karakoram, China		***2.6***	4750	~36°N	6 Jun- 30 Jul 1960	Zhang et al., 2006	
Yangbulake, Karakoram, China		4.3	4800	~36°N	1Jul - 5 Jul 1987	Zhang et al., 2006	
Meikuang, Kunlun Shan, China		3	4840	~36°N	7 May- Sep 1989	Zhang et al., 2006	
Halong, Kunlun Shan, China		4.7	4616	~36°N	15 Jun- 28 Jun 1981	Zhang et al., 2006	
Halong, Kunlun Shan, China		3.6	4900	~36°N	14 Jun 27 Jun 1981	Zhang et al., 2006	
Xiaodongkemadi, Tanggula, China		13.8	5425-5475	~32°30'N	Jul- Aug 1993	Kayastha et al., 2003	Zhang_et al., 2006
Qiyi, Qilian Shan, China		7.2	4305-4619	~39°N	Jul- Aug 2002	Kayastha et al., 2003	Zhang_et al., 2006
Kangwure, Himalaya, China		9	5700-6000		20 Jul-25 Aug 1993	Zhang et al., 2006	
Urumqi Glacier, Tien shan, China	5.2	8.4		~42°N	Summer	Cui, 2009	Xianzhong, et al., 2010

Urumqi Glacier, Tien shan, China	3.1	7.1		~42°N	Summer	Cui, 2009	Xianzhong, et al., 2010
Urumqi Glacier, Tien shan, China	5.2	7.1		~42°N	Summer	Cui, 2009	Xianzhong, et al., 2010
Urumqi Glacier, Tien shan, China		4		~42°N	Summer	Cui, 2009	Xianzhong, et al., 2010
Baishui Glacier, Hengduan, China		4.92	4200	26°00'N	26 Jun-11 Jul 1982	Liu, 1996	Xianzhong, et al., 2010
Baishui Glacier, Hengduan, China		10.3	4600	26°00'N	Sept 2008	Xianzhong, et al., 2010	
Baishui Glacier, Hengduan, China		13.6	4700	26°00'N	Sept 2008	Xianzhong, et al., 2010	
Baishui Glacier, Hengduan, China		14.1	4800	26°00'N	Sept 2008	Xianzhong, et al., 2010	
Baishui Glacier, Hengduan, China	2.4		4400	26°00'N	13 May-6 Jun 2009	Xianzhong, et al., 2010	
Baishui Glacier, Hengduan, China	2.8		4500	26°00'N	13 May-6 Jun 2009	Xianzhong, et al., 2010	
Baishui Glacier, Hengduan, China	4.6		4600	26°00'N	5 May - 6 Jun 2009	Xianzhong, et al., 2010	
Baishui Glacier, Hengduan, China	5.2		4700	26°00'N	13 May-6 Jun 2009	Xianzhong, et al., 2010	
Baishui Glacier, Hengduan, China	5.8		4800	26°00'N	13 May - 6 Jun 2009	Xianzhong, et al., 2010	
Dokriani Glacier, Himalaya	5.9		4000	31°45' N	4 Jun-6Jun 1995	Singh and Kumar, 1996	Hock, 2003
Dokriani Glacier, Himalaya	5.7	7.4	4000	31°45' N	4 days (1997-98)	Singh et al., 2000a,b	Hock, 2003
Glacier AX010, Himalaya	7.3	8.1	4956	27°45' N	Jun-Aug 1978	Kayastha et al., 2000a	Hock, 2003
Glacier AX010, Himalaya	8.7	8.8	5072	27°45' N	Jun-Aug 1978	Kayastha et al., 2000a	Hock, 2003
Glacier AX010, Himalaya	***11.6***		5245	27°45' N	1 Jun-31 Aug 1978	Kayastha et al., 2000a	Hock, 2003
Khumbu Glacier, Himalaya		16.9	5350	28°00'N	21 May-1 Jun 1999	Kayastha et al., 2000b	Hock, 2003
Rakhiot Glacier, Himalaya		6.6	3350	35°22'N	18 Jul-6 Aug 1986	Kayastha et al., 2000b	Hock, 2003
Yala Glacier, Himalaya		9.3	5120	28°14'N	1 Jun-31 Jul 1996	Kayastha, 2001	Hock, 2003
Yala Glacier, Himalaya		10.1	5270	28°14'N	1 Jun-31 Jul 1996	Kayastha, 2001	Hock, 2003
Central Asia means:	*5.4±2.3*	*7.9±3.6*					
Non-glaciated Sites							
Location	Snow	Ice	Elevation	Latitude	Duration	Reference	Cited in
Gooseberry Creek, Utah, USA	2.5		2650	~38°N	23 Apr-9 May 1928	Clyde, 1931	Hock, 2003
Weissfluhjoch, Switzerland	4.5		2540	46°48'N	Snowmelt season	Zingg, 1951	Hock, 2003
3 basins in USA	2.7				Several seasons	C. of Engineers, 1956	Hock, 2003
3 basins in USA	4.9				Several seasons	C. of Engineers, 1956	Hock, 2003
Former European USSR	5.5	7	1800-3700			Kuzmin, 1961, p. 117	Hock, 2003
12 sites in Finland	3.9			~60-68°N	1959-1978	Kuusisto, 1980	Hock, 2003
Non-glaciated site means:	*4.0±1.2*	*7.0*					
Mean meltfactor for all examples in the literature:	***4.5±1.7***	***7.7±3.2***					

2.9.3 Discussion of terminal moraine assumptions

In order to support our assumption that terminal moraines can form during advances driven by interannual variability without long term terminus standstills (< 50 years; a time scale supported by flowline modeling (see Roe, 2011 Fig. 4)), we present a review of the moraine sedimentological literature (Table 2.6), which shows that the majority of moraines with constrained formation periods form over periods less than 50 years. The development of a universal model for the timescale of moraine formation has been hampered by the complexity of formational processes, the abundance of unconstrainable variables and initial conditions. But it is important to note that all moraine formation timescales found in the literature were less than 50 years. The length of time needed to form terminal moraines is dependent on the process of formation and can be constrained only crudely. Ice marginal indicators are typically divided into glaciotectonic, push, hummocky, drop moraines, and ice-contact fans but composite moraines are common (Benn and Evans, 1998). For the purposes of justifying the short timescale of ice marginal deposit formation (<50 years), we further divide the indicators into those that are independent of terminus standstills (glaciotectonic, push and hummocky moraines) and those that are dependent on terminus standstills (drop moraines and ice-contact fans). Note the dominance of push moraines in the table. The authors made no attempt to bias the type of moraines presented in this table. Rather more research has been focused on push moraines or push moraines are more common. We use the broad, continuum definition of push moraines used in Bennett (2001).

Table 2.6 TABLE COMPILATION OF MORAINE FORMATION TIMES.

Region	Time period	Type	Sub-Category	Formation Time	Height	Reference
Moraines independent of terminus standstills						
Argentina	Modern	Glaciotectonic	Folding and Thrusting	<13 years	15-50m	Glasser & Hambrey, 2002
Svalbard	Modern	Push	Surge	Likely <5yrs	30-40m	Boulton et al., 1999
Svalbard	LIA	Push	Englacial thrusts		45m	Hambrey & Huddart, 1995
Chile	Neoglacial	Push	Formed of subglacial clasts		20-40m	Glasser et al., 2006
Svalbard	Neoglacial	Thrust	Melt out thrust	Formed upon retreat	40m	Bennett et al., 1996
Iceland	LIA	Glaciotectonic	Fold and thrust	2-6 days	10-40m	Benediktsson et al., 2010
Baffin I., Canada	Neoglacial	Push	Pushed outwash gravels	1 yr	40m	Boulton et al., 1986
Iceland	LIA	Push	Single large nappe and faulting	<39 likely 1 or 2 yrs	8m, 35m	Bennett et al., 2004
Svalbard	LIA	Push/Thrust	Surge	<1 yr	>30m	Hart & Watts, 1997
Svalbard	LIA	Ice Cored	Retreating from LIA maximum	Formed upon retreat	25-30m	Lysså & Lønne, 2001
Iceland	LIA	Glaciotectonic	Fold and thrust	12 yrs at terminus	25-30m	Bennett et al., 2000
Norway	Modern	Push?	2 year advance	2 years	20m	Benedict et al., 2013
Svalbard	LIA	Push	1882/1886 Surge	<1 yrs	1-20m	Boulton et al., 1996
New Zealand	LGM	Push/Thrust		Likely <30 yrs	10-15m	Hart, 1996
Iceland	Modern	Push	Imbricate	1 yr	1-10m	Humlum, 1985
Alaska	Modern	Push		Sustained adv.	10m	Motyka & Echelmeyer, 2003
Norway	LIA/ modern	Push	Bulldozing and thrusting	1-10 yrs	3-8m	Burki et al., 2009
Yukon,Canada	LIA/ modern	Ice Cored	Debris thickness reported		1-6m	Johnson, 1972
Iceland	Modern	Push	Polygenetic push	Seasonal	.4-5.25m	Sharp, 1984
Iceland	LIA	Push/Thrust	1890 Surge	1 day	5m	Benediktsson et al., 2008
Iceland	Modern	Push	Annual moraines	Seasonal	4m	Sharp, 1984
Iceland	Modern	Push/Basal Freezing		1 year	3.5-4m	Krüger, 1993
Iceland	Modern	Push		1 year	3.5m	Krüger, 1993
Norway	Modern	Push	From six separate glaciers	1 year sustained adv	1-3m	Winkler & Matthews, 2010
Alaska	Modern	Ice Cored/ Push	Readvance in a surging glacier	1 year	3m	Johnson, 1971
Iceland	Modern	Ice Cored	Debris thickness reported	1 year	1-3m	Krüger & Kjær, 2000
Argentina	Modern	Push		1 yr	2.5m	Rabassa et al., 1979
Iceland	Modern	Push		Seasonal	1-2m	Boulton, 1986
Switzerland	Modern	Push	Annual winter advances	Seasonal	<1.5m	Lukas, 2012
Norway	Modern	Push	Annual winter advances	Seasonal	<1m	Benedict et al., 2013
Iceland	Modern	Push	Lodgement freeze on	Seasonal	.3 -.7m	Krüger, 1995
New Zealand	Modern	Ice Cored	Debris thickness reported	1-2 years	.4m	Brook & Paine, 2011
Region	Time period	Type	Sub-Category	Formation Time	Height	Reference
Moraines dependent on terminus standstills						
Colorado, USA	LGM	Ice Contact Fan	Debris flow and alluvium	<20 years	25m	Johnson and Gillham, 1995
France	LIA	Ice Contact Fan/Dump	Formed over 3 advances	~10 years	20m	Nussbaumer & Zumbühl, 2012
Scotland, UK	Younger Dryas	Ice Contact Fan/push	Debris flow and alluvium	3-9 or 7-19 years	15m	Benn & Lukas, 2006
Iceland	Modern	Ice Contact Fan	Outwash fans/ sandar	<10years	10m	Boulton, 1986
Iceland	Modern	Dump/push	Initially push	7 years sustained adv.	4-7m	Krüger et al., 2002

* LIA refers to the Little Ice Age
** LGM refers to the Last Glacial Maximum

2.9.3.1 Moraines independent of glacial standstills

The most rapidly forming moraines require the propagation of debris in front of an advancing ice front (e.g. Krüger, 1995; Benediktsson, et al., 2010; Benediktsson et al., 2008; Boulton, 1986; Humlum, 1985). Because the material is bulldozed or thrust in front of the glacier, the moraine can form during any advance and retreat cycle irrespective of time spent in standstill. The formation of glaciotectonic and push moraines is more dependent on the availability of sediment or permafrost in the foreland than it is on the glaciological conditions (Bennett, 2001). *Glaciotectonic Moraines* are formed when the stress imposed by an advancing glacier excavates and elevates (associated with thrusting and folding) proglacial bedrock and/or quaternary sediments. *Push Moraines* are formed by the bulldozing of proglacial sediment and typically have steep proximal and gentle distal slopes. Advances over long distances can result in formation of a more extensive set of moraine ridges. *Hummocky and ice-cored moraines* form when heavily debris-covered ice is dynamically separated from an active, retreating glacier (Lyså and Lonne, 2001). As these moraines are in place as soon as the ice is dynamically separated from the active glacier, all that remains is for the ice core to waste away. Ice-cored and hummocky moraines do not require a glacial standstill to form (Glassner and Hambrey, 2002; Johnson, 1972) and their identification in the moraine record implies that the moraine was emplaced instantaneously for the timescales of interest for this study.

2.9.3.2 Moraines dependent on glacial standstills

Latero-frontal fans and dump moraine sizes are dependent on the debris flux off the glacier and the length of time the glacier terminus remains stationary. A glacier that advances and retreats without a terminus standstill will not likely form an ice-contact fan or a dump moraine, although there are reported occurrences in the literature. One of these potential

influences is thick supraglacial debris-cover, which can slow terminus oscillations and provide the debris fluxes to create large moraines. *Ice-contact fans* form by the coalescence of debris fans and glaciofluvial processes at the glacier terminus. Although latero-frontal fans can form over short periods and even in a single short-lived advance, these fans are typically on the order 10 meters in height whereas fans that limit subsequent ice advances are typically 100s of meters in height (Benn and Lukas, 2006; Benn and Evans, 1998). *Dump Moraines* are formed by the delivery of supraglacial material derived from rockfall onto the glacier or the melt out of basal debris septa that flows or falls off the terminal ice slope. Paleoglacier valleys with large ice-contact fans (>100 m in height) or dump moraines should be treated with more caution than moraines that are independent of glacial standstills. Nearly all documented terminal moraine formation durations are less than 20 years (Table 2.6). Further sedimentological and stratagraphic investigation of LGM terminal moraines is needed to constrain the importance of moraine formation timescale on paleoclimate reconstruction (e.g., Johnson and Gillam, 1995).

2.9.3.3 Terminal moraines do not limit subsequent advances

We have assumed that the furthest length excursion from the mean glacier length forms the maximum terminal moraine. In effect, this requires that that previously formed moraines do not limit the extent of subsequent advances. The only moraine types that have been shown to limit subsequent advances are large latero-frontal moraines or scree aprons; these are common in tectonically active regions such as the Himalaya or the Andes. These moraines can become sufficiently massive to dam glacier ice and cause subsequent glacial advances to terminate at the same location (Lliboutry, 1977; Thorarinsson, 1956). This effect is especially apparent where large lateral moraines are deposited outside of cirques and steep valleys and are therefore less susceptible to paraglacial processes (Thorarinsson, 1956). Cases where latero-terminal moraines

could have limited ice extent are easily identifiable by the height and extent of the latero-frontal moraines. These situations are uncommon in LGM terminal moraines in the Western US.

2.9.3.4 Overridden terminal moraines are destroyed

Moraines can be overrun by subsequent advances and still be identifiable upon retreat (Karlén, 1973; Bennett et al., 2000). Overrun moraines may be differentiated from moraines that haven't been overrun by their subdued topography compared to moraines down valley, the presence of fluted till overriding the moraine, and the presence of lateral continuations of the moraine that have not been overridden that exhibit a sharper morphology (Karlén, 1973). Preservation of overrun moraines is rare and the potential for preservation depends on the local bedrock topography and the amount of time the overrun moraine is subjected to subglacial processes. An overrun moraine could potentially pose a problem for paleoclimatic or mean glacial length reconstruction only if a moraine is overrun and there is no indication of the maximum extent of the overriding glacier. The overrun moraine would then be interpreted as the maximum extent of the glacier for the time period of interest and could produce substantial error. This situation is unlikely for LGM moraines, as any overrun moraine would have been smoothed by the overriding glacier and then subjected to at least 10 thousand years of diffusional surface process that would further obliterate the morainal form.

2.9.4 LGM moraine complexes

LGM 'terminal moraines' in the western US are often composed of a conglomeration of moraines formed during numerous glacier advances. We call these clusters of moraines, terminal moraine complexes keeping in mind that it is possible that these clusters of ridges were formed by a single advance and the individual moraines interpreted as terminal moraines are actually fault bend folds from a glaciotectonic push moraine. Below in figure 2.4 we present a LiDAR hillshade of the Teton Glacier LGM terminal moraine and our interpretation of distinct terminal

moraines and the subjective limits of the terminal moraine complex. This hillshade allows us to define many more ice marginal features than possible without detailed field surveys. The terminal moraines defined in figure 2.4 are likely formed between the LGM mean length and the maximum terminal moraine (labeled 1) and are therefore likely candidates for moraines formed by glacier length fluctuations driven by interannual variability.

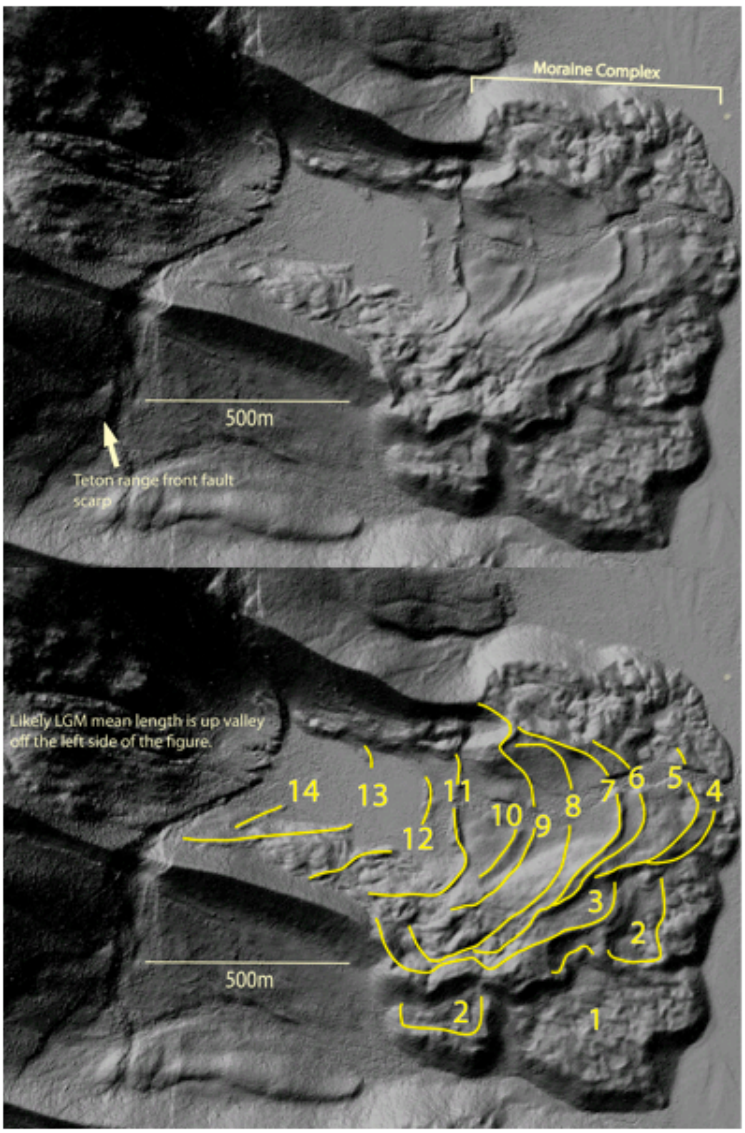

Figure 2.4 LiDAR of the LGM Teton glacier terminal moraines. In the bottom panel we show what we interpret to be 14 distinct ice margins revealed by the LiDAR. The LiDAR is courtesy of OpenTopography.

2.9.5 Relative sensitivity due to temperature and precipitation variability

Roe and O'Neal (2009) show that the relative sensitivity of a glacier's fluctuations to temperature vs. precipitation variability is given by:

$$R = \frac{A_{T>0}\mu\sigma_T}{A_{tot}\sigma_P} \quad . \tag{2.4}$$

The R values for Front Range glaciers greater than 4 km^2 range between 2.2 and 2.9 with a mean of 2.5, suggesting that year-to-year variations in summer temperature were two to three times as important for driving length perturbations as were variations in annual precipitation. This dominant sensitivity to summertime temperature variation is expected in continental climates.

2.9.6 Flowline model description

We follow standard equations for the shallow-ice-approximation incorporating glacier sliding (e.g., Oerlemans, 2001):

$$\frac{dH(x)}{dt} = \dot{b}(x) - \frac{dF(x)}{dx};\ F(x) = \rho^3 g^3 \left(f_d H(x)^2 + f_s \right) H(x)^3 \left(\frac{dz_s}{dx} \right)^3, \tag{2.5}$$

where $H(x)$ is ice thickness at position x, $\dot{b}(x)$ is the local net mass balance, $F(x)$ is the depth-integrated ice flux, ρ is ice density, g is the acceleration due to gravity, dz_s/dx is the local ice surface slope, f_d = 1.9 x 10^{-24} Pa^3 s^{-1} and f_s = 5.7 x 10^{-20} Pa^3 m^2 s^{-1} (the coefficients of deformation and sliding).

2.9.7 Model discussion

By exploring a very wide parameter space, we have constrained the effects of interannual variability on glacial length and moraine formation over extreme bounds. The range of parameter uncertainty could be better constrained by examining how the climate parameters vary in space from the LGM to the present. The most uncertain climate parameters, Γ, σ_P, and σ_T, could be better constrained by using atmospheric circulation model output, and better minimum estimates

of D could be obtained by reducing the uncertainty in moraine-derived dates. It should also be determined if using higher order ice physics models changes the effects of interannual variability on glacier length, although we anticipate that parameter uncertainty will swamp any differences between models. In the climate forcing presented here, we have assumed that T and P are uncorrelated from year-to-year (white noise), as is generally the case for centennial-scale instrumental observations of T and P and glacier mass balance records (e.g., Burke and Roe, 2013); on longer time-scales, paleoclimate records show that a degree of persistence (correlation from year-to-year) does exist (e.g., Huybers and Curry, 2006). Even a small degree of persistence can substantially increase the magnitude of fluctuations (e.g. Reichert et al., 2001). For this reason and others outlined in Roe and O'Neal (2009), we feel that our estimates of the fluctuation of glacier length about the mean length are conservative.

2.9.8 Explanation of Interannual Variability

Interannual climate variability refers to changes in the mean value of climate parameters (air temperature, precipitation, etc.) from year-to-year. Think of last year's mean summer temperature compared to this year's mean summer temperature (same can be done for total winter precipitation or annual precipitation). The variation from one year to the next is what we refer to as interannual variability. When long records of mean summer temperature (or annual precip) are tested for year-to-year correlation (if we have a warm summer relative to the long term mean this year are we more likely to have a warm summer next year?) there is little evidence of correlation (Burke and Roe, 2013). Interannual records of summer temperature show very little or no correlation from one year to the next and are best represented as white noise (equal power at all frequencies). The change in weather from year-to-year is not considered a climate change so glacier fluctuations forced by interannual variability are independent of

climate change.

2.9.9 References for supplementary material

Anderson, B.M., 2004, The response of "Ka Roimata o Hine Hukatere" Franz Josef Glacier to climate change [Ph.D. Thesis]: Christchurch, University of Canterbury, 106 p.

Anderson, B.M., Lawson, W., Owens, I., and Goodsell, B., 2006, Past and future mass balance of "Ka Roimata o Hine Hukatere" Franz Josef Glacier, New Zealand: Journal of Glaciology, v. 52, no. 179, p. 597–607, doi: 10.3189/172756506781828449.

Anslow, F.S., Hostetler, S., Bidlake, W.R., and Clark, P.U., 2008, Distributed energy balance modeling of South Cascade Glacier, Washington and assessment of model uncertainty: Journal of Geophysical Research, v. 113, no. F2, p. F02019, doi: 10.1029/2007JF000850.

Arendt, A., and Sharp, M., 1999, Energy balance measurements on a Canadian high arctic glacier and their implications for mass balance modelling: IAHS Publication, 165-172.

Benediktsson, Í.Ö., Möller, P., Ingólfsson, Ó., Van der Meer, J.J.M., Kjær, K.H., and Krüger, J., 2008, Instantaneous end moraine and sediment wedge formation during the 1890 glacier surge of Brúarjökull, Iceland: Quaternary Science Reviews, v. 27, no. 3-4, p. 209–234, doi: 10.1016/j.quascirev.2007.10.007.

Benediktsson, Í.Ö., Schomacker, A., Lokrantz, H., and Ingólfsson, Ó., 2010, The 1890 surge end moraine at Eyjabakkajökull, Iceland: a re-assessment of a classic glaciotectonic locality: Quaternary Science Reviews, v. 29, no. 3-4, p. 484–506, doi: 10.1016/j.quascirev.2009.10.004.

Benn, D. I., and Evans, D. J., 1998, Glaciers and glaciation: London. Edward Arnold. 734 p.

Benn, D.I., and Lukas, S., 2006, Younger Dryas glacial landsystems in North West Scotland: an assessment of modern analogues and palaeoclimatic implications: Quaternary Science Reviews, v. 25, no. 17-18, p. 2390–2408, doi: 10.1016/j.quascirev.2006.02.015.

Bennett, M.R., 2001, The morphology, structural evolution and significance of push moraines: Earth-Science Reviews, v. 53, no. 3-4, p. 197–236, doi: 10.1016/S0012-8252(00)00039-8.

Bennett, M., Huddart, D., Hambrey, M.J., and Ghienne, J.F., 1996, Moraine development at thehigh-arctic valley glacier Pedersenbreen, Svalbard: Geografiska Annaler. Series A, v. 78, no. 4, p. 209–222.

Bennett, M.R., Huddart, D., and McCormick, T., 2000, An integrated approach to the study of glaciolacustrine landforms and sediments: a case study from Hagavatn, Iceland: Quaternary Science Reviews, v. 19, no. 7, p. 633–665, doi: 10.1016/S0277-3791(99)00013-X.

Bennett, M., Huddart, D., Waller, R., Cassidy, N., Tomio, a, Zukowskyj, P., Midgley, N., Cook, S., Gonzalez, S., and Glasser, N., 2004, Sedimentary and tectonic architecture of a large

push moraine: a case study from Hagafellsjökull-Eystri, Iceland: Sedimentary Geology, v.172, no. 3-4, p. 269–292, doi: 10.1016/j.sedgeo.2004.10.002.

Benson, L., Madole, R., Landis, G., and Gosse, J., 2005, New data for Late Pleistocene Pinedale alpine glaciation from southwestern Colorado: Quaternary Science Reviews, v. 24, no. 1-2, p. 49–65, doi: 10.1016/j.quascirev.2004.07.018.

Bøggild, C., Reeh, N., and Oerter, H., 1994, Modelling ablation and mass-balance sensitivity to climate change of Storstrømmen, northeast Greenland: Global and Planetary Change, v. 9, p. 79–90.

Boulton, G., 1986, Push-moraines and glacier-contact fans in marine and terrestrial environments: Sedimentology, v. 33, p. 677–698.

Boulton, G.S., Van Der Meer, J.J.M., Hart, J., Beets, D., Ruegg, G.H.J., Van Der Waterer, Jarvis, J., 1996, Till and moraine emplacement in a deforming bed surge— An example from a marine environment: Quaternary Science Reviews, v. 15, no. 95, p. 961–987.

Boulton, G.S., Van Der Meer, J.J.M., Beets, D.J., Hart, J.K., and Ruegg, G.H.J., 1999, The sedimentary and structural evolution of a recent push moraine complex : Holmstrombreen, Spitsbergen: Quaternary Science Reviews, v. 18, p. 339–371.

Box, J., and Rinke, A., 2003, Evaluation of Greenland ice sheet surface climate in the HIRHAM regional climate model using automatic weather station data: Journal of Climate, v. 16, p.1302–1319.

Braithwaite, R.J., 1981, On glacier energy balance, ablation, and air temperature. Journal of Glaciology, v. 27, p. 381–391.

Braithwaite, R.J., and Zhang, Y., 2000, Sensitivity of mass balance of five Swiss glaciers to temperature changes assessed by tuning a degree-day model: Journal of Glaciology, v. 46, no. 152, p. 7–14.

Braun, M., and Hock, R., 2004, Spatially distributed surface energy balance and ablation modelling on the ice cap of King George Island (Antarctica): Global and Planetary Change, v. 42, no. 1-4, p. 45–58, doi: 10.1016/j.gloplacha.2003.11.010.

Brock, B.W., Mihalcea, C., Kirkbride, M.P., Diolaiuti, G., Cutler, M.E.J., and Smiraglia, C., 2010, Meteorology and surface energy fluxes in the 2005–2007 ablation seasons at the Miage debris-covered glacier, Mont Blanc Massif, Italian Alps: Journal of Geophysical Research, v. 115, no. D9, p. D09106, doi: 10.1029/2009JD013224.

Brook, M.S., and Paine, S., 2012, Ablation of Ice-Cored Moraine in a Humid, Maritime Climate: Fox Glacier, New Zealand: Geografiska Annaler: Series A, Physical Geography, v. 94, no. 3, p. 339–349, doi: 10.1111/j.1468-0459.2011.00442.x.

Brugger, K.A., 2010, Climate in the Southern Sawatch Range and Elk Mountains, Colorado, U.S.A., during the Last Glacial Maximum: Inferences using a simple degree-day model:

Arctic, Antarctic, and Alpine Research, v. 42, no. 2, p. 164–178, doi: 10.1657/1938-4246-42.2.164.

Brugger, K.A., 2007, Cosmogenic ^{10}Be and ^{36}Cl ages from Late Pleistocene terminal moraine complexes in the Taylor River drainage basin, central Colorado, USA: Quaternary Science Reviews, v. 26, no. 3-4, p. 494–499, doi: 10.1016/j.quascirev.2006.09.006.

Burki, V., Larsen, E., Fredin, O., and Margreth, A., 2009, The formation of sawtooth moraine ridges in Bødalen, western Norway: Geomorphology, v. 105, no. 3-4, p. 182–192, doi: 10.1016/j.geomorph.2008.06.016.

Buttstadt, M., Moller, M., Iturraspe, R., and Schneider, C., 2009, Mass balance evolution of Martial Este Glacier , Tierra del Fuego (Argentina) for the period 1960 – 2099: Advances in Geosciences, v. 22, p. 117–124.

Denby, B., and Greuell, W., 2000, The use of bulk and profile methods for determining surface heat fluxes in the presence of glacier winds: Journal of Glaciology, v. 46, no. 154, p. 445–452, doi: 10.3189/172756500781833124.

Gardner, A.S., Sharp, M.J., Koerner, R.M., Labine, C., Boon, S., Marshall, S.J., Burgess, D.O., and Lewis, D., 2009, Near-surface temperature lapse rates over Arctic glaciers and their implications for temperature downscaling: Journal of Climate, v. 22, no. 16, p. 4281–4298, doi: 10.1175/2009JCLI2845.1.

Glasser, N.F., and Hambrey, M.J., 2002, Sedimentary facies and landform genesis at a temperate outlet glacier: Soler Glacier, North Patagonian Icefield: Sedimentology, v. 49, no. 1, p. 43– 64, doi: 10.1046/j.1365-3091.2002.00431.x.

Glasser, N.F., Jansson, K., Mitchell, W. a., and Harrison, S., 2006, The geomorphology and sedimentology of the “Témpanos” moraine at Laguna San Rafael, Chile: Journal of Quaternary Science, v. 21, no. 6, p. 629–643, doi: 10.1002/jqs.1002.

Gosse, J.C., Klein, J., Lawn, B., Middleton, R., and Evenson, E.B., 1995, Beryllium-10 dating of the duration and retreat of the last Pinedale glacial sequence: Science (New York, N.Y.), v. 268, no. 5215, p. 1329–33, doi: 10.1126/science.268.5215.1329.

Grabiec, M., Budzik, T., and G!owacki, P., 2012, Modeling and hindcasting of the mass balance of Werenskioldbreen (Southern Svalbard): Arctic, Antarctic, and Alpine Research, v. 44, no. 2, p. 164–179.

Greuell, W., and Smeets, P., 2001, Variations with elevation in the surface energy balance on the Pasterze (Austria): Journal of Geophysical Research, v. 106, no. D23, p. 31717–31727.

Gümundsson, S., Björnsson, H., Palsson, F., and Haraldsson, H.H., 2003, Physical energy balance and degree-day models of summer ablation on Langjökull ice cap, SW-Iceland: National Power Company of Iceland.

Hambrey, M.J., and Huddart, D., 1995, Englacial and proglacial glaciotectonic processes at the snout of a thermally complex glacier in Svalbard: Journal of Quaternary Science, v. 10, p. 313–326.

Hanna, E., Huybrechts, P., Janssens, I., Cappelen, J., Steffen, K., and Stephens, A., 2005, Runoff and mass balance of the Greenland ice sheet: 1958–2003: Journal of Geophysical Research, v. 110, no. D13, p. D13108, doi: 10.1029/2004JD005641.

Hart, J.K., 1996, Proglacial glaciotectonic deformation associated with glaciolacustrine sedimentation, Lake Pukaki, New Zealand: Journal of Quaternary Science, v. 11, no. 2, p. 149–160, doi: 10.1002/(SICI)1099-1417(199603/04)11:2<149::AID-JQS227>3.0.CO;2-2.

Hart, J.K., and Watts, R.J., 1997, A comparison of the styles of deformation associated with two recent push moraines, South Van Keulenfjorden, Svalbard: Earth Surface Processes and Landforms, v. 22, no. 12, p. 1089–1107, doi: 10.1002/(SICI)1096-9837(199712)22:12<1089::AID-ESP804>3.0.CO;2-8.

He, X., Du, J., Ji, Y., Zhang, N., Li, Z., Wang, S., and Theakstone, W.H., 2010, Characteristics of DDF at Baishui Glacier No. 1 region in Yulong Snow Mountain: Journal of Earth Science, v. 21, no. 2, p. 148–156, doi: 10.1007/s12583-010-0013-4.

Hock, R., 2003, Temperature index melt modelling in mountain areas: Journal of Hydrology, v. 282, no. 1-4, p. 104–115, doi: 10.1016/S0022-1694(03)00257-9.

Hock, R., and Holmgren, B., 2005, A distributed surface energy-balance model for complex topography and its application to Storglaciären, Sweden: Journal of Glaciology, v. 51, no. 172, p. 25–36.

Hodgkins, R., Carr, S., Pálsson, F., Gu"mundsson, S., and Björnsson, H., 2013, Modelling variable glacier lapse rates using ERA-Interim reanalysis climatology: an evaluation at Vestari- Hagafellsjökull, Langjökull, Iceland: International Journal of Climatology, v. 33, no. 2, p. 410–421, doi: 10.1002/joc.3440.

Howat, I.M., Tulaczyk, S., Rhodes, P., Israel, K., and Snyder, M., 2006, A precipitation-dominated, mid-latitude glacier system: Mount Shasta, California: Climate Dynamics, v. 28, no. 1, p. 85–98, doi: 10.1007/s00382-006-0178-9.

Humlum, O., 1985, Genesis of an imbricate push moraine, Höfdabrekkujökull, Iceland: The Journal of Geology, v. 93, p. 185–195.

Johnson, M.D., and Gillam, M.L., 1995, Composition and construction of late Pleistocene end moraines, Durango, Colorado: GSA Bulletin, v. 107, no. 10, p. 1241–1253.

Johnson, P.G., 1971, Ice cored moraine formation and degradation, Donjek Glacier, Yukon Territory, Canada: Geografiska Annaler: Series A, Physical Geography, v. 53, no. 3/4, p. 198–202.

Johnson, P.G, 1972, A possible advanced hypsithermal position of the Donjek Glacier: Arctic, v. 25, n. 4, p. 302-305.

Karlén, W., 1973, Holocene glacier and climatic variations, Kebnekaise mountains ,Swedish Lapland: Geografiska Annaler., Series A, v. 55, no. A, p. 29–63.

Kayastha, R.B., Ageta, Y., Nakawo, M., Fujita, K., Sakai, A., and Matsuda, Y., 2003, Positive degree-day factors for ice ablation on four glaciers in the Nepalese Himalayas and Qinghai- Tibetan Plateau: Bulletin of glaciological research, v. 20,p. 7-14.

Kirkbride, M.P., 1995, Relationships between temperature and ablation on the Tasman Glacier, Mount Cook National Park , New Zealand Relationships between temperature and ablation on the Tasman Glacier , Mount Cook National Park , N: New Zealand Journal of Geologyand Geophysics, v. 38, p. 17–27.

Konya, K., Matsumoto, T., and Naruse, R., 2004, Surface heat balance and spatially distributedablation modelling at Koryto Glacier, Kamchatka peninsula, Russia: Geografiska Annaler: Series A, v. 86, no. 4, p. 337–348.

Krüger, J., 1993, Moraine-ridge formation along a stationary ice front in Iceland: Boreas, v. 22, no. 2, p. 101–109.

Krüger, J., 1995, Origin, chronology and climatological significance of annual-moraine ridges at Myrdalsjökull, Iceland: The Holocene, v. 5, no. 4, p. 420–427.

Krüger, J., and Kjær, K.H., 2000, De-icing progression of ice-cored moraines in a humid, subpolar climate, Kötlujökull, Iceland: The Holocene, v. 10, no. 6, p. 737–747, doi: 10.1191/09596830094980.

Krüger, J., Kjær, K.H., Van Der Meer, J.J.M., 2002, From push moraine to single-crested dump moraine during a sustained glacier advance: Norwegian Journal of Geography, no. 4, p. 37– 41.

Laabs, B.J.C., Marchetti, D.W., Munroe, J.S., Refsnider, K.A., Gosse, J.C., Lips, E.W., Becker, R.A., Mickelson, D.M., and Singer, B.S., 2011, Chronology of latest Pleistocene mountain glaciation in the western Wasatch Mountains, Utah, U.S.A.: Quaternary Research, v. 76, no. 2, p. 272–284, doi: 10.1016/j.yqres.2011.06.016.

Laabs, B.J.C., Plummer, M.A., and Mickelson, D.M., 2006, Climate during the last glacial maximum in the Wasatch and southern Uinta Mountains inferred from glacier modeling: Geomorphology, v. 75, no. 3-4, p. 300–317, doi: 10.1016/j.geomorph.2005.07.026.

Laumann, T., and Reeh, N., 1993, Sensitivity to climate change of the mass balance of glaciers in southern Norway: Journal of Glaciology, v. 39, no. 133.

Li, J., Liu, S., Zhang, Y., and Shangguan, D., 2011, Surface energy balance of Keqicar Glacier, Tianshan Mountains , China , during ablation period: Sciences in Cold and Arid Regions, v. 3, no. 3, p. 197–205, doi: 10.3724/SP.J.1226.2011.00197.

Licciardi, J.M., Clark, P.U., Brook, E.J., Elmore, D., and Sharma, P., 2004, Variable responses of western U.S. glaciers during the last deglaciation: Geology, v. 32, no. 1, p. 81, doi:

10.1130/G19868.1.

Lliboutry, L., Arnao, B.M., and Schneider, B., 1977, Glaciological problems set by the control of dangerous lakes in Cordillera Blanca, Peru. III Study of moraines and mass balances at Safuna: Journal of Glaciology, v. 18, no. 79, p. 275–290.

Lukas, S., 2012, Processes of annual moraine formation at a temperate alpine valley glacier: insights into glacier dynamics and climatic controls: Boreas, v. 41, no. 3, p. 463–480, doi: 10.1111/j.1502-3885.2011.00241.x.

Lyså, A. and Lønne, I., 2001, Moraine development at a small high-arctic valley glacier: Rieperbreen, Svalbard: Journal of Quaternary Science, v. 16, no. 6, p. 519–529, doi: 10.1002/jqs.613.

MacDougall, A.H., and Flowers, G.E., 2011, Spatial and temporal transferability of a distributed energy-balance glacier melt model: Journal of Climate, v. 24, p. 1480–1498, doi: 10.1175/2010JCLI3821.1.

Mair, D., Burgess, D.O., and Sharp, M.J., 2005, Thirty-seven year mass balance of Devon Ice Cap, Nunavut, Canada, determined by shallow ice coring and melt modeling: Journal of Geophysical Research, v. 110, no. F1, p. F01011, doi: 10.1029/2003JF000099.

Marshall, S.J., and Sharp, M.J., 2009, Temperature and Melt Modeling on the Prince of Wales Ice Field, Canadian High Arctic: Journal of Climate, v. 22, no. 6, p. 1454–1468, doi: 10.1175/2008JCLI2560.1.

Marshall, S., Sharp, M., Burgess, D.O., and Anslow, F.S., 2007, Near−surface temperature lapse rates on the Prince of Wales Icefield, Ellesmere Island, Canada: Implications for regional downscaling of temperature: International journal of ..., v. 398, no. September 2006, p. 385–398, doi: 10.1002/joc.

Mihalcea, C., Mayer, C., Diolaiuti, G., Lambrecht, A., Smiraglia, C., and Tartari, G., 2006, Ice ablation and meteorological conditions on the debris-covered area of Baltoro glacier, Karakoram , Pakistan: Annals of Glaciology, v. 43, no. 1894, p. 292–300.

Motyka, R.J., and Echelmeyer, K. a., 2003, Taku Glacier (Alaska, U.S.A.) on the move again: active deformation of proglacial sediments: Journal of Glaciology, v. 49, no. 164, p. 50–58, doi: 10.3189/172756503781830962.

Munroe, J.S., Laabs, B.J.C., Shakun, J.D., Singer, B.S., Mickelson, D.M., Refsnider, K. A., and Caffee, M.W., 2006, Latest Pleistocene advance of alpine glaciers in the southwestern Uinta Mountains, Utah, USA: Evidence for the influence of local moisture sources: Geology, v. 34, no. 10, p. 841, doi: 10.1130/G22681.1.

Nussbaumer, S.U., Nesje, A., and Zumbuhl, H.J., 2011, Historical glacier fluctuations of Jostedalsbreen and Folgefonna (southern Norway) reassessed by new pictorial and written evidence: The Holocene, v. 21, no. 3, p. 455–471, doi: 10.1177/0959683610385728.

Nussbaumer, S.U., and Zumbühl, H.J., 2011, The Little Ice Age history of the Glacier des Bossons (Mont Blanc massif, France): a new high-resolution glacier length curve based on historical documents: Climatic Change, v. 111, no. 2, p. 301–334, doi: 10.1007/s10584-011-0130-9.gsa 2013 schedule

Oerlemans, J., Kuhn, M., Obleitner, F., Palsson, F., Smeets, C.J.P.P., Vugts, H.F., and Wolde, J.D.E., 1999, Glacio-meteorological investigations on Vatnajökull, Iceland, summer 1996: An overview: Boundary Layer Meteorology, v. 92, p. 3–26.

Oerlemans, J., and Vugts, H., 1993, A meteorological experiment in the melting zone of the Greenland ice sheet: Bulletin of the American Meteorological Society, v. 74, no. 3, p. 355–365, doi: 10.1175/1520-0477(1993)074<0355:AMEITM>2.0.CO;2.

Oerlemans, J., Glaciers and Climate Change: Lisse, NL, Swets and Zeitlinger, 160 p.

Pellicciotti, F., Brock, B., Strasser, U., Burlando, P., Funk, M., and Corripio, J., 2005, An enhanced temperature-index glacier melt model including the shortwave radiation balance#: development and testing for Haut Glacier d'Arolla, Switzerland: Journal of Glaciology, v. 51, no. 175, p. 573–587, doi: 10.3189/172756505781829124.

Petersen, L., and Pellicciotti, F., 2011, Spatial and temporal variability of air temperature on a melting glacier: Atmospheric controls, extrapolation methods and their effect on melt modeling, Juncal Norte Glacier, Chile: Journal of Geophysical Research, v. 116, no. D23, p. D23109, doi: 10.1029/2011JD015842.

Phillips, F., and Zreda, M., 1997, Cosmogenic ^{36}Cl and ^{10}Be ages of Quaternary glacial and fluvial deposits of the Wind River Range, Wyoming: GSA Bulletin, v. 109, no. 11, p. 1453– 1463.

Porter, S.C., and Swanson, T.W., 2008, ^{36}Cl dating of the classic Pleistocene glacial record in the northeastern Cascade Range, Washington: American Journal of Science, v. 308, no. 2, p. 130–166, doi: 10.2475/02.2008.02.

Rabassa, J., Rubulis, S., & Suárez, J., 1979, Rate of formation and sedimentology of (1976–1978) push-moraines, Frías Glacier, Mount Tronador (41 10$ S; 71 53$ W), Argentina: Moraines and Varves, 65-79.

Reinardy, B.T.I., Leighton, I., and Marx, P.J., 2013, Glacier thermal regime linked to processes of annual moraine formation at Midtdalsbreen, southern Norway: Boreas, no. 1971, p. n/a–n/a, doi: 10.1111/bor.12008.

Roe, G.H., 2011, What do glaciers tell us about climate variability and climate change?: Journal of Glaciology, v. 57, no. 203, p. 567–578, doi: 10.3189/002214311796905640.

Roe, G.H., and O'Neal, M.A., 2009, The response of glaciers to intrinsic climate variability: observations and models of late-Holocene variations in the Pacific Northwest: Journal of Glaciology, v. 55, no. 193, p. 839–854, doi: 10.3189/002214309790152438.

Schildgen T.F., and Dethier D.P., 2000, Fire and ice: using isotopic dating techniques to interpret the geomorphic history of Middle Boulder Creek, Colorado. Geological Society of America Abstracts with Programs 32(7): 18.

Schneider, C., Kilian, R., and Glaser, M., 2007, Energy balance in the ablation zone during the summer season at the Gran Campo Nevado Ice Cap in the Southern Andes: Global and Planetary Change, v. 59, no. 1-4, p. 175–188, doi: 10.1016/j.gloplacha.2006.11.033.

Sharp, M., 1984, annual moraine ridges at Skalafellsjökull southeast Iceland: Journal of Glaciology, v. 30, no. 104, p. 82–93.

Six, D., Wagnon, P., Sicart, J.E., and Vincent, C., 2009, Meteorological controls on snow and ice ablation for two contrasting months on Glacier de Saint-Sorlin, France: Annals of Glaciology, v. 50, p. 66–72.

Steffen, K., and Box, J., 2001, Surface climatology of the Greenland ice sheet: Greenland Climate Network 1995–1999: Journal of Geophysical Research, v. 106, no. D24, p. 33951– 33964.

Strasser, U., Corripio, J., Pellicciotti, F., Burlando, P., Brock, B., and Funk, M., 2004, Spatial and temporal variability of meteorological variables at Haut Glacier d'Arolla (Switzerland) during the ablation season 2001: Measurements and simulations: Journal of Geophysical Research, v. 109, p. D03103, doi: 10.1029/2003JD003973.

Szafraniec, J., 2002, Influence of positive degree % days and sunshine duration on the surface ablation of Hansbreen, Spitsbergen glacier: Polish Polar Research, v. 23, no. 3, p. 227–240.

Thorarinsson, S., 1956, On the variations of Svinafellsjökull, Skaftafellsjökull and Kviarjökull in Oraefi: Jökull, v. 6, p. 1–15.

Van den Broeke, M.R., Smeets, C.J.P.P., and Van de Wal, R.S.W., 2011, The seasonal cycle and interannual variability of surface energy balance and melt in the ablation zone of the west Greenland ice sheet: The Cryosphere, v. 5, no. 2, p. 377–390, doi: 10.5194/tc-5-377-2011.

Van de Wal, R., 1992. Ice and climate. PhD Thesis, Utrecht University, 144 pp.

Ward, D.J., Anderson, R.S., Guido, Z.S., and Briner, J.P., 2009, Numerical modeling of cosmogenic deglaciation records, Front Range and San Juan mountains, Colorado: Journal of Geophysical Research, v. 114, no. F1, p. F01026, doi: 10.1029/2008JF001057.

Winkler, S., and Matthews, J. A., 2010, Observations on terminal moraine-ridge formation during recent advances of southern Norwegian glaciers: Geomorphology, v. 116, no. 1-2, p. 87–106, doi: 10.1016/j.geomorph.2009.10.011.

Worsley, P., and Alexander, M.J., 1976, Glacier and Environmental Changes. Neoglacial Data from the Outermost Moraine Ridges at Engabreen, Northern Norway: Geografiska Annaler. Series A, Physical Geography, v. 58, no. 1/2, p. 55, doi: 10.2307/520743.

Yong, Z., Shiyin, L., and Yongjian, D., 2007, Glacier meltwater and runoff modelling, Keqicar Baqi glacier, southwestern Tien Shan, China: Journal of Glaciology, v. 53, no. 180, p. 91–98, doi: 10.3189/172756507781833956.

Young, N.E., Briner, J.P., Leonard, E.M., Licciardi, J.M., and Lee, K., 2011, Assessing climaticand nonclimatic forcing of Pinedale glaciation and deglaciation in the western United States: Geology, v. 39, no. 2, p. 171–174, doi: 10.1130/G31527.1.

Zhang, Y., Liu, S., and Ding, Y., 2006, Observed degree-day factors and their spatial variationon glaciers in western China: Annals of Glaciology, v. 43, no. 1, p. 301–306.

Zumbühl, H.J., Steiner, D., and Nussbaumer, S.U., 2008, 19th century glacier representations and fluctuations in the central and western European Alps: An interdisciplinary approach: Global and Planetary Change, v. 60, no. 1-2, p. 42–57, doi: 10.1016/j.gloplacha.2006.08.005.

Chapter 3 Numerical modeling of debris-covered glaciers: transient effects of debris on the length and dynamics of valley glaciers

Leif S. Anderson[1] and Robert S. Anderson[1]

[1]*Institute of Arctic and Alpine Research, and Department of Geological Sciences, University of Colorado, Campus Box 450, Boulder, Colorado 80309, USA*

3.1 Abstract

Debris cover can significantly affect the length and dynamics of valley glaciers. However, the difficulty in measuring relevant variables such as ice thickness and sub-debris mass balance at the decadal scale limits documentation of the dynamic response of glaciers to debris cover. As a result, there is considerable uncertainty about how debris cover on glaciers will affect water resources in high relief settings and sea level rise. It is imperative that we create a conceptual framework that honors the effect of debris on ice dynamics. We developed a 2D long-valley shallow-ice approximation numerical glacier model modified with longitudinal coupling. The model allows transient feedbacks between englacial debris, surface debris, sub-debris melt, and ice dynamics. In our model simulations, we varied debris input from headwall sources while maintaining a steady climate, using parameters loosely designed to replicate Khumbu, Nepal, debris-covered glaciers. Model results replicate debris-cover surface velocity and debris thickness patterns from a range of Central Asian debris-covered glaciers.

Debris deposited on the glacier surface in the accumulation zone travels through the glacier to emerge in the ablation zone. Once on the glacier surface, debris is advected down glacier, and increases in thickness through the ablation zone. Debris reduces melt, leading to elongated glaciers. Even in steady state, debris reduces ice surface slopes, ice thickness

gradients, ice discharge gradients, and englacial velocities in the ablation zone. We show that debris thickness is dependent on debris emergence rates and the surface velocity field, while also providing a means to interpret debris thickness patterns on modern glaciers. Steady state glacier length is nonlinearly related to debris deposition rates. Glacier surfaces can become saturated with debris, at which point adding more debris to the glacier leads to insignificant changes in glacier length. Surface debris emerging near the terminus suppresses glacier-wide net melt more than debris emerging near the ELA. Ice thickness perturbations caused by emerging debris are diffused up the glacier leading to lower ice surface slopes and larger ice thicknesses up glacier of the debris covered reach.

3.2 Introduction

The effect of debris on glaciers is of intrinsic interest to the glaciological and glacial geologic communities. Debris cover can significantly lengthen glaciers, potentially effecting the interpretation of the moraine record. Debris cover also increases the volume of glaciers, which has important implications for water resources in arid environments. For example, most of the glacial ice in the Himalaya and Hindu Kush is preserved in glaciers with more than 20% debris cover (Scherler et al., 2011). Additionally, Himalayan debris-covered glaciers are not responding coherently to climate change: some Himalayan debris-covered glaciers are advancing, others are stationary, and some are retreating (Scherler et al., 2011). This highlights the importance of debris cover in understanding glacier retreat and global sea level rise (e.g., Raper and Braithwaite, 2006). Through this paper, we refer to *debris-covered glaciers* as any glacier with continuous debris cover across the full width of the glacier regardless of the percentage of the total glacier covered with debris (after Kirkbride, 2011).

Most recent work on debris-covered glaciers focuses on understanding the effect of debris cover on glacier mass balance, and has lead to important advances in our understanding of the insulating effects of debris on sub-debris melt rates (e.g., Reid and Brock, 2010; Nicholson and Benn, 2008). These studies tend to be limited in time and space because of the inherent difficulty and danger of collecting in-situ data on debris-covered glaciers. On the other hand, increasingly available remotely sensed data allows for efficient documentation of debris covered glacier extent, surface velocities, and ice thickness changes at a regional scale (e.g., Kirkbride, 1995; Scherler et al., 2011a; Scherler et al., 2011b; Bolch et al., 2008; Quincey et al., 2009). While this approach allows for broad documentation of glacier change it struggles to account for the processes driving the change and is often limited in temporal scope.

Because of the limitations of these approaches, feedbacks between debris-covered glacier mass balance and glacier dynamics have been difficult to quantify. Yet, a process-based approach to debris-ice dynamics feedbacks is a prerequisite for the development of rigorous theory of debris-covered glacier response to climate change. Numerical glacier models are logical tools for exploring feedbacks within debris-covered glaciers (e.g., Scherler et al., 2011; Konrad and Humphrey, 2000). These models couple debris-perturbed mass balance with ice physics, bridging the temporal and spatial gap between the previously mentioned approaches.

Debris-covered glacier models must connect ice physics to supraglacial debris-cover (e.g., Vacco et al., 2010, Naito, et al., 2000; Konrad and Humphrey, 2000; Konrad et al., 1999). Naito et al. (2000) used a one-dimensional shallow-ice-approximation model with supraglacial debris advection to simulate the response of the Khumbu Glacier, Nepal. With a constant climate and englacial debris concentration, the model simulated the formation of a large depression on the debris-covered tongue. Konrad and Humphrey (2000) used a 2-dimensional steady state

model with a constant surface slope to explore rock glacier dynamics. In their model, debris was deposited on the glacier surface below the equilibrium line altitude (*ELA*) and then advected along the glacier surface. With high rates of debris input, rock glaciers formed several-meter debris covers, which reduced sub-debris melt to zero, and resulted in infinite glacier lengths. The model demonstrated that in steady state debris cover decreases the vertical component of englacial velocity (w), leading to flow paths parallel to the horizontal component of ice velocity (u) (Konrad and Humphrey, 2000). These models highlight the importance of supraglacial debris cover distribution on the response of debris-covered glaciers.

However, in many debris-covered glacier systems supraglacial debris is largely deposited on the glacier surface in the accumulation zone by rockfalls, rock slides, or within avalanches from steep valley headwalls and sidewalls (e.g., Boulton and Eyles, 1979; Owen and Derbyshire, 1989; Benn and Owen, 2002; Benn et al., 2012). Debris deposited in the accumulation zone advects through the glacier until it melts out in the ablation zone; only there does it perturb the local mass balance. Debris advection through the glacier must therefore be accounted for in transient debris cover models. Only then can the feedbacks between englacial debris, supraglacial debris, melt, and glacier length be simulated.

We used a new fully transient 2-dimensional numerical model that tracks englacial debris advection, debris emergence, and supraglacial debris advection to explore the feedbacks within idealized debris-covered glaciers. We primarily focus on steady state results for simplicity and to lay the theoretical background for modeling the effect of climate change on debris-covered glaciers. Debris-covered glaciers are complicated: in addition to variable climate forcings and geometries they also respond to differing erosion rates and modes of debris entrainment. In order to capture a fraction of this diversity, we chose one constant climate state for our calculations but

allowed the debris deposition location and rate to vary on the glacier. In the model, debris deposition occurs only in the accumulation zone. Extreme erosion rates (both high and low) represent a wide range of erosional regimes.

In this paper, we compare the results of bare-ice models with results from models incorporating debris under the same climate forcing to isolate the effect of debris on glacial length and dynamics. We first describe the numerical model set up, parameters, and assumptions. Second, we present results of glaciers in steady state with a constant debris deposition rate in the accumulation zone. This is followed by a presentation of the transient response of the modeled glacier to a step change increase in the debris deposition rate. Third, we provide explanations for the results in the previous sections. Last, we discuss the implications of this work and place in context with real debris-covered glaciers.

3.3 Methods: Theory and Numerical Methods

We developed a two-dimensional finite difference numerical model (in x and z) that simulates the transient evolution of temperate valley glaciers. The model tracks the advection of debris through and on the glacier surface. This allows us to simulate transient feedbacks between debris cover, sub-debris melt, ice dynamics, and climate change. Forced by a time series of ELAs and a prescribed mass balance gradient, the model calculates ice surface elevations above a longitudinal profile by solving equations for ice flux and mass conservation. The modeled longitudinal path represents the glacier centerline. A number of authors have used the shallow-ice-approximation and basal sliding parameterizations in numerical glacier models (e.g., Nye 1965; Budd and Jensen (1975); Oerlemans 1986; Kessler et al., 2006). We used a similar approach, but also included a longitudinal stress coupling parameterization (Marshall et al., 2005). The model is efficient, allowing for a wide exploration of parameter space over millennia.

3.3.1 Conservation of ice mass

Mass conservation is at the core of the ice physics model. Assuming uniform ice density, and ignoring variations in the width of the glacier, conservation of ice requires that

$$\frac{\partial H}{\partial t} = \dot{b} - \frac{\partial Q}{\partial x} \tag{3.1}$$

where H is the local thickness of the glacier, and $\dot{b}$ is the local specific balance. Here Q is the specific volume discharge of ice [=] $m^3/m/yr$.

3.3.2 Annual surface mass balance of ice without the effects of debris

Glacier surface mass balance links climate to glacier response. We ignore mass change from englacial and subglacial sources, and use a simple mass balance scheme, which limits the number of parameters while also honoring the fundamentals of valley glacier mass balance.

3.3.3 Annual surface mass balance

Our mass balance scheme combines surface accumulation and ablation into a single thresholded linear mass balance as a function of elevation:

$$\dot{b}_z = \min\left(\frac{d\dot{b}_z}{dz}(Z_{ice} - ELA), \dot{b}_z^{\max} \right) \tag{3.2}$$

in which $\frac{d\dot{b}_z}{dz}$ is the mass balance gradient with elevation, Z_{ice} is the ice surface elevation, the ELA is the long term average of the elevation of zero net mass balance, and $\dot{b}_z^{\max}$ is the prescribed maximum mass balance that accounts for the depletion of moisture available for precipitation at higher elevations. These parameters reproduce the general characteristics of measured mass balance profiles from glaciers in the Khumbu region, Himalaya (Wagnon et al., 2014). In the calculations shown here we used values for the mass balance gradient ($\frac{d\dot{b}_z}{dz}$ = 7.5 m/yr/km), ELA (5000 m), and maximum mass balance ($\dot{b}_z^{\max}$ = 2 m/year). We assume that

supraglacial debris has no impact on mass balance in this parameterization. The following section describes our parameterization of the effect of supraglacial debris on $\dot{b}_z$.

3.3.4 Annual surface mass balance: effect of supraglacial debris

Sub-debris melt rate decreases non-linearly with increasing debris thickness (e.g. Østrem, 1959; Nicholson and Benn, 2008). For debris thicknesses less than ~2 cm, debris can increase melt rates relative to bare ice. For debris thicknesses greater than ~2 cm, debris suppresses sub-debris melt rates (e.g., Nicholson and Benn, 2008). The heat sink created by the debris layer buffers the sub-debris ice from the energy absorbed at the top of the debris, leading to a reduction in energy available for melt at the base of the debris layer. For simplicity, we neglect melt rate amplification due to debris thicknesses less than 2 cm thickness. We use an exponential debris thickness vs. melt rate curve:

$$\dot{b} = \dot{b}_z e^{\frac{-h_{debris}}{h_*}} \tag{3.3}$$

where $\dot{b}$ is the net mass balance including the effects of supraglacial debris, $\dot{b}_z$ is the prescribed mass balance profile not including the effects of debris (see equation 3.2), h_{debris} is the supraglacial debris thickness, and h_* is the e-folding length scale which defines pattern of melt fall off with increasing supraglacial debris (after Anderson, 2000; Vacco et al., 2010). While equation 3.3 is a simple empirical relationship between debris thickness and the local annual surface mass balance, more complicated energy balance schemes could easily be integrated into the model (e.g., Nicholson and Benn, 2008; Reid and Brock, 2010).

3.3.5 Ice flux

In this model, ice is transferred by internal ice deformation and sliding at the bed, and adjusted by longitudinal stress gradients. The ice flux down glacier is:

$$Q = H\bar{u} \tag{3.4}$$

in which H is the local ice thickness and $\bar{u}$ is the depth-averaged bed parallel velocity which results from the sum of the ice deformation velocity (modulated by variations longitudinal stress) and ice sliding velocity.

3.3.6 Deformation: shallow ice approximation

Within a glacier, ice deformation transports mass down slope. We use the shallow-ice-approximation where horizontal stress gradients are assumed negligible relative to vertical gradients of horizontal shear stress (e.g., Cuffey and Patterson, 2010). This assumption reduces the momentum balance equations to expressions for vertical shear stress as a function of the local ice surface slope and ice thickness. The depth-averaged horizontal velocity due to internal deformation, after Glen's flow law, is

$$\bar{u}_{def} = \frac{2\bar{\eta}}{n+2}(\rho_i g \alpha)^{n-1} H^n \tau_{bx}, \tag{3.5}$$

where A is the creep parameter, ρ_i the density of ice (we use 917 kg m^{-3} throughout the domain), g the acceleration due to gravity, α the local ice surface slope, H the local ice thickness, and τ_{bx} is the local basal shear stress. $\bar{\eta}$ is allowed to vary based on the local τ_{bx}, $\bar{\eta} = \frac{1}{2}\left[A\tau_E^{n-1}\right]^{-1}$ where we assume that $\tau_{E,}$ the effective stress, is approximated by the local τ_{bx} (after Cuffey and Patterson, 2010). We assume that all ice is temperate and therefore held at 0°C. A is therefore 24 x 10^{-25} [Pa^{-3} s^{-1}] (Cuffey and Patterson, 2010).

3.3.7 Sliding

In addition to internal deformation, temperate glaciers transfer mass via basal slip, which combines ice sliding over the bed with the deformation of the bed itself. We assume that all basal slip is accomplished by sliding over bedrock, and follow the formulation of Kessler et al. (2005):

$$U_{sliding} = U_c e^{1-\frac{\tau_c}{\tau_{bx}}}, \tag{3.6}$$

where U_c is a typical sliding velocity, τ_c is the gravitational driving stress that gives rise to the typical sliding velocity, and τ_{bx} is the gravitational driving stress in the *x*-direction. This sliding parameterization is not as sensitive to high τ_b values as many other sliding laws, and provides a more conservative estimate of sliding velocities when $\tau_b > \tau_c$ (Kessler et al., 2005).

3.3.8 Longitudinal stress coupling and the shapefactor

We have improved the shallow-ice-approximation equations with two modifications: 1) We include parameterizations of longitudinal stress coupling (after Marshall et al. (2005); Cuffey and Patterson (2010); and Kamb and Echlemeyer, 1986); and 2) We include a shapefactor, which includes the effect of valley wall drag. A detailed derivation of the longitudinal stress coupling parameterization is found in Marshall et al. (2005). Vertically averaged ice velocities are therefore based on

$$\bar{u} = U_{sliding} + \frac{2\bar{\eta}}{n+2}(\rho_{ice} g \alpha)^{n-1} H^n \tau_{bx}, \tag{3.7}$$

in which $\bar{\eta}$ is the effective viscosity, *n* is an empirically derived power law coefficient equal to 3, and τ_{bx} is the basal shear stress in the *x*-direction, including the effects of longitudinal coupling. τ_{bx} is defined as

$$\tau_{bx} = f\left(\rho g H \alpha + 4\bar{\eta}\frac{\partial^2 u}{\partial x^2} + 4\frac{\partial \bar{\eta} H}{\partial x}\frac{\partial u}{\partial x}\right), \tag{3.8}$$

in which f is the shapefactor. We use an f of 0.75 to approximate the effects of sidewall drag from a parabolic valley cross-section with the half-width 3 times the ice thickness (Cuffey and Patterson, 2010). This parameterization allows the local gravitational driving stress to be perturbed by compression or extension upstream and/or downstream. Note that the components of τ_{bx} can be separated to define terms for $\bar{u}_{def}$ and $u_{coupling}$ when combined with equation 3.7.

3.3.9 Coordinate transformation and ice velocities within the glacier

In order to calculate the englacial vertical velocity field, $w(x,z)$, we perform a coordinate transform in which each column of ice is divided into an equal number of cells, m. The thickness of each cell in a column of thick ice is larger than the thickness of each cell in a thinner portion of the glacier (Fig. 3.1). We solve for the vertical component of velocity using the continuity equation for an incompressible fluid, which in two dimensions (x,z) becomes:

$$\frac{\partial w}{\partial z} = -\frac{\partial u}{\partial x}. \tag{3.9}$$

Assuming no basal melt, w at the bed equals zero. We solve for the vertical velocity in each column by integrating vertically:

$$w = -\int_{o}^{z}\left(\frac{\partial u}{\partial x}\right)dz \ . \tag{3.10}$$

Solving equation 3.10 requires knowledge of the vertical profile of the horizontal velocity due to internal deformation, $u_{def}(z)$. We know the mean velocity in the x direction at any position x from equation 3.7. We define F, which converts $\bar{u}_{def}$ into an estimate of the vertical profile of $u_{def}(z)$ ($F = \frac{u(z)}{\bar{u}_{def}}$). $U_{\xi}(x,\xi)$ is the u velocity structure defined on a 2D grid (Fig. 3.1):

$$U_{\xi}(x,\zeta) = \bar{u}_{def}(x)F + u_{sliding}(x) + u_{coupling}(x) \tag{3.11}$$

where ζ is the non-dimensional height z/H and $u_{coupling}$ is the vertically-integrated velocity effect due to longitudinal stress coupling, determined by subtracting $\bar{u}_{def}$ from $\bar{u} - u_{sliding}$. F can alternatively be expressed as a fourth degree polynomial that relates the internal deformation profile shape to mean deformation speed:

$$F = (5(\zeta - 1.5\zeta^2) + \zeta^3 - \frac{1}{4}\zeta^4). \tag{3.12}$$

With the horizontal velocity *u(x,z)* in hand, we integrate equation 3.10 to solve for the vertical velocity *w(x,z)* field.

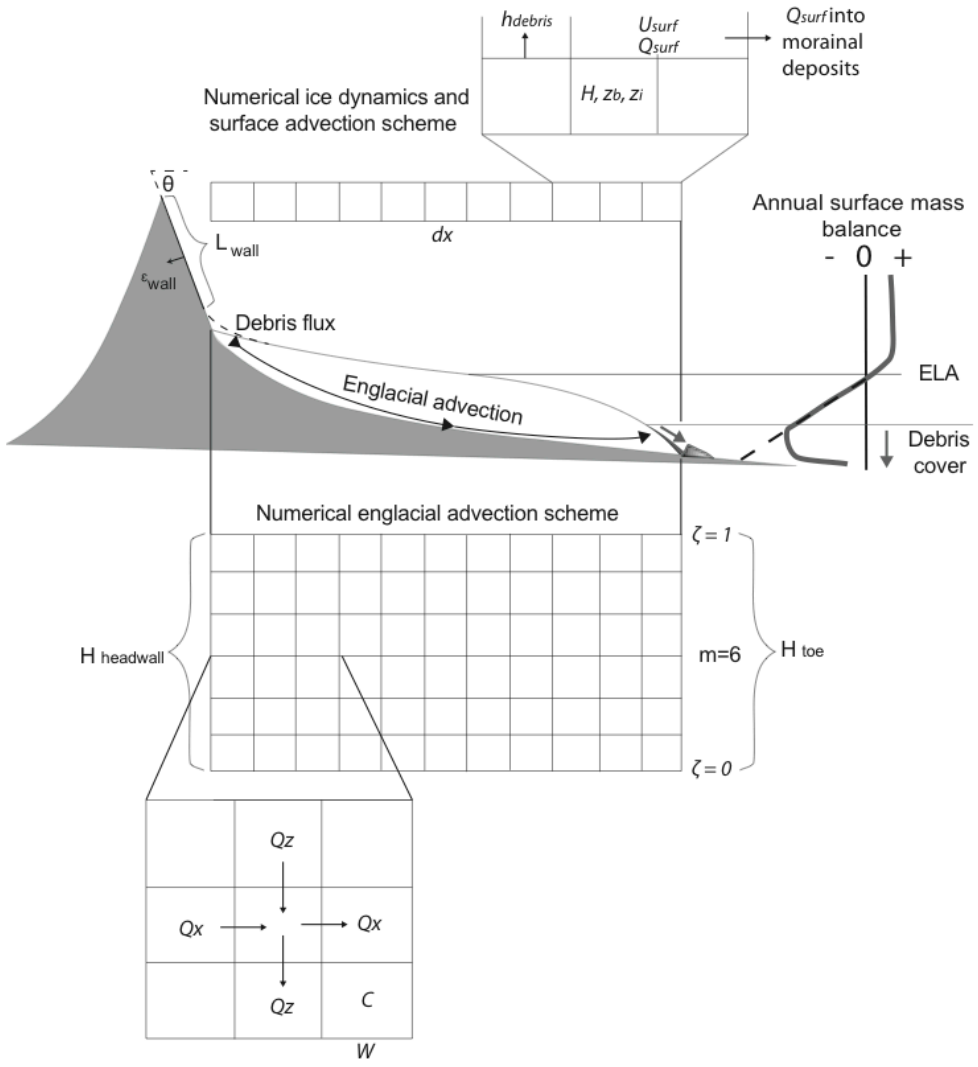

Figure 3.1 Schematic of the model set up. Debris eroded from the headwall or sidewalls is deposited on the glacier. Debris deposited on the glacier is either advected through the glacier and/or advected down the surface of the glacier. Debris is advected through the englacial environment using a 2D rectangular grid and coordinate transform. Ice physics and supraglacial debris advection is treated on a 1D grid.

3.3.10 Debris-related processes

In this model, debris is deposited on the glacier accumulation zone by rock fall (Fig. 3.1). The debris is then advected into and through the glacier until it melts out in the ablation zone. Debris that melts out forms a supraglacial debris layer that in turn perturbs the local mass balance. Supraglacial debris is advected toward the terminus until it is deposited in the proglacial environment as morainal material. In the following sections we discuss the differential equations and parameterizations used to model debris transport by englacial and supraglacial advection through temperate glaciers.

3.3.11 Debris source

Debris can be entrained in the glacier at either the upper glacier surface or at the glacier bed. Supraglacial debris deposition largely occurs by mass wasting from cliffs and hillslopes above glaciers, while sub-glacial debris entrainment occurs through regelation and net freeze-on. Basal debris emergence at the glacier surface is typically limited to the glacier toe and plays a minor role in the formation of extensive debris-covers (Benn and Evans, 2010). We focus on debris sourced from valley head and side walls for two reasons: 1) headwall erosion rates are better constrained than rates of subglacial debris entrainment (Messerli and Zurbuchen, 1968; Arsenault and Meigs, 2005; Heimsath and McGlynn, 2007; O'Farrell et al., 2008); and 2) rock falls and avalanches from head and sidewall cliffs are the primary processes of debris delivery onto many valley glaciers (Messerli and Zurbuchen, 1968 (European Alps from Humlum, 2000); Owens and Derbyshire, 1989 (Karakorum); Ballantyne and Harris, 1994; Humlum, 2000 (West Greenland); Benn and Owen, 2002 (Himalaya); Humlum, 2005 (Svalbard); Arsenault and Meigs, 2005 (Southern Alaska); O'Farrell et al., 2008 (Southern Alaska); Benn and Evans, 2010; Scherler et al., 2011 (Central Asia)). In high relief ranges such as the European Alps and

Himalaya, debris delivered by snow avalanching provides the primary source of debris to the glacial environment (e.g., Benn and Evans, 2010; Benn et al., 2012).

The model replicates the entrainment of debris onto the glacier surface and the advection of debris through the glacier. These processes combine to form the equivalent of *Ablation dominant* and *Avalanche-type* medial moraines on the modeled glacier surface (Benn and Evans, 2010). For simplicity, we neglect englacial thrusting and ice-stream interaction moraines (see Eyles and Rogerson, 1978; Anderson, 2000; Benn and Evans, 2010).

We assume that the rate of delivery of rocky debris to the glacier surface decays exponentially with distance from the headwall:

$$\dot{d} = D_{factor} \frac{\rho_{rock} H_{wall} \dot{\varepsilon}_{wall}}{\sin(\theta) x_*} e^{\frac{-x}{x_*}} = D_{factor} \dot{d}_0 e^{\frac{-x}{x_*}}, \qquad (3.13)$$

where $\dot{d}$ is the mass flux to the surface [=] M/L^{2}T, ρ_{rock} is the mean density of rock in the headwall, H_{wall} is the height of the headwall, $\dot{\varepsilon}_{wall}$ is the slope-normal erosion rate of the wall, θ is the headwall slope angle, x_* is a length scale characterizing the decline of debris delivery rate with distance from the headwall, D_{factor} is a debris delivery enhancement factor and $\dot{d}_0$ is the mass flux onto the glacier at the base of the headwall. The D_{factor} term combines the effects of varying H_{wall}, $\dot{\varepsilon}_{wall}$, θ, and the funneling effect of drainage basins on the headwall. Debris is deposited onto glaciers from sidewalls as well. In this case, we take $\dot{d}$=0< x_i, and $\dot{d} = D_{factor} \dot{d}_0 e^{\frac{-(x-x_i)}{x_*}}$ for x>x_i. The pattern of debris deposition presented in equation 3.13 is valid in cases where debris is delivered via rock falls and avalanches onto the glacier (e.g., Boulton and Eyles, 1979).

3.3.12 **Advection of englacial debris**

Debris deposited onto the glacier accumulation zone is advected into the glacier. Once embedded in the ice, debris concentration at a point will change only by straining of the ice. Taking the Eulerian point of view, the time rate of change of concentration of debris within a parcel of ice is:

$$\frac{\partial C}{\partial t} = -\frac{C}{h_\xi}\frac{\partial h_\xi}{\partial t} - \frac{uC}{h_\xi}\frac{\partial h_\xi}{\partial x} - \frac{\partial (wC)}{\partial z} - \frac{\partial (uC)}{\partial x}, \tag{3.14}$$

where C is the concentration of englacial debris [=] kg/m^3 and h_ξ is the cell height in a given ice column. The first term on the right hand side represents the rate of change of debris concentration due to strain of the ice in the vertical dimension. Note that if the strain rate is negative, signifying vertical thinning of an ice column, the concentration of the debris in the ice will increase. The second term represents the rate of change of debris concentration due to the change in cell height from one horizontal cell to the next cell down glacier. The third and fourth terms represent changes in concentration due to advection in the vertical and the horizontal directions, respectively.

The rock is added to the uppermost cells in the accumulation zone based on the annual rate of debris deposition on the glacier surface. $\dot{d}$ and the local annual positive mass balance $\dot{b}$ govern the englacial debris concentration in the cells nearest the glacier surface in the accumulation zone. Debris passed through the englacial environment to the top cells in the ablation zone is melted out based on the local surface melt rate and transferred to the supraglacial debris advection scheme.

3.3.13 Advection of debris on the glacier surface

We track both the melt-out of englacial debris and the advection of supraglacial debris on the glacier surface. The rate of change of debris thickness at a point on the glacier surface is defined by

$$\frac{dh_{debris}}{dt} = -\frac{C\dot{b}'}{(1-\phi)\rho_{rock}} - \frac{\partial u_{surf} h_{debris}}{\partial x}, \tag{3.15}$$

where h_{debris} is the mean debris thickness within a cell, and u_{surf} is the surface velocity of the glacier (after Naito et al., 2000; Konrad and Humphrey, 2000; Vacco et al., 2010). The first term captures the addition of debris to the surface layer from melt of debris-laden ice and is hereafter referred to as $\dot{\varepsilon}_{debris}$, the debris emergence rate. The second term represents the advection of debris down glacier.

Few studies have documented porosity, ϕ, in supraglacial debris. The range of porosity should be expected to vary widely depending on the sorting, grain size and geometry of individual supraglacial clasts. Supraglacial debris porosity may vary depending on debris thickness, as the percentage of fine material in supraglacial debris tends to increase as debris thickens (e.g., Owen et al., 2003). Most published studies assume constant values of ϕ for supraglacial debris, where the published values range from 0.2 to 0.45 based on a range of support from theoretical arguments to in-situ measurements (e.g., Nicholson and Benn, 2008; Conway and Rassmussen, 2000; Kirkbride and Warren, 1999; Bozhinskiy, et al, 1986). For this study we assume a constant ϕ of 0.3.

Near the terminus shallow-ice-approximation (*SIA*) models produce unrealistic surface velocities (Leysinger and Gudmundsson, 2004). The spike in velocities is caused by the dependence of the *SIA* on the local surface slope. Because the slope tends toward infinity at the terminus, surface velocities spike to unrealistic values. In order to correct for these unreasonable

velocities— which would produce unrealistic surface debris thicknesses near the glacier terminus— we find the lowest surface velocities in the ablation zone of the glacier and set the surface velocity to that number for the last few cells of the glacier.

3.3.14 Conservation of debris

The debris conservation is the core of the numerical advection scheme. The total debris mass within the system is tracked by summing all debris in the model:

$$M_{input} = M_{englacial} + M_{surf} + M_{moraine}, \tag{3.16}$$

where M_{input} is the total rock mass input to the system from the headwall, $M_{englacial}$ is the total mass in the englacial system, M_{surf} is the total debris mass resting on the surface of the glacier, and $M_{moraine}$ is the total mass deposited in the proglacial environment. We track these quantities in order to assure that debris is conserved (Fig. 3.2). In Figure 3.2, the 'total debris in the model' is the sum of the englacial, surficial, and proglacial debris. 'Total debris input' is the total amount of mass deposited on the glacier from headwall erosion over the course of the calculation. If 'Total debris in the model' equals 'total debris input' debris mass is conserved in the mode

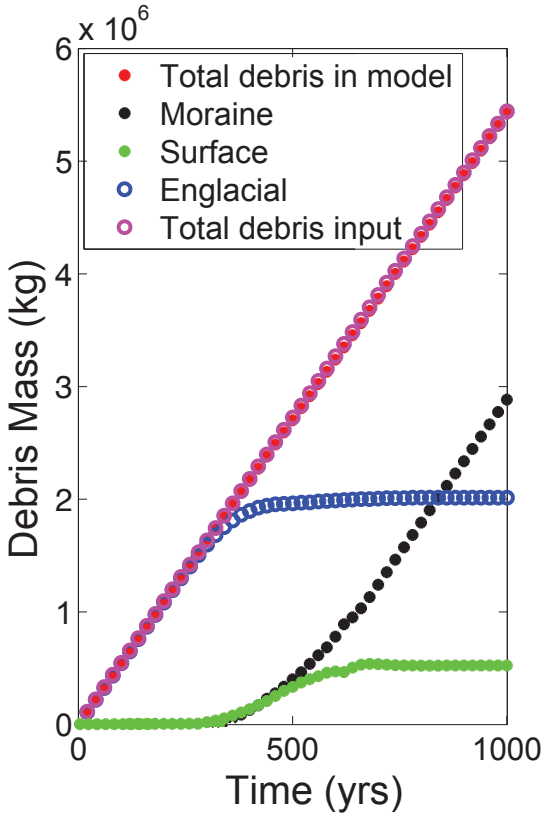

Figure 3.2 Example of model output demonstrating conservation of debris through time. The steady state debris-free glacier receives a step increase in debris input at time =0. The rate of debris input remains constant through time and for the first ~280 years all of the debris is englacial. After 280 years the englacial debris concentration asymptotes toward steady state as debris emerges in the ablation zone, and is deposited in the proglacial environment. Once the supraglacial debris mass has also reached steady state the rate of debris input equals the rate of debris deposition to the proglacial environment.

3.3.15 Numerics

We now describe the organization of the model. First, surface mass balance is calculated for both debris-free and debris-covered ice. Next, we use a forward centered difference scheme, in-time and in-space, for ice fluxes and hence $H(x,t)$. dt is the timestep for the ice physics-relevant calculations (dt =0.02 years). All ice columns are segmented into m heights (i.e. ζ = 0:(1/m):1). Advection schemes are performed every dt_{advect}, where is the timestep for the calculation of both englacial and supraglacial debris advection (dt_{advect} =0.1 years).

Advection schemes lacking correction diffuse numerically. To ensure that advected debris is not diffused numerically, we employ the two-step anti-diffusion correction scheme of Smolarkiewicz (1983). The two-step scheme works by calculating an anti-diffusion velocity from the velocities produced by the ice physics scheme described above. The anti-diffusion velocity is then used to transfer the diffused debris back to its original cells. A second corrective step based on the first iteration of anti-diffusion velocities is then used to correct the debris concentration and thickness again. We test advection scheme stability using the Courant-Friedrichs-Lewy (CFL) condition, which ensures that mass is not advected beyond adjacent cells in a single timestep. The maximum CFL number is checked in each timestep. Last, the mass conservation is checked before proceeding to the next iteration.

3.4 Results: Numerical Experiments

We present results that highlight the effects of debris on glacier length and glacier dynamics. We explore the effects of debris deposition rate, $\dot{d}_0$, and debris input location on the glacier. First, we show the advection of debris through a glacier with no supraglacial debris. Second, we show model calculations of debris-perturbed and debris-free glaciers at steady state (Sections 3.2). We then vary the debris deposition rate and the location of debris deposition and

present steady state results (Sections 3.3 and 3.4). We then show transient glacier length and response time results (Section 3.5). Last, we present the transient glacier response to debris addition in Section 3.6. We show changes in ice thickness, ice flux, surface debris thickness, and surface mass balance through time.

All calculations run on the same linear glacier bed profile. The model parameters were selected to loosely represent glaciers in the Khumbu Himalaya which are arguably the most well researched sub-set of debris-covered glaciers (e.g., Benn et al., 2012). The model is run with a basal slope of 5 %, based on an approximate surface slope of debris-covered glaciers in the Khumbu Himal (see Scherler, 2014). The maximum glacier bed elevation is 5200 m (Scherler, 2014). We use a baseline $\frac{d\dot{b}}{dz} = 0.0075$ yr^{-1} derived from nearby debris-free glaciers in the Khumbu region (Mera and Pokalde glaciers: after Wagnon et al., 2014). All model calculations presented below start with the same steady state debris-free glacier profile with a steady ELA at 5000 m.

Because changing the headwall height, slope, or erosion rate all have the same effect on the debris delivery to the glacier, we opt to use a single parameter to capture this, the debris factor, D_{factor}. A step change in $\dot{d}_0$ from zero to 1377 kg/yr times the D_{factor} is imposed at the start of each calculation. For $D_{factor} = 1$, the input rate is simply $\dot{d}_0$, which we base on a headwall that is 150 m tall, 60° from the horizontal that is eroding at a rate of 3 mm/yr. The debris factors explored are 1, 2, 3, 4, 5, 6, 8, 10, and 12 corresponding to $\dot{d}_0 * D_{factor} = 1377$, 2755, 4130, 5510, 6885, 8262, 11016, 13770, and 16525 kg/yr. We use $D_{factor} = 1$, 3, and 5 as our base parameter selection. Debris deposit location is also varied over six locations in the accumulation zone: 12, 30, 47, 65, 82, 100% from the headwall to the ELA, although most results are presented for the 12%, 47% and 100% debris deposition locations.

3.4.1 Background: advection through a steady glacier with no supraglacial debris

Each calculation starts with a steady state debris-free glacier to which a steady debris flux is added above the *ELA*. Debris advects through the glacier with no initial surface debris cover. Because the englacial velocity field controls englacial advection, we first present the steady state englacial velocity structure of our baseline, debris-free glacier as a control. In steady state, vertical velocities, w, at the glacier surface are equal in magnitude to the surface mass balance field. w decreases in magnitude to zero at the glacier bed (Fig. 3.3). The horizontal surface velocity field (u_{surf}) increases from the headwall to the *ELA* and then decreases again toward the glacier terminus. Englacial horizontal velocities decrease with depth. The slowest horizontal velocities in each ice column occur at the glacier bed (Fig. 3.4A).

Based on the field of englacial velocities, debris input at different locations in the accumulation zone will travel different englacial paths and will emerge at different times (Fig. 3.3). Debris deposited near the headwall is advected more deeply into the glacier than debris deposited near the ELA because of the large vertical speeds and low horizontal speeds near the headwall. Debris deposited near the ELA where vertical speeds are low and horizontal speeds are high leads to a shallow advection path and a short time in the englacial environment (Fig. 3. 3). Without any feedbacks between the surface debris cover and ice dynamics, debris deposited in the accumulation zone will emerge nearly symmetrically about the ELA following the englacial flowlines (Fig. 3.3). Once the co-evolution between supraglacial debris, ice dynamics, and englacial debris concentration is allowed, the internal velocity structure will be perturbed and the englacial debris concentration seen in Figure 3.3 will be altered

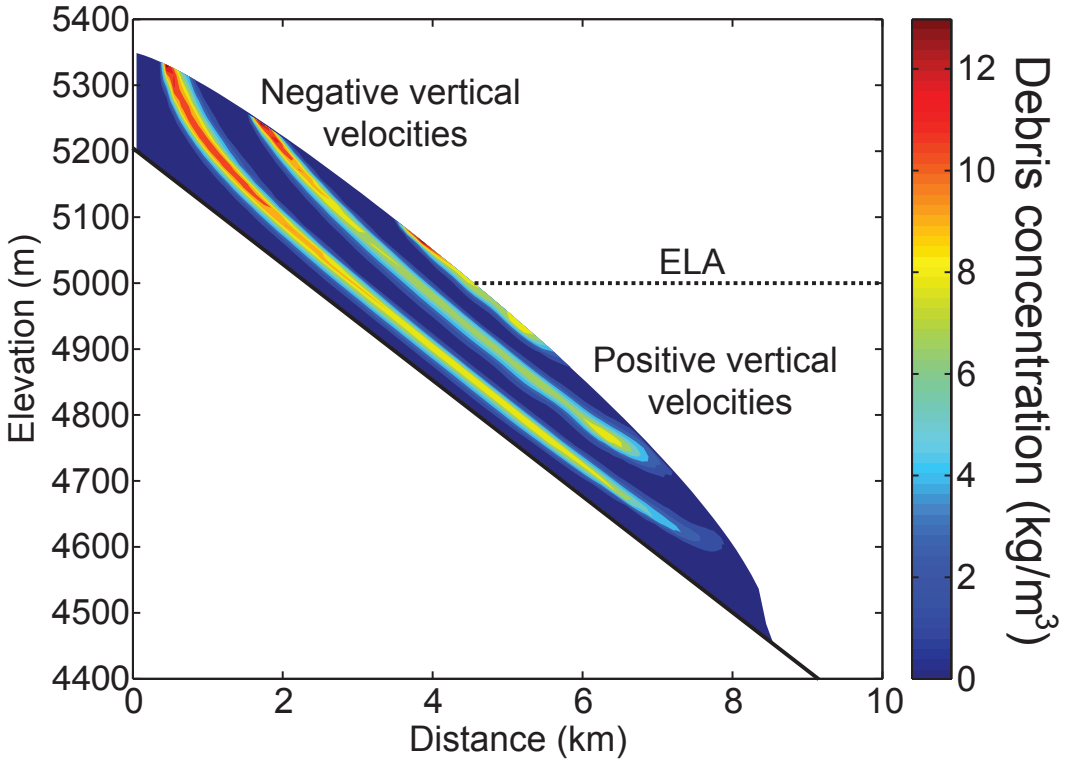

Figure 3.3 The advection of debris through a steady state glacier, unperturbed by surface debris. Englacial debris concentrations are plotted when supraglacial debris from each pathway is > 0.002 m. Three debris deposition locations are 12%, 47% and 100% from the headwall to the ELA. Changes in debris concentration through the glacier are the result of the englacial strain history and negligible numerical diffusion.

3.4.2 Comparison of modeled debris-free and debris-covered glaciers at steady state

We now present differences between the steady state modeled debris-free and debris-perturbed glaciers using the base parameter set (debris deposition at 47% between the headwall and the ELA and D_{factor} = 3). We compare the surface mass balance, surface velocity, ice thickness and ice discharge patterns between the two-modeled glaciers in turn. Under the same climate forcing, the steady state debris-covered glacier is 5 km longer than the steady state debris-free glacier (Fig. 3.4).

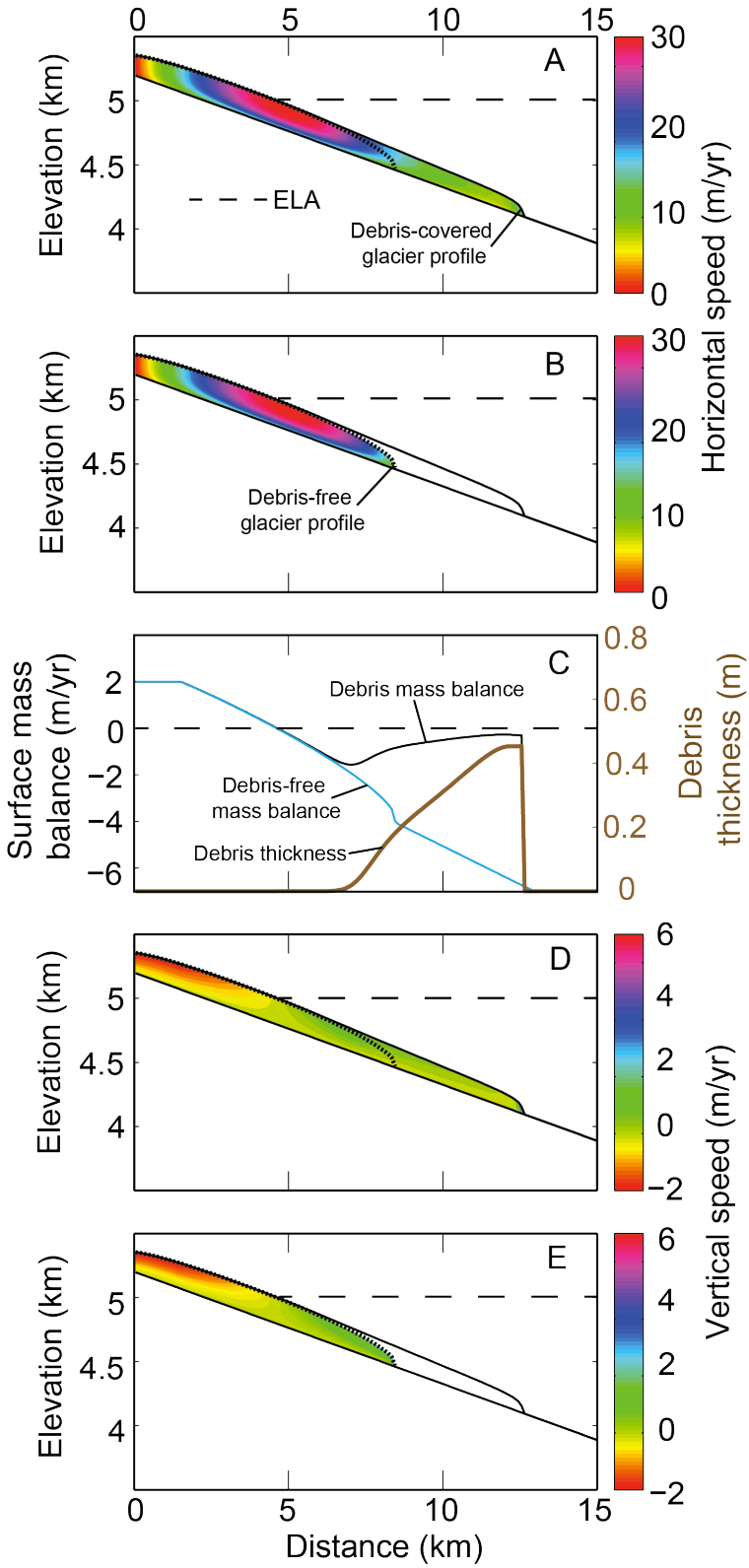
A
B
C
D
E
Elevation (km)
ELA
Debris-covered
glacier profile
Debris-free
glacier profile
Horizontal speed (m/yr)
Surface mass
balance (m/yr)
Debris mass balance
Debris-free
mass balance
Debris thickness
Debris
thickness (m)
Vertical speed (m/yr)
Distance (km)

Figure 3.4 Comparison of modeled internal glacier velocities for debris-covered and debris-free glaciers with the same climate forcing. A) The horizontal component of englacial velocities for the debris-covered glacier. The blue line shows the extent of the debris-free glacier. B) The horizontal component of englacial velocities for the debris-free glacier. The black line shows the extent of the debris-covered glacier. C) Annual surface mass balance of the modeled glaciers. D) The vertical component of englacial velocities for the debris-covered glacier. The blue line shows the extent of the debris-free glacier. E) The vertical component of englacial velocities for the debris-free glacier. The black line shows the extent of the debris-covered glacier.

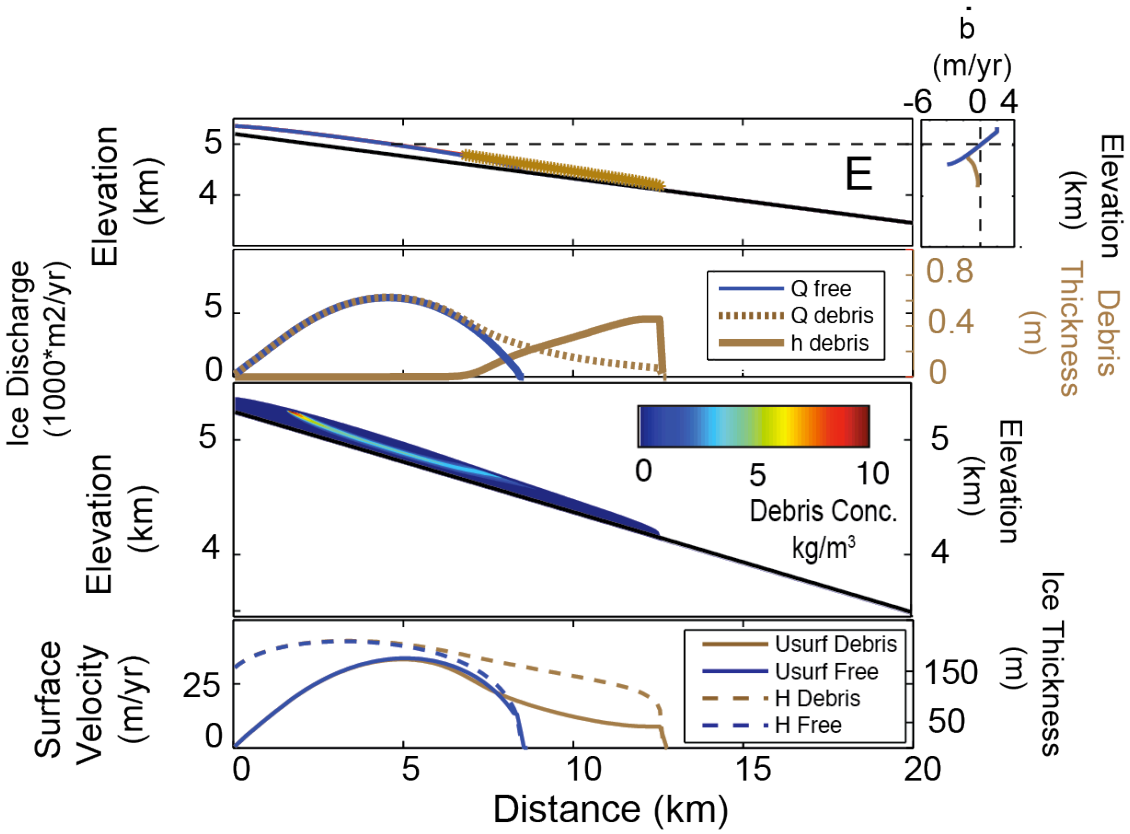

Figure 3.5 Comparison between a debris-covered glacier and a debris-free glacier in steady state, both in equilibrium with the same climate. A) Debris-covered glacier profile showing the ELA and the extent of debris cover. B) Comparison of the debris-free and debris-perturbed ice discharge patterns resulting from the surface debris thickness profile. C) The englacial debris concentration of the debris-perturbed glacier. D) Comparison of debris-free and debris-perturbed glacier surface velocities and glacier thicknesses. E) The surface mass balance profiles of the debris-perturbed and debris-free glaciers.

3.4.2.1 Surface mass balance differences

The debris-free glacier mass balance profile is determined by the glacier surface elevation and the *ELA*. The mass balance profile of the debris-covered glacier reflects both the elevation dependence of mass balance and the effects of the supraglacial debris (Fig. 3.5B and 3.5E). The mass balance gradient down-glacier from the point of initial debris emergence reverses relative to the debris-free profile and monotonically decreases toward zero.

3.4.2.2 Glacier velocity differences

The horizontal component of the englacial velocities for both the debris-free and debris-covered glaciers are similar through the extent of the debris-free glacier (Fig. 3.4A and 3.4B. Horizontal englacial velocities in the debris-covered glacier beyond the toe of the debris-free glacier are reduced compared those expected from a debris free glacier of equal geometry. A debris-free glacier of equal size would have a roughly parabolic surface velocity pattern with distance similar to the debris-free glacier surface velocity shown in Figure 3.5D. The internal horizontal velocity structures are very similar near the headwall. The debris-free glacier surface velocity pattern decreases sharply below the ELA in parabolic form (Fig. 3.5D). The debris-perturbed glacier surface velocity deviates from the debris-free glacier surface velocity at the ELA. It is slightly lower than the debris-free glacier surface velocity in the upper portion of the ablation zone, and departs radically from the parabolic form in the debris-laden tongue, only slowly declining toward the terminus.

The debris-free glacier vertical velocity at the surface becomes increasing positive from the *ELA* to the terminus, reflecting the monotonically decreasing negative mass balance in the ablation zone (Fig. 3.4D). In the debris-covered glacier case, *w* increases from the *ELA* to where surface debris-cover is first present there velocities decline toward the terminus.

3.4.2.3 Glacier thickness and surface slope differences

The ice thicknesses are similar for the debris-free and debris-perturbed glaciers from the headwall to the ELA. Below the ELA ice thicknesses diverge. The debris-free glacier thickness decreases rapidly below the ELA to its terminus. The debris-perturbed glacier thickness decreases slowly until very near its terminus where ice thicknesses decrease rapidly (Fig. 3.5B). Below the ELA the debris-perturbed glacier has lower surface slopes than the debris-free glacier (Fig. 3.5).

3.4.2.4 Ice discharge differences

The debris-free and debris-perturbed glacier ice discharges deviate near the point of debris emergence. The debris-free glacier ice discharge follows a parabolic shape dictated by the integral of the surface mass balance profile. From the headwall to the location of debris emergence, the debris-perturbed ice discharge pattern follows the debris-free discharge pattern. Below the point of debris emergence, the ice discharge declines slowly similar to the surface speed profile.

3.4.3 Changes in debris deposition rate

We now change the magnitude of debris deposition rate, $\dot{d}_0$ by varying D_{factor}. In these calculations we show the steady state properties of a glacier with three chosen debris delivery rates (D_{factor} = 1,3, and 5). The debris input location is held at 47% from the headwall to the *ELA*. The inclusion of debris extends the length of each modeled glacier from the debris-free initial profile. The glacier with the highest debris deposition rate produced the longest glacier (17.5 km (D_{factor}=5) compared to 12.5 km (D_{factor}=3) and 8 km (D_{factor}=1) (Fig. 3.6).

The maximum debris emergence rate increases non-linearly with a linear increase in $\dot{d}_0$ (Fig. 3.7). The width of the debris emergence zone also increases with a higher $\dot{d}_0$ (Fig. 3.7).

While the up-glacier edge of the zone of debris emergence remains fixed among the calculations, the down glacier edge of the zone of debris emergence moves closer to the glacier terminus as D_{factor} increases. Changing the debris deposition rate also leads to changes in the shape of the steady state debris pattern (Fig. 3.6 and 3.7). Both the maximum debris thickness and the percentage of the ablation zone covered with debris increases with a larger D_{factor}. The increase in the percentage of the ablation area covered with debris corresponds with the increase in glacier length.

Steady state glacier length increases non-linearly with debris deposition rate (Fig. 3.8). The larger the debris input rate, the more amplified the steady state length differences become among the different debris input locations (Fig. 3.8). For avalanche locations near the headwall, the steady state glacier length change has a different relationship to D_{factor} than avalanche locations near the *ELA*.

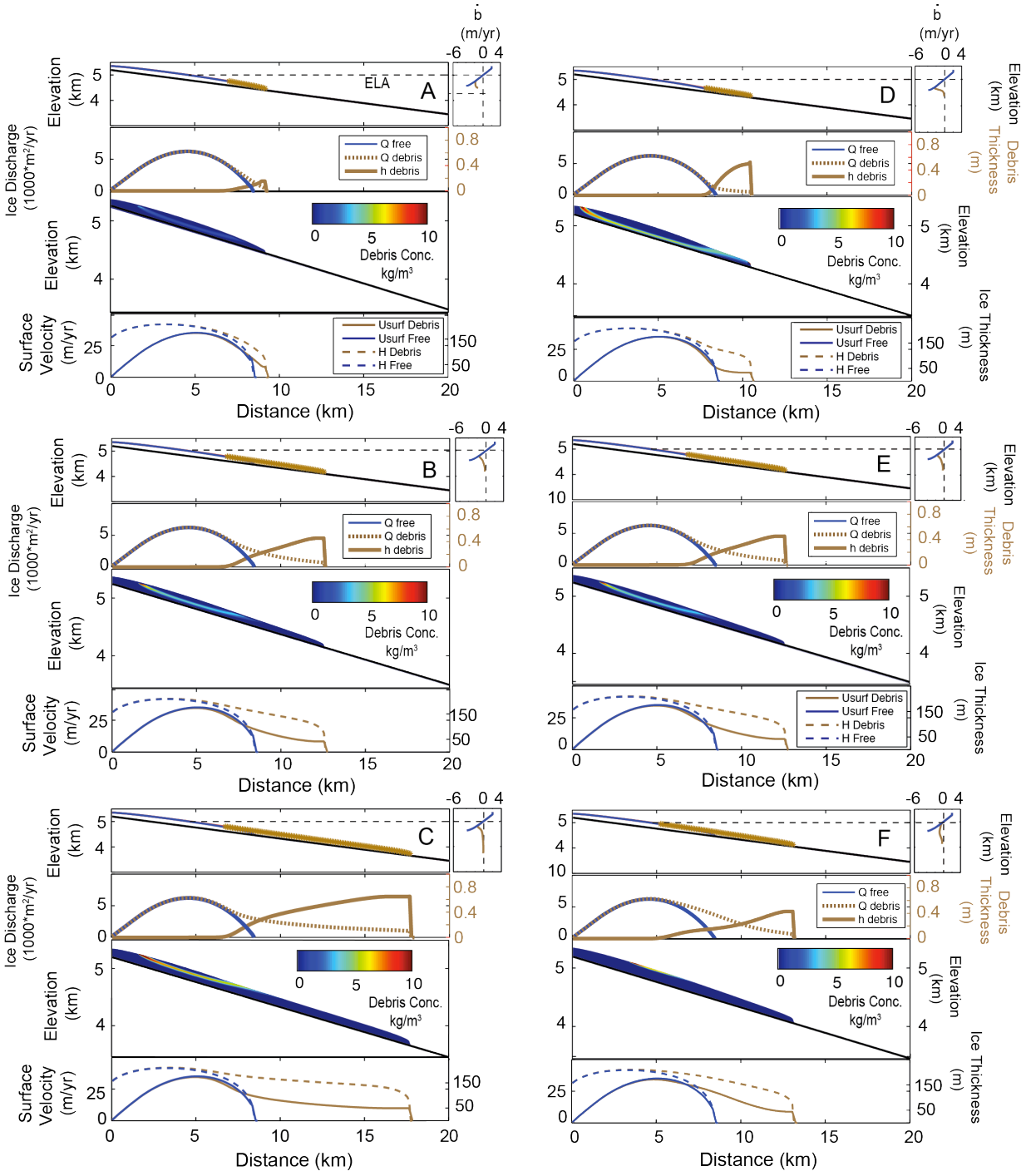
A
B
C
D
E
F
ELA
Q free
Q debris
h debris
Debris Conc.
kg/m³
Usurf Debris
Usurf Free
H Debris
H Free
Elevation (km)
Ice Discharge (1000*m²/yr)
Surface Velocity (m/yr)
Debris Thickness (m)
Ice Thickness (m)
ḃ (m/yr)
Distance (km)

Figure 3.6 Model output showing the effect of changing the headwall/sidewall erosion rate on the glacier (A-C) and the effect of changing the debris input location (D-F). A) Avalanche input location at 47% and D_{factor} = 1 B) Avalanche input location at 47% and D_{factor} = 3. C) Avalanche input location at 47% and D_{factor} = 5. D) Avalanche input location at 12% and D_{factor} = 3. E) Avalanche input location at 47% and D_{factor} = 3. F) Avalanche input location at 100% and D_{factor} = 3.

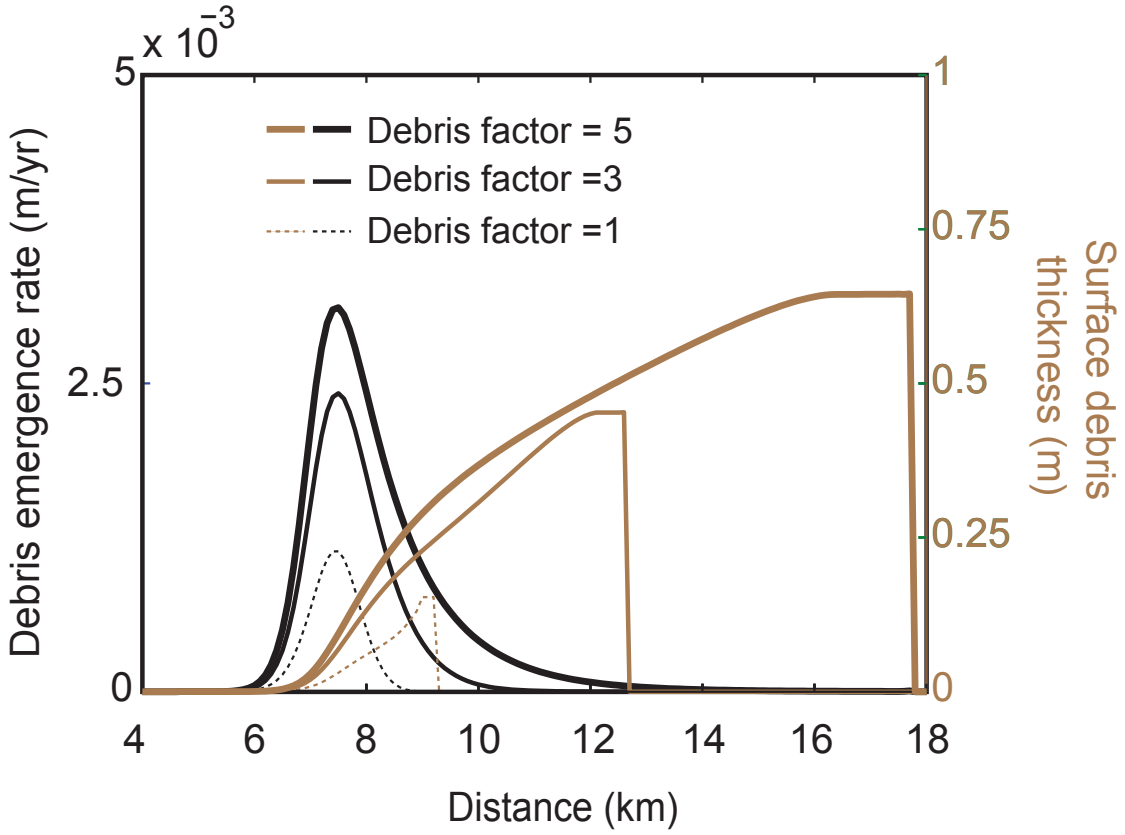

Figure 3.7 Debris thickness and debris emergence rate for D_{factor} = 1, 3, and 5. All debris is deposited in the accumulation zone 47% to the ELA from the headwall.

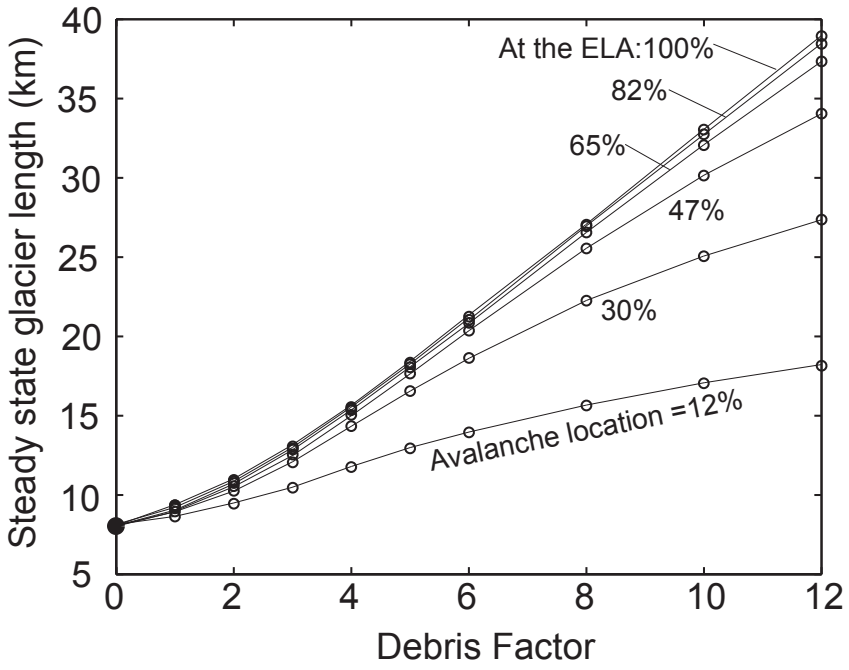

Figure 3.8 Steady state glacier length versus the debris input rate for the six debris input locations in the accumulation zone.

3.4.4 Changes in debris deposition location

We now vary the debris input location on the modeled steady-state glaciers. In these calculations we show the steady state properties of a glacier with a constant D_{factor} equal to 3. The debris input location is varied through six input locations from the headwall to the ELA (Fig. 3.8). The inclusion of debris in the model extends the length of each modeled glacier. The calculation with debris input nearest the ELA formed the longest glacier (13 km (100% to the ELA) compared to 12.5 km (47% from the headwall to the ELA) and 11 km (input 12% from the headwall to the ELA; Fig. 3.6D-F).

The maximum debris emergence rate increases the closer the debris is deposited to the headwall. The zone of debris emergence is wider when debris is deposited near the *ELA* (Fig. 3.9). The maximum debris cover thickness decreases the closer the debris is input to the ELA. Debris cover thickness increases most rapidly when debris is input near the headwall. For glaciers where the debris-cover is input closer to the ELA the debris thickness increases slower (Fig. 3.9). The steady state debris thickness profile also varies considerably. The further up glacier debris first emerges, the larger the percentage of the debris cover in the ablation zone.

For each D_{factor}, we also varied the debris input location (Fig. 3.10). A non-linear relationship exists between debris input location and the steady state glacier length. Changes in debris input location near the headwall lead to larger changes in steady state glacier length than changes in debris input location near the *ELA*. The larger the D_{factor} the more amplified this relationship becomes (Fig. 3.10).

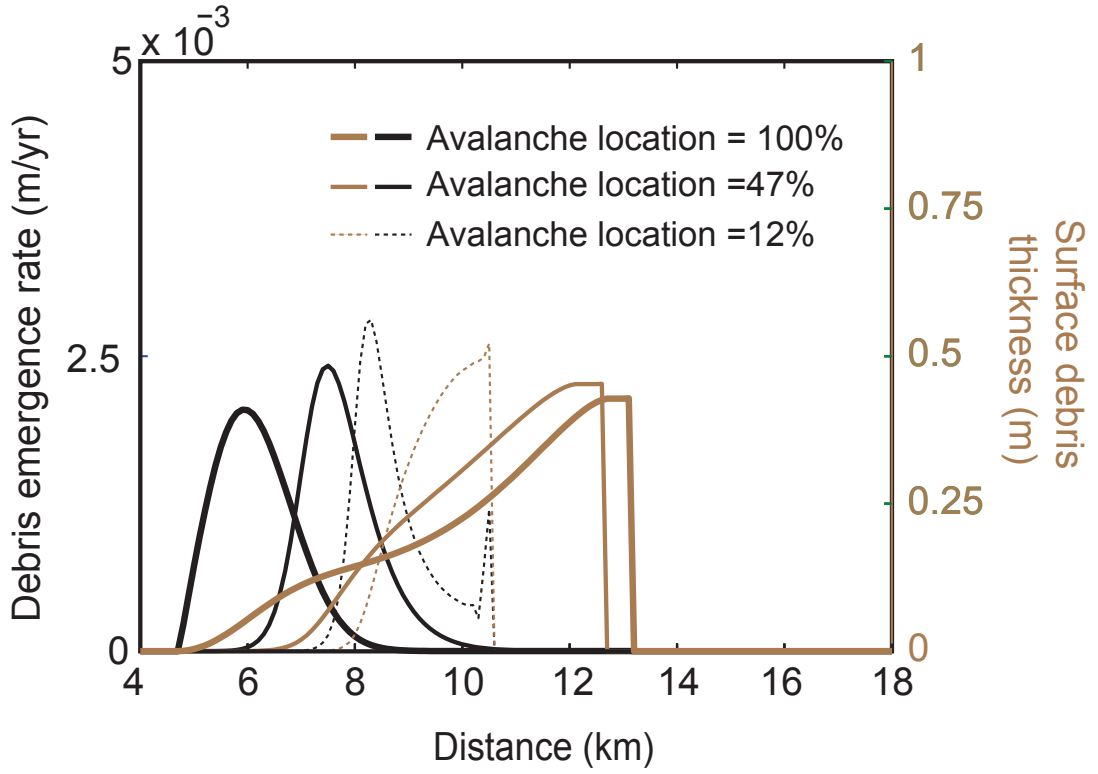

Figure 3.9 Debris thickness and debris emergence rate for model calculations with D_{factor} =3, with variable debris deposition locations from 12%, 47%, to 100% from the headwall to the ELA. Spike in the toe emergence rate of the 12% case is the result of debris concentration increase and advection due to low melt rates under the debris.

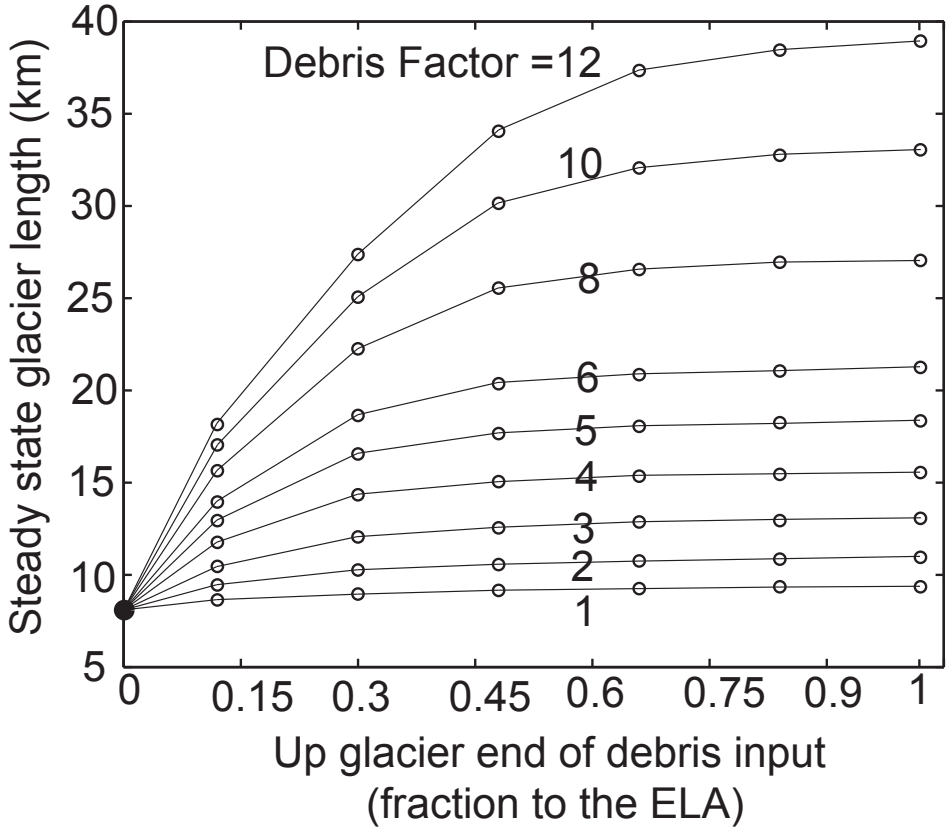

Figure 3.10 Steady state glacier length versus the location of debris input for nine different debris input rates. Changes in debris input location near the headwall produce the largest glacier length changes.

3.4.5 Response times

The addition of debris to a debris-free glacier causes a transient glacier length response that is similar to the response of a debris-free glacier to a climate change (e.g., Oerlemans, 2000; Fig. 3.11). The shape of the glacier length response curves in Figure 3.11 is similar to the shape of response curves modeled glaciers responding to a uniform, glacier-wide increase in mass balance (e.g., Roe and Baker, 2014; Oerlemans, 2000). The closer the debris is deposited to the ELA, the faster the glacier starts advancing (Fig. 3.11A). The greater the debris deposition rate, the longer it takes the glacier to reach steady state. Debris travels through the glacier faster when deposited near the ELA (Fig. 3.12). Slightly countering this effect, the time between initial debris emergence and glacier advance is longer when the debris emerges near the ELA (Fig. 3.12).

We also calculate the e-folding timescale of the modeled glaciers length response to the addition of debris to a debris-free glacier. The e-folding timescale for each calculation is based on the glacier length response in the period between initial debris emergence and when the glacier reaches its maximum, steady length. The e-folding response time increases as D_{factor} is increased (Fig. 3.13), even though rates of terminus advance are higher for large D_{factor} calculations than calculations with low D_{factor} (Fig. 3.14). Similarly, the closer debris is deposited to the *ELA*, the faster the maximum rates of advance and the further the glacier needs to advance to reach steady state (Fig. 3.11A). E-folding response times vary widely from 200 years to 1400 years.

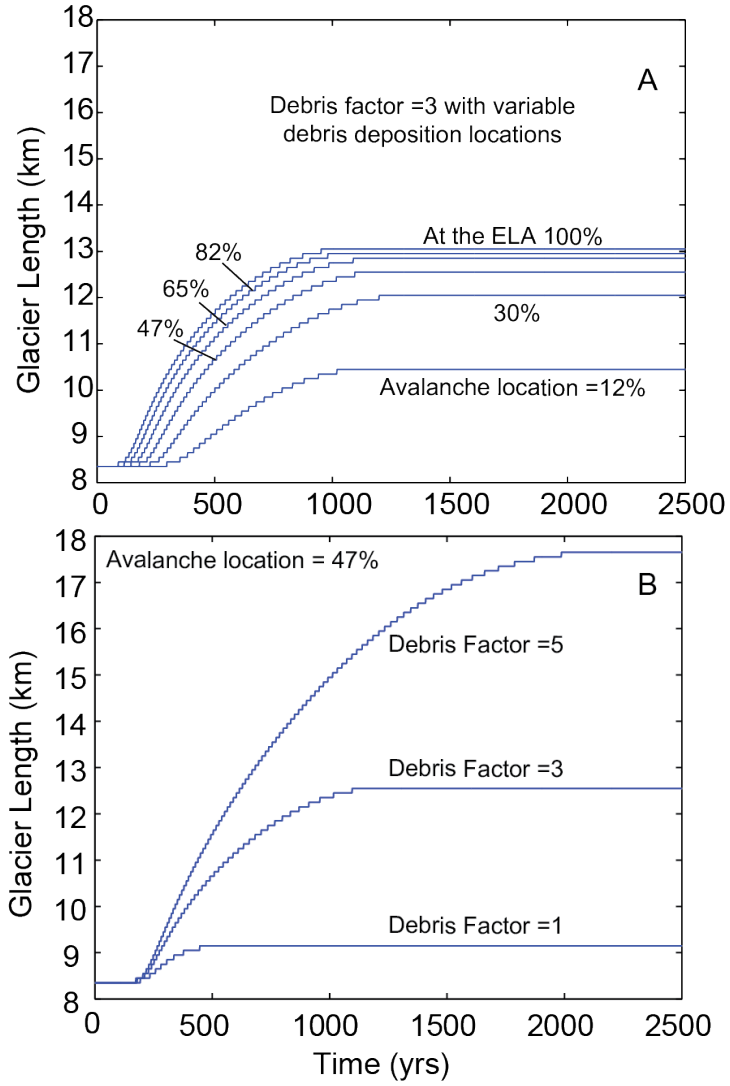

Figure 3.11 A) Glacier length response due to a step change in debris deposition rate at time zero. D_{factor} is 3 for all cases shown. B) Glacier length response due to a step change in debris deposition rate at time zero the debris factors are 1, 3, and 5. In all cases debris is deposited 47% from the headwall to the ELA.

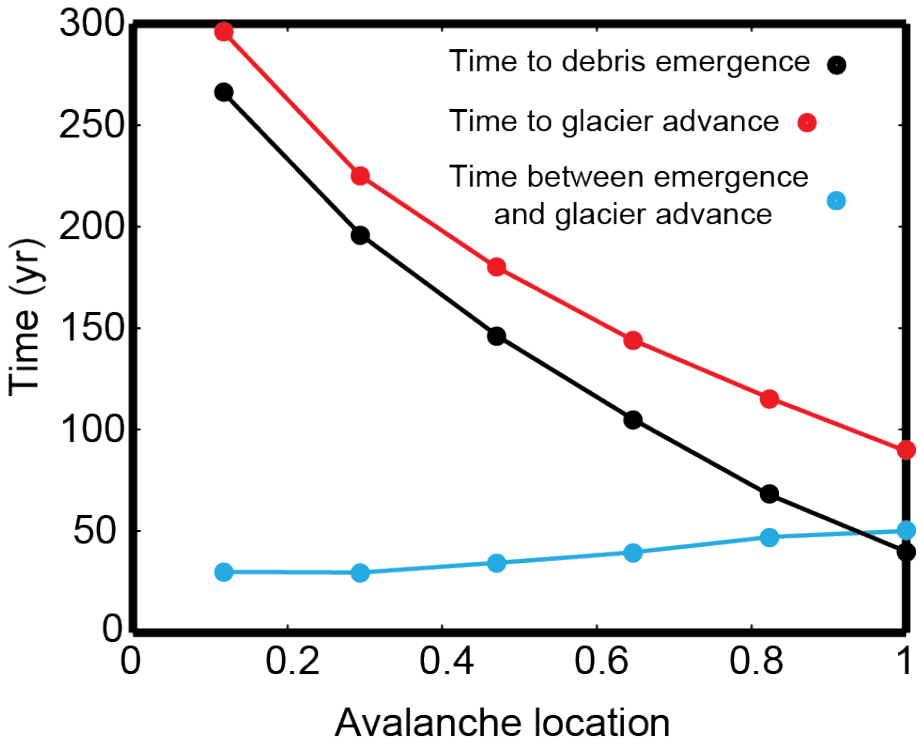

Figure 3.12 Time to debris emergence, time to glacier advance and the time needed for the glacier to advance once the debris emerges. Data from calculations with a D_{factor} =3 and all modeled rock avalanche input locations. A similar pattern exists for other deposition rates.

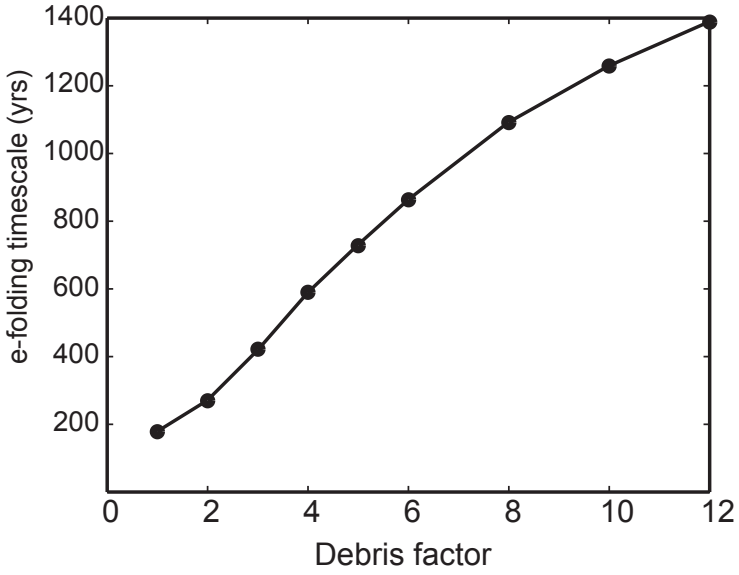

Figure 3.13 E-folding timescale for the response of the modeled glaciers to a step change in debris deposition. The more debris input to the system, the longer the e-folding response time. Debris avalanche location set to 47% from the headwall to the ELA in all cases shown.

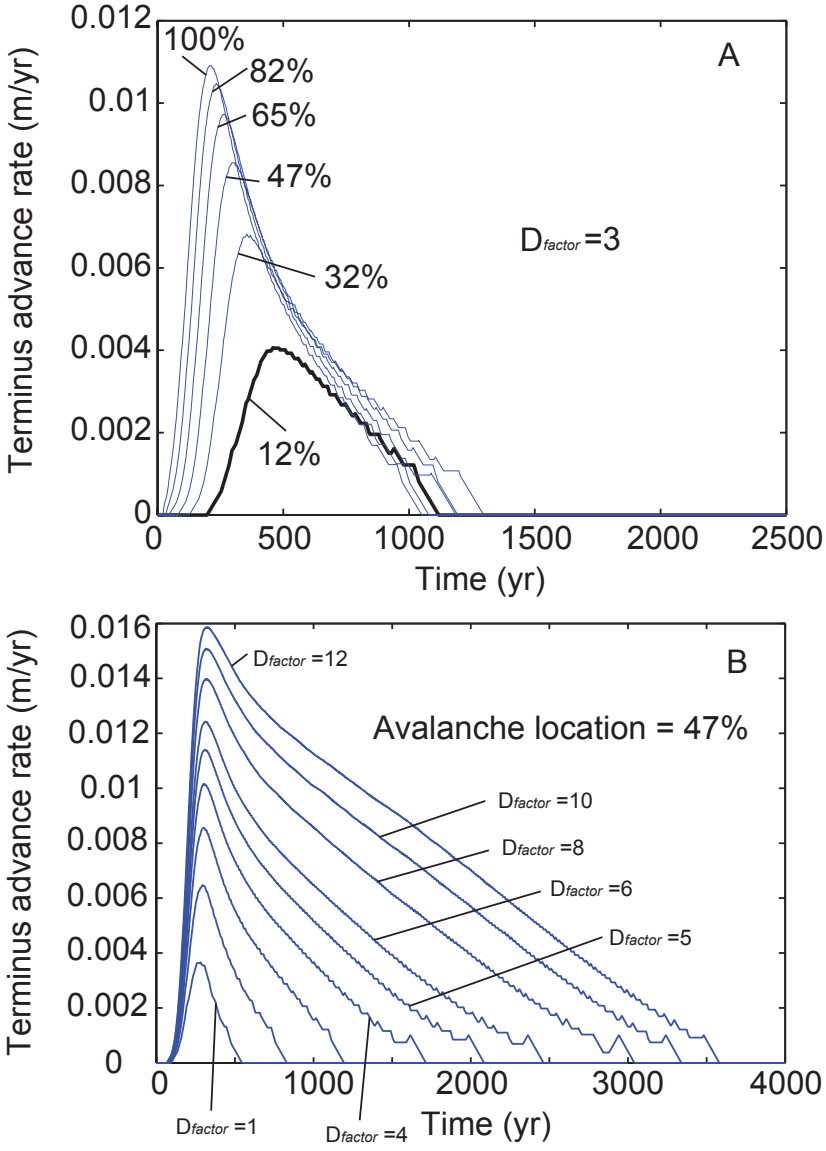

Figure 3.14 Comparisons of terminus advance rates depending on the D_{factor} and avalanche input location. (A) Smoothed terminus advance rates with D_{factor} =3 and the full range of avalanche input locations. (B) Smoothed terminus advance rates with the avalanche input location at 47% from the headwall to the ELA.

3.4.6 Dynamic response to the emergence of englacial debris

We now describe the transient response of our baseline debris-free glacier to a step change in debris deposition in the accumulation zone. At time zero the total debris deposited onto each modeled glacier per year is increased from zero to $\dot{d}_0$* (D_{factor}=3). We vary the avalanche input location from 12%, 45%, to 100%. Debris is deposited in the accumulation zone, incorporated into the glacier and then advected through the glacier until it emerges in the ablation zone. Upon debris emergence, the glacier starts to thicken due to a reduced $\dot{b}$ (Fig. 3.15). The ice surface slope is initially increased down glacier of the ice thickness perturbation caused by the debris (Fig. 3.15). Because of the local thickening and ice surface slope increase near the glacier toe, the terminus advances.

The most rapid rate of debris cover thickness increase and spatial coverage increase occurs within the first 150 years after initial debris emergence (or the first 3 blue curves after the red steady state curves in Fig. 3.15 C,F,I). This rapid increase in debris coverage coincides with the most rapid thickening rates in the debris-covered portion of the glacier. In each ice discharge plot in Figure 3.15 a bulge in ice discharge can be seen propagating toward the glacier toe as the terminus advances in the first 150 years of the calculation (Fig. 3.15 B,E,H). The local increase in ice discharge gradient associated with this bulge leads to the greatest rates of terminus advance (Fig. 3.11). After the initial 150-200 year period of rapid debris emergence, significant changes in the debris cover and surface mass balance profiles are solely the result of glacier toe advance. The debris thickness and surface mass balance created in the new cells reach their steady state values rapidly (Fig. 3.15 C,F,I).

There are several notable differences between the three transient cases presented. In the avalanche location = 12% case, the emergence of debris close to the terminus results in a rapid

change in surface melt rate under debris, but a slower change in glacier-wide mass balance (Fig. 3.15C and 3.16). The more gradual decrease in surface mass balance in the avalanche location = 100% case is also reflected in the ice thickness and discharge patterns (Fig. 3.15G-I).

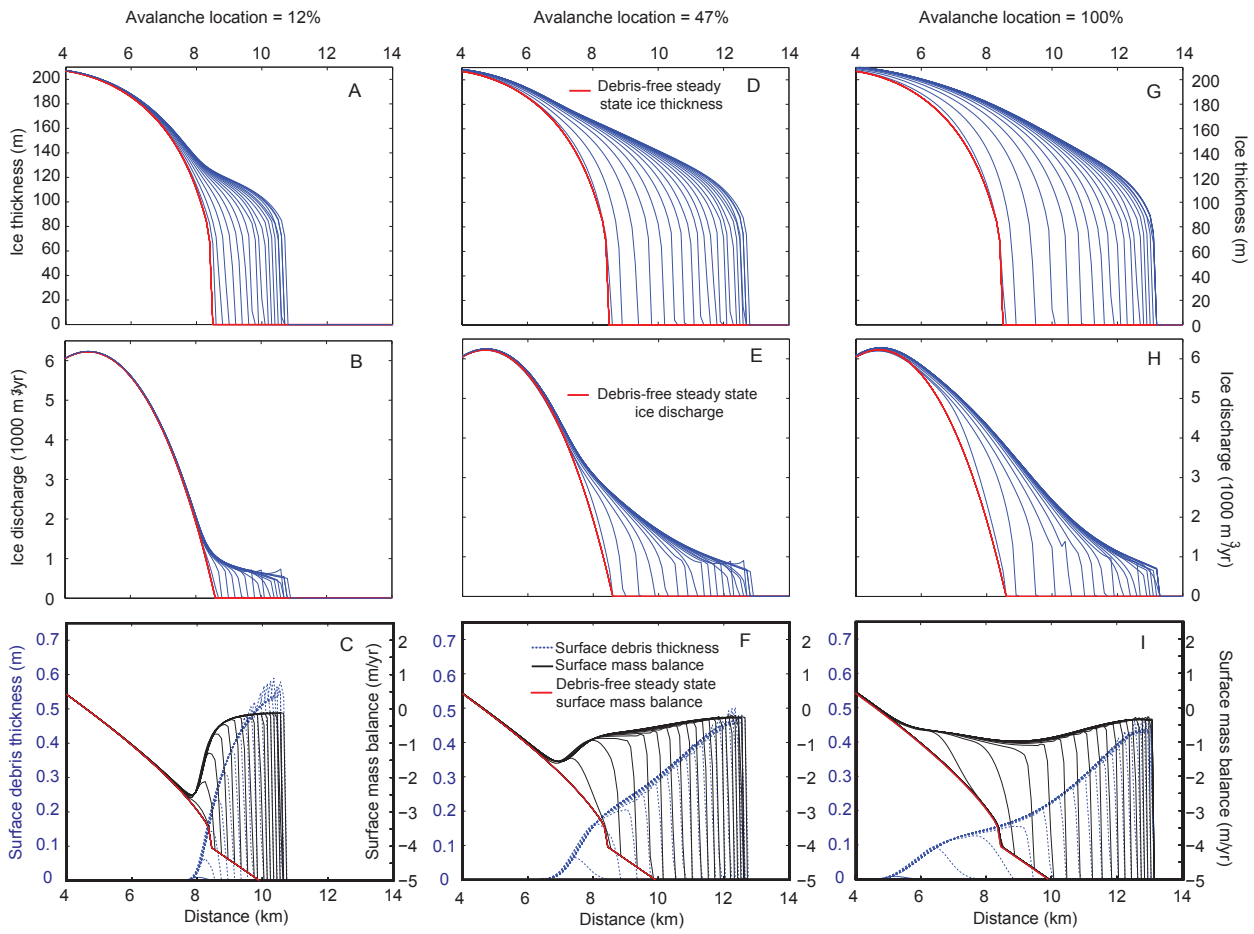

Figure 3.15 The transient response of ice thickness, ice discharge, surface debris thickness, and the surface mass balance to a step change increase in debris deposition in the accumulation zone. Red lines indicate the initial debris-free steady state profiles. All model output show is for a D_{factor} =3. Results are plotted every 50 years. (A-C) model results where the avalanche location = 12%. (D-F) model results where the avalanche location = 47%. (G-I) model results where the avalanche location = 100%.

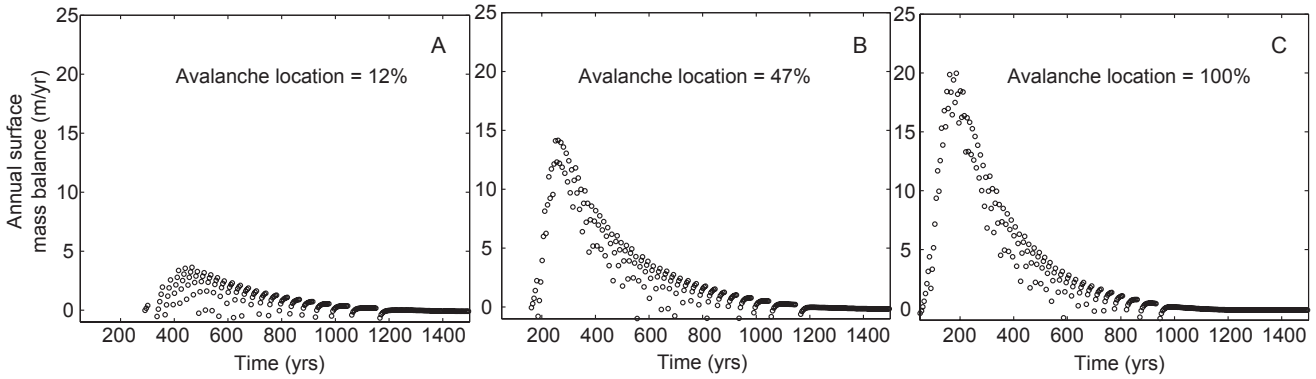

Figure 3.16 The annual surface mass balance from the time of debris emergence to steady state for the three transient cases. The closer debris is deposited to the ELA the larger the maximum annual surface mass balance is perturbed from 0.

3.5 Discussion

We now attempt to explain differences between the modeled debris-perturbed and debris-free glaciers illustrated above. First we explain the steady state results. Next, we provide an explanation for the steady state patterns of debris seen in the model output above based on equation 3.15, the surface velocity profile and the debris emergence rate. This leads to explanations for the glacier response to variations in debris deposition rate and debris deposition location. Finally, we discuss the response times of the modeled glaciers to a step change in debris deposition rate. Last, we describe the transient, dynamic response of the glacier to a step change in debris deposition rate from the debris-free steady state to the debris-perturbed steady state.

3.5.1 Explanations for the steady state debris-covered glacier

The most notable difference between the debris-free and debris-covered glaciers in Figure 3.4 and 3.5 is the difference in the surface mass balance profiles. Where debris begins to emerge on the glacier surface, the mass balance gradient switches from decreasing down-glacier to increasing down-glacier. Recall that the spatial gradient in ice discharge at steady state must equal the local mass balance $\dot{b}$ ($\dot{b} = \frac{dQ}{dx}$). Because $\dot{b}$ increases toward zero in the debris-covered portion of the glacier, the ice discharge gradient must also decrease toward zero toward the glacier terminus. Debris-covered glaciers are longer than debris-free glaciers because they must extend to lower elevations to counter the reduced $\frac{dQ}{dx}$ and insulating effects of surface debris.

As $Q = H\bar{u}$, u_{surf} and H must also display reduced spatial gradients in the ablation zone. u_{surf} decreases up glacier from the initial zone of emergence relative to the debris-free glacier, even though ice thickness is larger in the debris-perturbed case (Fig. 3.5). Ice discharge is not

reduced relative to the debris-free case, up glacier from the start of the zone of debris emergence (Fig. 3.5). While the ice thickness is increased for the debris-covered glacier, the ice surface slope is simultaneously reduced. The increase in H up glacier from the point of initial debris emergence has a larger effect on ice discharge than the glacier surface velocities. Ice surface velocities (here we only address velocities due to internal deformation) vary with $(\sin\alpha)^3$ and H^4 (equations 3.4 and 3.5), while ice discharge varies with $(\sin\alpha)^3$ and H^5. For surface velocity, the reduction in ice surface slope between the debris-free and debris-perturbed cases leads to a larger magnitude reduction in velocity compared to the increase caused by changes in H. For ice discharge, the reduction in ice surface slope between the debris-free and debris-perturbed cases leads to a smaller magnitude reduction in discharge compared to the increase caused by changes in H.

Scherler et al. (2011) presents an extensive debris-covered glacier data set from Central Asia. They show that glacier surface speed declines within debris cover. Our steady state model shows similar patterns (Fig. 3.17). The steady state surface debris pattern is discussed in Section 4.4.

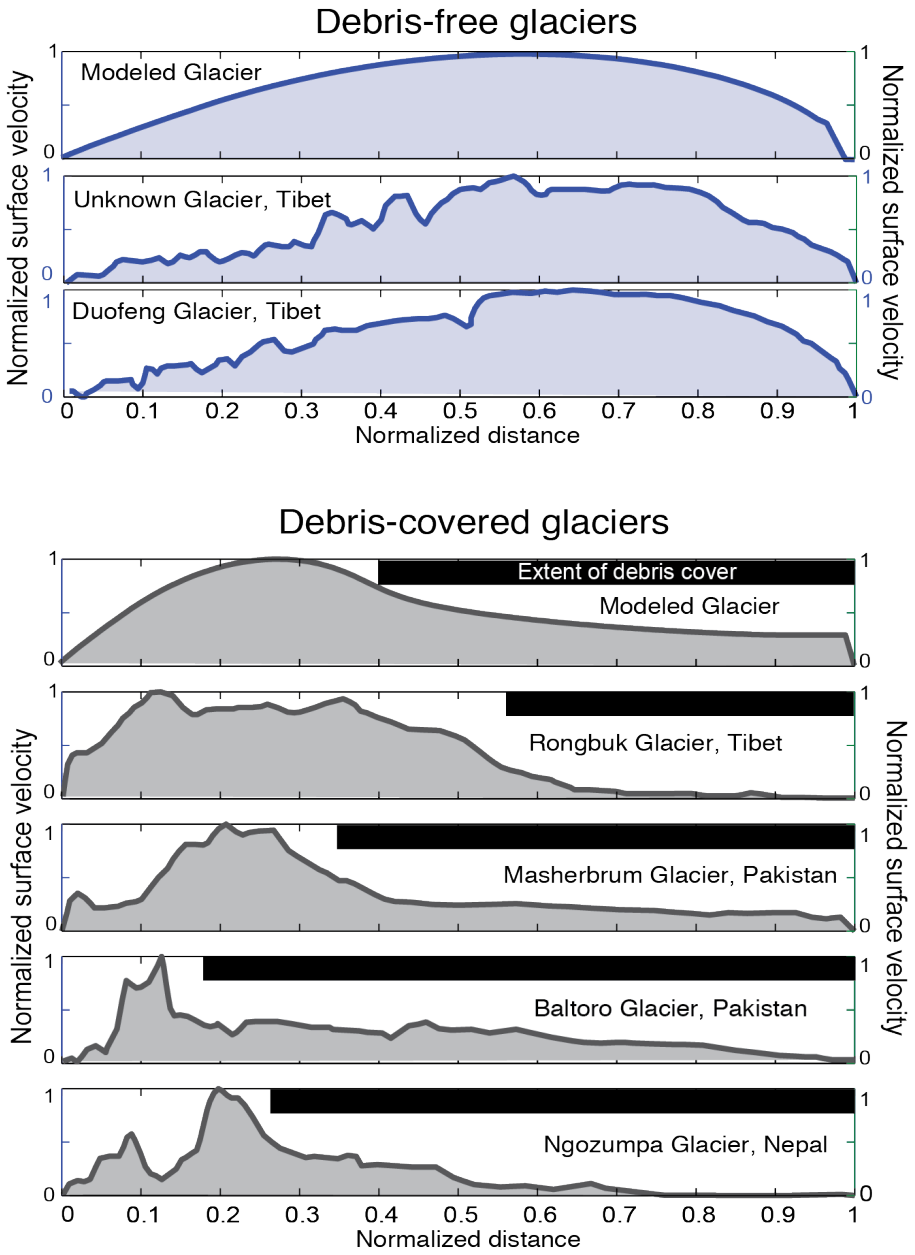

Figure 3.17 A comparison of model output with debris-covered and debris-free glacier surface velocities from Central Asia. All data is normalized for comparison and from Scherler et al., 2011. Maximum velocities are much larger for the presented debris-covered glaciers than the debris-cover model output. This difference stems from the model's linear bed profile and simple hypsometry.

3.5.2 Explanations for the pattern of steady state supraglacial debris thickness

Modeled debris thickness profiles are similar to debris thickness profiles from debris-covered glaciers (Fig. 3.18). All modeled and actual debris thickness profiles generally increase with distance down glacier. More data are needed to identify the full range of debris thickness profiles. We now present explanations for modeled variations in debris cover thickness.

A combination of the englacial debris concentration, C, field, the sub debris-melt rate, $\dot{b}'$ and the u_{surf} field determines pattern of surface debris. The surface debris thickness, h_{debris}, is therefore dependent on the co-evolution of variables that are themselves dependent on $h_{debris.}$ Two variables combine to determine the steady state supraglacial debris profile: 1) the debris emergence rate, $\dot{\varepsilon}_{debris} = \frac{C\dot{b}'}{(1-\phi)\rho_{rock}}$ and 2) the spatial pattern of u_{surf}.

The debris advection path determines the debris emergence rate as the local melt rate depends upon position relative to the ELA. Debris input near the ELA results in emergence that is spread over a larger area than debris input near the headwall. Near the *ELA*, low net melt rates and high near-surface u velocities smear out the zone of debris emergence. In contrast, debris input near the headwall emerges near the terminus, where melt rates are high and u velocities are low, resulting in a narrow zone of debris emergence.

In steady state, h_{debris} in the ablation zone is defined by

$$h_{debris} = \frac{1}{u_{surf}} \int_{x_{ELA}}^{x} \frac{C\dot{b}'}{\rho_{rock}(1-\phi)} dx, \tag{3.17}$$

where the x_{ELA} is the x-position of the ELA and x is the position of interest down glacier from the *ELA*. The up-glacier integral of $\dot{\varepsilon}_{debris}$ dominates the flux of surface debris between cells in the zone of debris emergence. The flux of debris between cells in the zone of debris emergence must therefore increase (Fig. 3.19).

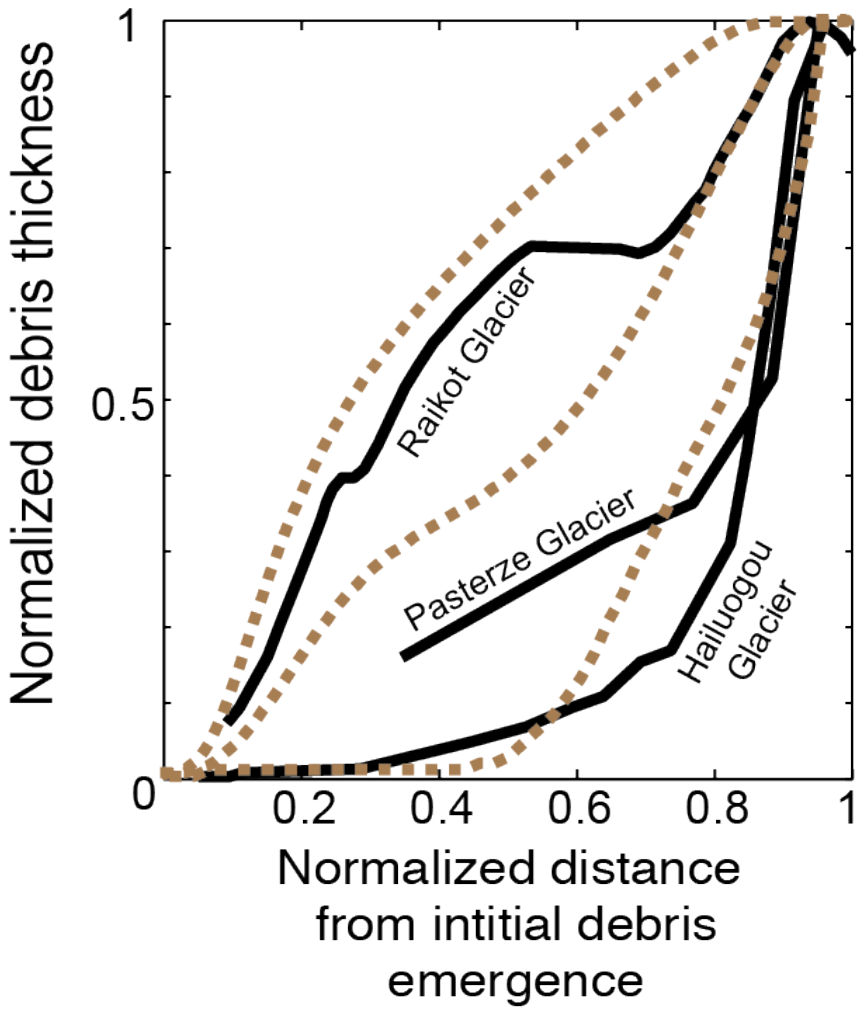

Figure 3.18 A comparison of modeled steady-state debris cover thickness to debris thickness from three glaciers. The x-axis shows the normalized distance from the point of initial debris emergence to the glacier terminus. Raikot Glacier, Pakistan data is from the centerline, while Pasterze Glaicer, Austria and Hailuogou Glacier, China data are mean debris thicknesses (Owen et al., 2002; Kellerer-Pirklbauer, 2008; Zhang et al., 2010). Modeled debris thickness output is from Figures 3.6A-F.

The debris emergence rate $\dot{\varepsilon}_{debris}$ is negligible if either C or $\dot{b}'$ is near zero. If $\dot{\varepsilon}_{debris}$ is negligible, the temporal rate of change of debris-cover reduces to

$$\frac{\partial h_{debris}}{\partial t} = \frac{\partial (h_{debris} u_{surf})}{\partial x}. \tag{3.18}$$

In steady state this reduces further to $h_{debris} u_{surf} = c$, where the constant, c, is the flux of debris at the point where emergence rate declines to zero, which we call $q_{\dot{\varepsilon}_{debris}=0}$. Equation 3.17 therefore becomes

$$h_{debris} = \frac{q_{\dot{\varepsilon}_{debris}=0}}{u_{surf}}, \tag{3.19}$$

in which $q_{\dot{\varepsilon}_{debris}=0}$ is the integral of emergence rate up glacier of this point: $\int_{x_{ELA}}^{x_{\dot{\varepsilon}_{debris}=0}} \frac{C\dot{b}'}{\rho(1-\phi)} dx$, which has units of [m^2/yr]. The pattern of surface speed, $\frac{1}{u_{surf}}$, dominates the surface debris thickness pattern (Fig. 3.18). Because $\frac{\partial u_{surf}}{\partial x}$ is always negative, debris thickness will always increase toward the glacier toe below the zone of debris emergence. In other words, the debris thickens by strain associated with the surface speed gradient.

While most debris-covered glaciers are experiencing periods of negative mass balance, it may be possible to apply equations 3.17 to 3.19 to real debris-covered glaciers. Known surface velocity and debris thickness would allow you to infer $q_{\dot{\varepsilon}_{debris}}$, and potentially the $\dot{\varepsilon}_{debris}$ pattern. The glacier must be in steady state for this to apply.

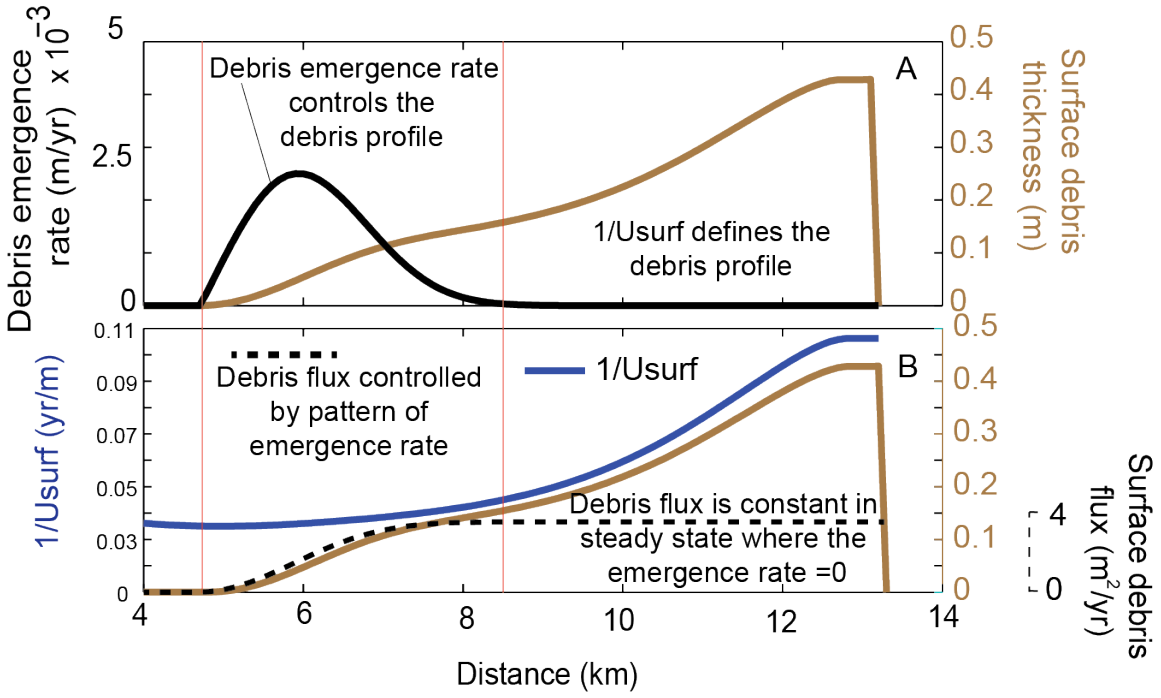

Figure 3.19 A) Debris emergence rate and surface debris thickness for the debris factor = 3, avalanche location = 100% case. B) Surface debris thickness compared to the $1/U_{surf}$ and the steady state surface debris flux. Debris emergence dominates the debris cover profile until the debris emergence rate nears zero; thereafter, surface strain dominates.

The spatial distribution of the zone of debris emergence depends on 1) the concentration of debris in the ice and 2) the surface mass balance. The debris deposition location in the accumulation zone and the englacial velocity field controls the up glacier end of the debris emergence zone. The pattern of englacial debris and the debris input rate control the down glacier end of debris emergence. A larger debris input rate leads to thicker debris covers, which reduces the sub-debris ablation rate. A reduced ablation rate then reduces the rate of debris emergence by the direct dependence of the emergence rate on the surface mass balance. If $\dot{b}$ goes to zero, the emergence rate also goes to zero. The reduction of $\dot{b}$ leads to the reduction of englacial vertical velocities. Because *w* is reduced, the *u* component of velocity dominates englacial advection under thick debris, leading to an expanded zone of high englacial debris concentration (Fig. 3.7). The expansion of the englacial zone of high debris concentration then leads to an expansion of the zone of debris emergence.

3.5.3 Explanations for glacier response to erosion rate and debris input location change

Increases in debris deposition rate lead to increases in emergence rate which in turn lead to thicker debris on the glacier surface. If the net mass balance increases, due to debris emergence, the glacier must extend to lower elevations so net accumulation is equal to net ablation. Adding more debris to the glacier leads to a longer glacier. But there is a feedback that limits the effect of increasing debris deposition rates. Supraglacial debris thicknesses increase most rapidly down glacier when debris emerges near the terminus (Fig. 3.9). A rapid increase in debris thickness means that the surface mass balance is also reduced quickly toward zero (Fig. 3.6). Adding another characteristic debris thickness (h_*) of debris to a surface debris layer that has already reduced melt rates to near zero has a decreasing effect on the suppression of surface mass balance. The glaciers in figure 3.8 are becoming saturated with surface debris. Adding

more debris to the glacier surface has a smaller and smaller effect on the mass balance the therefore the glacier length. Sub-debris melt rate saturation leads to the sigmoidal shape seen in figure 3.8 for avalanche locations 12%, 30%, and 47% (Fig. 3.15C). Deposition locations nearer to the ELA require a larger volume of debris to reach saturation because the entire ablation zone needs to be saturated in order for an increase in debris deposition rate to no longer effect the net mass balance and the glacier length.

Glaciers are more sensitive to debris cover near the terminus than near the ELA. Changes in debris deposition location near the headwall lead to large changes in steady state glacier length. Likewise, an equal change in debris deposition location near the ELA will lead to a smaller change in the steady state length (Fig. 3.10). A meter of debris at high elevations in the ablation zone, where debris-free melt rates are, for example, 1 m/yr would suppresses the net melt of the glacier considerably less than one meter of debris near the glacier terminus where debris-free melt rates are 7 m/yr. Debris emerging near the terminus of an initially debris-free glacier has a larger effect on the net mass balance than debris emerging near the ELA.

3.5.4 Response timescales

The coupling between debris emergence, debris thickness, and ice dynamics complicates the response of glaciers to debris. We define three timescales for the adjustment of a debris-free glacier to a step change input of debris in the glacier accumulation zone. The first timescale is the time it takes for debris to advect through the glacier. The time debris spends in the model varies by 200 years. Debris deposited near the headwall will therefore see a significant lag between the time of debris deposition and emergence. This timescale may have implications for interpreting cosmogenic radionuclide dates of Holocene terminal moraines. If the debris advection time through the glacier varies by hundreds of years the ages of boulders on a moraine

will also vary by hundreds of years. The englacial advection timescale may help explain cosmogenic radionuclide boulder age scatter.

A second timescale is the time between debris emergence and glacier advance. The closer the debris emerges to the terminus the shorter this timescale. This is an expected result, as debris thickness perturbations will propagate to the toe faster when the thickness perturbation is closer to the terminus. The timescale between emergence and advance slightly counters the englacial advection timescale but is ultimately secondary.

The e-folding time of the glacier length response to the addition of debris varies widely from 200 to 1400 years and increases with a larger D_{factor}. The larger the D_{factor}, the larger the surface debris thickness and therefore the more the glacier is out of glacier wide surface mass balance and therefore the longer it takes for the glacier to advance to a new steady state. Because debris cover can reduce melt rates to nearly zero, debris-covered glaciers take a considerable amount of time to reach steady state, if they reach it at all.

3.5.5 Explanations for the transient glacier length response to a step change debris input

We now explain the transient response of a debris-free glacier to the addition of debris in the accumulation zone of the glacier (Section 3.6). After the debris as been advected through the glacier it melts out in the ablation zone. This emerging debris decreases the local surface mass balance causing a glacier to thicken locally because $\dot{b}$ becomes less negative. From the mass conservation equation for a constant width glacier, $\frac{\partial H_{ice}}{\partial t} = \dot{b} - \frac{\partial Q}{\partial x}$, an increase in $\dot{b}$ in the ablation zone will lead to local thickening as $\dot{b}$ is no longer equal the gradient in Q. The local thickening and increase in ice surface slope causes an increase in ice discharge at the lower edge of the thickened portion of the glacier. This increase in ice discharge is propagated down glacier by both advection and diffusion.

The largest $\frac{dH}{dt}$ is coincident with the largest $\frac{dh_{debris}}{dt}$ (within the first 100-150 years of the transient calculations). Surface debris thicknesses equilibrate with debris emergence rates faster than ice thicknesses equilibrate with the debris perturbed surface mass balance (Fig. 3.15 F, I). The local thickening caused by the debris decreases the ice surface slope on the up-stream side of the emerging debris patch. Reducing α reduces the ice flux gradient upstream of the emerging debris, which leads to thickening and a reduction of ice surface slope up glacier from the debris. The ice thickness perturbation caused by the debris emergence is propagated up glacier, where the ice thickness change from the debris-perturbed case to the debris-free case decreases in magnitude the further up glacier from the actual debris cover (e.g., Nye 1963; Alley and Willans, 1984; Cuffey and Patterson, 2010). When the glacier advances into a new cell the toe cell thickens until the ice thickness is nearly steady and $\dot{b} \approx \frac{\partial Q}{\partial x}$. The toe advances until a new steady state is reached. The length of the glacier depends on the parameterization of glacier terminus mass balance.

3.5.6 The problem at the terminus

The 100 m *dx* limits the model's ability to accurately represent the debris-covered terminus. When a new cell is formed during advance, the cell is initially debris-free. Because of the different ice physics (*dt*) and debris advection (*dt_advect*) time steps the ice advected from the toe cell into the foreland is subject to a non-debris perturbed melt rate. If non-debris perturbed melt rate * *dx* is larger in magnitude than the ice passed from the glacier toe cell into the first foreland cell, the glacier will no longer advance. Our results therefore depend on how the glacier toe is parameterized. With that said, glaciers further with net mass balances further

As debris thickens to the point were sub-debris melt rates approach zero, $\frac{dQ}{dx}$ also tends toward zero. If $\frac{dQ}{dx}$ does reach zero, the glacier would theoretically continue to advance in perpetuity. Konrad and Humphreys, 2000 applied the same argument to rock glaciers. Mechanisms exist to limit the extent of debris-covered glaciers even where $\dot{b}$ nearly declines to zero. If $\dot{b}$ is nearly zero, the change H and $\bar{u}$ in space will also be nearly zero. Debris-covered termini may support bare ice faces or thinner debris that increase mass loss and may limit glacier extent (e.g., Benn and Lehmkuhl, 2000; Shroder et al., 2000; Anderson et al., in review). Debris-covered glaciers are also primed to produce large drop moraines or latero-frontal fans; if the mass advected off the glacier is large, the glacier can become mired in the very debris it transported, leading to exceptional moraines that impede glacier advance (Benn and Evans, 2010).

3.5.7 Implications and future work

While these model calculations represent idealized conditions, our results provide a theoretical backdrop for understanding the effect of debris-covered on glaciers. We now provide a brief summary of our results. Debris cover on glaciers, independent of climate change 1) reverses mass balance gradients; 2) extends glacier lengths; 3) reduces ice discharge gradients; 4) lowers glacier surface slopes (and therefore ice thickness gradients); 5) reduces the magnitude and gradient of u_{surf}; and 6) reduces englacial velocities (both u and w).

The greater the rate of debris deposition in the accumulation zone, the more perturbed the glacier mass balance will become, and the longer the glacier will extend. This is true until the supraglacial environment becomes saturated with debris, at which point adding more debris to the glacier has a declining effect. Glaciers with zones of debris emergence near the glacier

terminus will tend to saturate at lower deposition rates than glaciers with debris emergence zones near the ELA.

A 1 meter thick debris cover near the terminus is more effective at perturbing the annual surface mass balance of a glacier than a 1 meter thick debris cover just below the ELA. Debris emerging near the terminus can also lead to significant bulges in ice thickness (e.g., Fig. 3.15A).

Debris-cover influences ice velocities and thickness up-glacier from the extent of the debris cover. The thickness perturbations caused by emerging debris are diffused up glacier, leading to lower ice surface slopes and greater ice thicknesses than on a debris-free glacier of comparable size.

With measured glacier surface velocities and debris cover thickness it may be possible to determine the relative importance of supraglacial debris strain and debris emergence rate on surface debris thickness profiles. We also highlight the need for more field studies of debris dynamics at glacier termini, as the processes of ablation at the terminus are poorly understood.

Most importantly, our model calculations lay the foundation for future efforts to assess the response of debris-covered glaciers to climate change. We hope that this work serves as a catalyst for linking in-situ and remotely sensed debris-covered glacier data to numerical modeling of the system. Future modeling efforts could explore 1) the effect of ice faces or surface melt ponds on the dynamics and extent of debris-covered glaciers; 2) potential feedbacks between glacial sliding and debris cover (How does melt suppression effect basal sliding?); 3) assess the importance debris-cover on ice dynamics using higher order ice physics models; 4) the effect of interannual debris deposition variability; 5) the effect of interannual climate variability on debris-covered glacier length; 6) the effect of using a full energy balance model for sub-debris melt; 7) exploring additional debris sources; or 8) allow the mean climate to cycle, and see how

debris-covered glaciers respond over multiple climate cycles, with potential implications for the moraine record.

3.6 References Cited

Anderson, R.S., 2000, A model of ablation-dominated medial moraines and the generation of debris-mantled glacier snouts: Journal of Glaciology, v. 46, no. 154, 459–469, (doi: 10.3189/172756500781833025).

Arsenault, A.M. and Meigs A.J., 2005, Contribution of deep-seated bedrock landslides to erosion of a glaciated basin in southern Alaska: Earth Surface Processes and Landforms, v. 30, no. 9, 1111–1125, (doi: 10.1002/esp.1265).

Ballantyne C.K., 1994, The Periglaciation of Great Britain: CUP Archive.

Benn D.I., Bolch T., Hands K., Gulley J., Luckman A., Nicholson L.I., Quincey D., Thompson S., Toumi R. and Wiseman S., 2012, Response of debris-covered glaciers in the Mount Everest region to recent warming, and implications for outburst flood hazards: Earth-Science Reviews, v. 114, no. 1-2, 156–174, (doi: 10.1016/j.earscirev.2012.03.008).

Benn, D. I., and Evans, D.J.A., 1998, Glaciers and glaciation: London. Edward Arnold. 734 p.

Benn, D.I. and Owen, L.A., 2002, Himalayan glacial sedimentary environments: a framework for reconstructing and dating the former extent of glaciers in high mountains: Quaternary International, v. 98, p. 3–25, (doi: 10.1016/S1040-6182(02)00048-4).

Bolch T., Buchroithner M., Pieczonka T. and Kunert A., 2008, Planimetric and volumetric glacier changes in the Khumbu Himal, Nepal, since 1962 using Corona, Landsat TM and ASTER data: Journal of Glaciology, v. 54, no. 187, 592–600, (doi: 10.3189/002214308786570782).

Boulton G. and Eyles N., 1979, Sedimentation by valley glaciers: a model and genetic classification: In Moraines and Varves (C. Schluchter, Ed.): Balkema, Rotterdam.

Bozhinskiy, A.N., Krass, M.S. and Popovnin V.V., 1986, Role of debris cover in the thermal physics of glaciers: Journal of Glaciology, v. 32, no. 111, 255–266.

Budd W.F. and Jenssen D., 1975, Numerical modelling of glacier systems. IAHS Publ., v. 104**,** 257–291.

Conway H. and Rasmussen L.A., 2000 Summer temperature profiles within supraglacial debris on Khumbu Glacier, Nepal, in Debris-covered Glaciers: Proceedings of an International Workshop Held at the University of Washington in Seattle, Washington, USA, 13-15 September 2000, p. 89.

Cuffey K.M. and Paterson W.S., 2010, The physics of glaciers: Elsevier, Oxford, UK.

Eyles, N. and Rogerson, R.J., 1978, A framework for the investigation of medial moraine formation: Austerdalsbreen, Norway, and Berendon Glacier, British Columbia, Canada: Journal of Glaciology, v. 20, 99–113.

Heimsath, A.M. and McGlynn, R., 2008, Quantifying periglacial erosion in the Nepal high Himalaya. Geomorphology, v. 97, no. 1-2, 5–23, (doi: 10.1016/j.geomorph.2007.02.046).

Humlum, O., 2000, The geomorphic significance of rock glaciers : estimates of rock glacier debris volumes and headwall recession rates in West Greenland. Geomorphology, v. 35, 41-67.

Humlum, O., 2005, Holocene permafrost aggradation in Svalbard. Geological Society, London, Special Publications, v. 242, no. 1, 119–129, (doi: 10.1144/GSL.SP.2005.242.01.11).

Kessler, M.A., Anderson, R.S. and Stock, G.M., 2006, Modeling topographic and climatic control of east-west asymmetry in Sierra Nevada glacier length during the Last Glacial Maximum: Journal of Geophysical Research, v. 111, no. F2, F02002, (doi: 10.1029/2005JF000365).

Kirkbride, M.P., 1995, Ice Flow Vectors on the Debris-Mantled Tasman Glacier, 1957-1986: Geografiska Annaler, Series A: Physical Geography, v. 77, no. 3, 147–157.

Kirkbride, M.P. and Warren, C.R., 1999, Tasman Glacier, New Zealand: 20th-century thinning and predicted calving retreat. Global and Planetary Change, **22**(1-4), 11–28, (doi: 10.1016/S0921-8181(99)00021-1).

Konrad, S.K. and Humphrey, N.F., 2000, Steady-state flow model of debris-covered glaciers (rock glaciers). IAHS PUBLICATION, 255–266.

Konrad, S.K., Humphrey, N.F., Steig, E.J., Clark, D.H., Potter, N., and Pfeffer, W.T., 1999, Rock glacier dynamics and paleoclimatic implications. Geology, v. 27, no. 12, 1131, (doi: 10.1130/0091-7613, 1999)027<1131:RGDAPI>2.3.CO;2).

Marshall, S.J., Bjornsson, H., Flowers, G.E. and Clarke, G.K.C., 2005, Simulation of Vatnajökull ice cap dynamics: Journal of Geophysical Research, v.110, no. F3, 126–135, (doi: 10.1029/2004JF000262).

Messerli, B., 1968, Block gletscher im Weissmies und Aletsch und ihre photogrammetrische Kartierung. Die Alpen, v. 3, 139–152.

Naito, N., Nakawo, M., Kadota, T. and Raymond, C.F., 2000, Numerical simulation of recent shrinkage of Khumbu Glacier, Nepal Himalayas, in Debris-covered Glaciers: Proceedings of an International Workshop Held at the University of Washington in Seattle, Washington, USA, 13-15 September 2000, p. 245.

Nicholson, L. and Benn, D.I., 2006, Calculating ice melt beneath a debris layer using meteorological data: Journal of Glaciology, v. 57, no. 178, 463–470, (doi: 10.3189/172756506781828584).

Nye, J., 1965, The frequency response of glaciers: Journal of Glaciology, v. 5, no. 41, 567–587.

Oerlemans J., 1986, An Attempt to Simulate Historic Front Variations of Nigardsbreen, Norway. Theoretical and applied climatology, v. 37, 126–135.

Oerlemans, J. 2001, Glaciers and Climate Change: Lisse, NL, Swets and Zeitlinger, 160 p.

O'Farrell, C.R., Heimsath, A.M., Lawson, D.E., Jorgensen, L.M., Evenson, E.B., Larson, G. and Denner, J., 2009, Quantifying periglacial erosion : insights on a glacial sediment budget, Matanuska Glacier, Alaska. Earth Surface Processes and Landforms. v. 34, 2008–2022, (doi: 10.1002/esp).

Östrem G., 1959, Ice Melting under a Thin Layer of Moraine, and the Existence of Ice Cores in Moraines Ridges. Geografiska Annaler, v. 41, no. 4, 228–230.

Owen, L.A. and Derbyshire E., 1989, The Karakoram Glacial Depositional System. Zeitschrift für Geomorphologie, Supplementary Issues, v. 46, 33–73.

Owen, L.A., Derbyshire, E. and Scott, C.H., 2003, Contemporary sediment production and transfer in high-altitude glaciers. Sedimentary Geology, v. 155, 13–36.

Quincey, D.J., Copland, L., Mayer, C., Bishop, M., Luckman, A. and Belo M., 2009a, Ice velocity and climate variations for Baltoro Glacier, Pakistan: Journal of Glaciology, v. 55, 194), 1061–1071.

Quincey, D.J., Luckman, A. and Benn, D., 2009b, Quantification of Everest region glacier velocities between 1992 and 2002, using satellite radar interferometry and feature tracking: Journal of Glaciology, v. 55, no. 192, 596–606, (doi: 10.3189/002214309789470987).

Raper, S.C.B. and Braithwaite, R.J., 2006, Low sea level rise projections from mountain glaciers and icecaps under global warming: Nature, v. 439, no. 7074, 311–3, (doi: 10.1038/nature04448).

Reid, T.D. and Brock, B.W., 2010, An energy-balance model for debris-covered glaciers including heat conduction through the debris layer: Journal of Glaciology, v. 56, no. 199, 903–916, (doi: 10.3189/002214310794457218).

Roe, G.H. and Baker, M.B., 2014, Glacier response to climate perturbations: an accurate linear geometric model: Journal of Glaciology, v. 60, no. 222, 670–684.

Scherler, D., 2014, Climatic limits to headwall retreat in the Khumbu Himalaya, eastern Nepal: Geology, (September), (doi: 10.1130/G35975.1).

Scherler, D., Bookhagen, B. and Strecker, M.R., 2011a, Hillslope-glacier coupling: The interplay of topography and glacial dynamics in High Asia: Journal of Geophysical Research, v. 116, no. F2, F02019, (doi: 10.1029/2010JF001751).

Scherler, D., Bookhagen, B. and Strecker, M.R., 2011b, Spatially variable response of Himalayan glaciers to climate change affected by debris cover: Nature Geoscience, v. 4, no. 3, 156–159, (doi: 10.1038/ngeo1068).

Smolarkiewicz, P.K., 1983, A simple positive definite advection scheme with small implicit diffusion: Monthly Weather Review, v. 111, no. 3, 479–486.

Vacco, D.A., Alley, R.B. and Pollard, D., 2010, Glacial advance and stagnation caused by rock avalanches: Earth and Planetary Science Letters, v. 294, no.1-2, 123–130, (doi: 10.1016/j.epsl.2010.03.019).

Wagnon P, Vincent C, Arnaud Y, Berthier E, Vuillermoz E, Gruber S, Ménégoz M, Gilbert A, Dumont M, Shea JM, Stumm D and Pokhrel BK, , 2013) Seasonal and annual mass balances of Mera and Pokalde glaciers (Nepal Himalaya) since 2007: The Cryosphere, v. 7, no. 6, 1769–1786, (doi: 10.5194/tc-7-1769-2013).

Chapter 4 Surface relief and ice cliffs on debris-covered glaciers: A case study from the Kennicott Glacier, Alaska, USA

Leif S. Anderson[1], Robert S. Anderson[1], and William H. Armstrong[1]

[1]*Department of Geological Sciences and Institute of Arctic and Alpine Research, University of Colorado Campus Box 450, Boulder, Colorado 80309, USA*

4.1 Abstract

Debris cover suppresses ice melt on glaciers. However, the retreat of debris-free ice cliffs within otherwise debris-covered glaciers counters the insulating effect of debris. Glacier surface processes (such as differential melt under debris, supraglacial stream erosion, englacial conduit collapse, etc.) control spatial distribution of ice cliffs. We provide a theoretical framework for the production and removal of ice cliffs and glacier surface topography on debris-covered glaciers. We apply this framework to assess the causes of cliff distribution and the mass loss due to ice cliff backwasting on the Kennicott Glacier, Wrangell Mountains, Alaska. Throughout the study area we measured ice cliff backwasting, ice cliff geometry and orientation, sub-debris melt rates, and debris thicknesses. Using Worldview 1 imagery we documented the spatial distribution of ice cliffs, lakes, and supraglacial streams, in addition to calculating ice surface velocities and glacier surface relief at 10^4 m^2 scale. Linear ice-cliff concentration, defined as the concentration of long-axis ice cliff length per area, increases and then decreases through the debris-covered portion of the glacier. Mean debris thickness appears to be the primary control on glacier surface relief and ice cliff concentration. Thin mean debris thicknesses correspond to the largest relief and ice cliff concentration increases down glacier. Supraglacial streams increase in sinuosity within the debris-covered portion of the glacier, potentially leading to a positive feedback between supraglacial streams, relief production and ice cliff formation. Approximately 30% of

net mass loss from the study area is due to the backwasting of ice cliffs. In some elevation bands approximately 55% of the total melt is due to ice cliff backwasting. Our results highlight the importance of ice cliff backwasting and the processes that control their distribution on debris-covered glacier surface mass loss.

4.2 Introduction

Debris-covered glaciers are prominent in highly erosive settings and are especially prominent in Asia, Alaska, and the Andes (Kirkbride, 2011). The effect of debris on glacier response depends on the percentage of a glacier covered with debris and the thickness of the debris cover. Debris cover greater than a few centimeters suppresses melt rates and can in some instances completely arrest ablation (Östrem, 1959). Debris cover therefore tends to suppress melt rates and decrease surface melt. Debris thicknesses range from millimeters up to about 2 meters or more for stagnant glacier termini (Kirkbride, 2011). We use the term *debris-covered glacier*, after Kirkbride (2011) to refer to glaciers on which any part of the ablation zone has a 'continuous' debris cover across the full glacier width (ice cliffs excluded, see below).

Debris is often incorporated into or deposited onto valley glaciers. Supraglacial debris in the ablation zone is held at the glacier surface until it is advected off the glacier. We refer to an area with debris resting on the glacier surface as a debris-covered area. Debris-covered areas are diverse and can vary considerably depending on the processes of debris transport and the volume of debris present within the area. We therefore present a classification scheme to help categorize and describe this variability. We use this classification scheme throughout the paper. Areas that are completely debris-covered (no ice exposed) are referred to as areas of *continuous* debris cover. If some ice is exposed within a larger area of continuous debris cover, it is *partially* debris-covered. These definitions are scale dependent. Partial-debris-covered areas can be

volume-limited, transport-limited, or *slope-limited*. A *volume-limited* area occurs where there is not enough debris to cover the entire area. The area is *transport-limited* if enough volume of debris exists to cover the area but there is no process to transport the debris across the entire area. Lastly, the area is *slope-limited* if there are debris-free slopes steeper than the angle of repose (i.e. ice cliffs) but enough debris volume to completely cover the area of interest. We focus on slope-limited debris-covered areas in this study.

Debris-covered glacier surface elevation can vary over short distances. It is important to differentiate between glacier surface slope averaged over hundreds of meters and smaller-scale fluctuations in debris-covered glacier topography. Steep local glacier surface topography is a prerequisite for the formation of ice cliffs on debris-covered glaciers; exposed ice can only be maintained if it is steeper than the angle of repose. Debris-cover itself plays the primary role in creating the glacier surface topography needed to form ice cliffs. Debris thicknesses can vary greatly over short distances, leading to local melt gradients, and the formation of surface topography (e.g. Benn and Evans, 2010), where here *local* refers to 50 m length scales.

Surface relief, R, is defined as:

$$R = z_{\max} - z_{\min} \tag{4.1}$$

where z_{max} is the maximum elevation and z_{min} is the minimum elevation over an area with horizontal length scale λ. An increase in local glacier surface relief corresponds to an increase of local glacier slopes, R/λ. Surface relief is always scale dependent. In this paper, we refer to surface relief over an area of 10,000 m^2 (λ = 100 m) or less. Increasing local relief and hence local slope increases the potential for debris to slide, expose bare ice, and form ice cliffs, which then melt perpendicular to the bare ice surface (i.e., backwaste).

Because many ice cliffs are ephemeral, models of debris-covered glacier mass balance must also account for the creation and destruction of ice cliffs. The formation and destruction of ice cliffs on debris-covered glaciers is inherently linked to a variety of glacier surface processes such as englacial conduit collapse, differential ablation under different local debris thicknesses, or the incision of a supraglacial stream increasing local glacier surface slopes (Reid and Brock, 2014; Sakai et al., 2002). The spatial variability of these processes controls the spatial pattern of ice cliffs. In order to develop models that account for the formation and destruction of ice cliffs in response to changing debris cover and warming climates, we must document and understand the processes setting the spatial distribution of ice cliffs. Our aims in this paper are twofold: 1) to link debris-covered glacier surface processes to glacier surface relief and the spatial distribution of ice cliffs on the Kennicott Glacier; and 2) to determine the importance of ice cliff spatial distribution on the surface mass balance of the debris covered portion of the Kennicott Glacier.

4.2.1 Study site

The Kennicott Glacier is located in the Wrangell Mountains, Alaska (Fig. 4.1; 61.48°, -142.92°; 42 km long; 387 km^2 area; Rickman and Rosenkrans, 1997; Anderson et al., 2003; Bartholomaus et al., 2008, 2011; Korn, 2010; Das et al., 2014). Twenty percent of the total glaciated area is covered with debris. The glacier supports 11 distinct ice-stream interaction medial moraines (see Eyles and Rogerson, 1978; referred to as medial moraines below), which coalesce 7 km from the terminus to form a continuous debris mantle (Fig. 4.1B). The Kennicott Glacier is both relatively high in latitude (61°N) and supports a high linear concentration (the total planview long-axis ice cliff length per area; Fig. 4.2) of ice cliffs in the lower 7 km of the glacier. The glacier hosts a variety of supraglacial debris-process domains including: *volume-limited* partial debris cover, *slope-limited* partial debris cover over active ice, and *slope-limited*

partial debris cover over “dead” ice These domains are characterized by specific combinations of relief-changing processes.

We first present our methodology. Second, we provide a review of the processes that control relief production, reduction, and maintenance on debris-covered portions of glaciers. Third, we describe how relief-changing glacier surface processes vary in space. Fourth, we present debris thickness, sub-debris melt rates, glacier surface relief, ice cliff geometry, ice cliff distribution in space, and ice cliff backwasting results. Last, we present melt rate calculations allowing estimates of the negative mass balance in the terminus reach, and discuss implications.

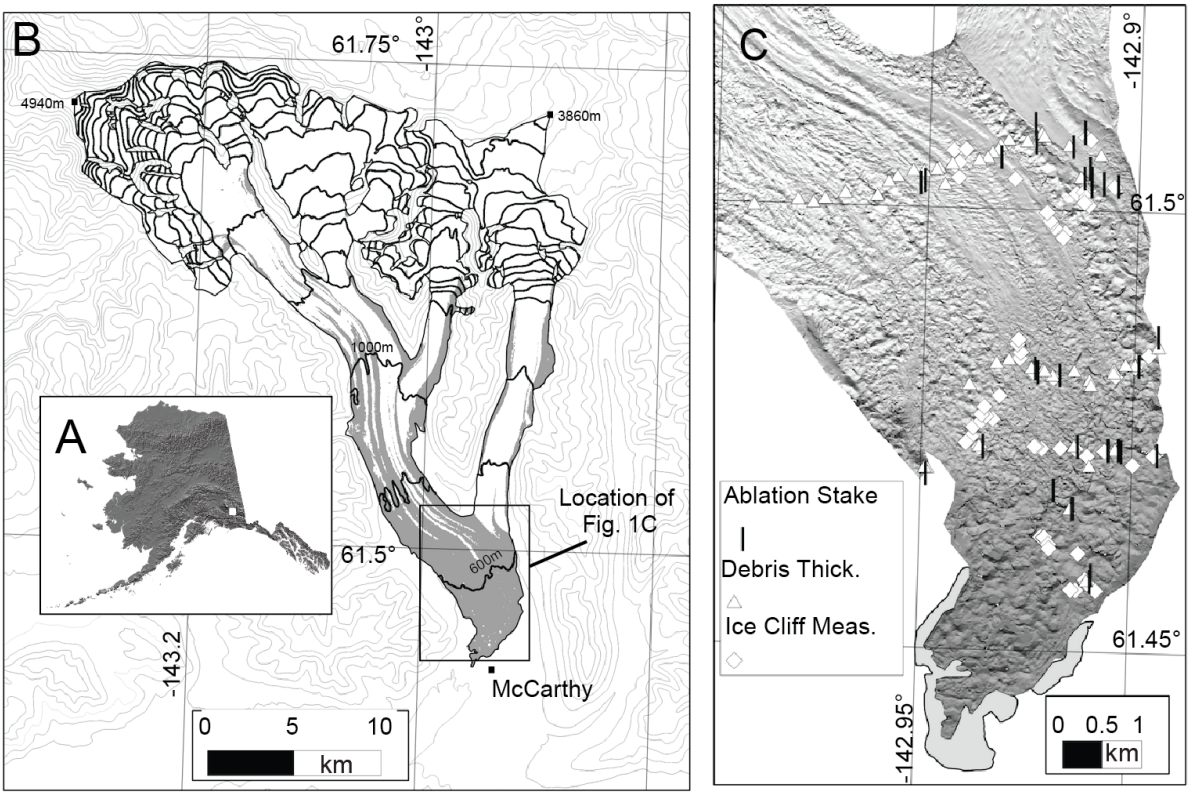

Figure 4.1 A) Map of Alaska showing the location of the Kennicott Glacier. B) Map of the Kennicott Glacier with contours derived from the 2009 SRTM DEM. C) Detailed hillshade of the glacier terminus showing the data collection sites. Proglacial lake Kennicott has existed in front of the glacier since at least 1990 and has been expanding since its inception. Subaerial melting, waterline melting, and flake calving are all causing ice loss from the ice-bounded lake margin (e.g., Benn et al., 2001).

4.3 Field Measurements and Methods

We conducted a two-month study on the Kennicott glacier between mid-June and August 2011 to measure debris thicknesses, sub-debris melt rates, ice cliff backwasting rates, ice cliff slopes, and ice cliff geometry. We used 0.5 m resolution WorldView 1 satellite imagery (WV1) to document the orientation and length of all ice cliffs, to trace supraglacial stream paths and supraglacial lakes, to produce glacier surface digital elevation models (DEMs), and to extract glacier surface velocities. The DEMs were used to calculate glacier surface relief across the study area.

4.3.1 Debris thickness and sub-debris melt measurements

We documented debris thicknesses at 165 locations throughout the study area (Fig. 4.1C; 4.2) and measured debris thicknesses at the top of ice cliffs or by digging pits through the debris to the ice surface (after Zhang et al., 2011). We measured the sub-debris ablation rate at 74 locations using PVC poles (Fig. 4.1C). We removed the debris, drilled holes into the ice, installed the poles and then replaced the debris (Fig. 4.2). We placed stakes at elevations ranging from 450 to 700 meters and in debris up to 40 cm thick in each of the 11 coalesced medial moraines (Fig. 4.1C).

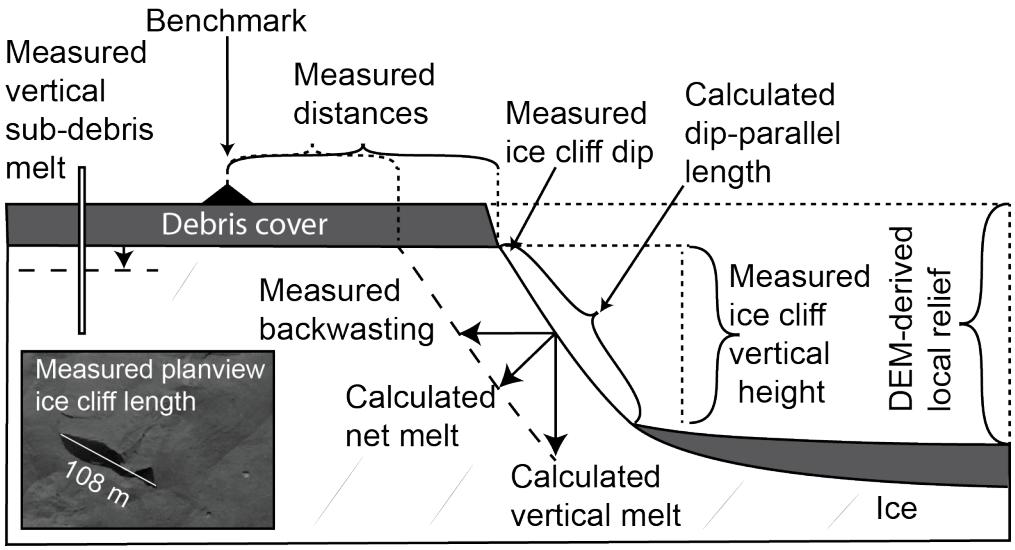

Figure 4.2 Schematic of field measurements and calculated rates and dimensions. Panel shows an ice cliff from the "dead" ice zone of the glacier and an example of the measurement of planview ice cliff length.

4.3.2 Ice cliff measurements

We collected melt rate and geometry data from 60 ice cliffs between 700 and 450 m elevation. Ice cliffs were selected so that all orientations (in 10° bins) were represented. We calculated ice cliff backwasting from repeat horizontal distance measurements between the upper ice cliff edge and a stationary marker (Fig. 4.1; 4.2; after Han et al., 2010). Ice cliff length and height were measured using a laser total station, while ice cliff slope (or dip) was measured using an inclinometer. We then calculated ice cliff area parallel to the ice cliff surface slope because net ice-cliff melt occurs perpendicular to this surface (Fig. 4.2). We manually traced the long-axis length and documented the orientation and elevation of all (~30,000) ice cliffs in the study area in QGIS using a WV1 image from August 2009 (~0.5 m resolution).

4.3.3 Supraglacial stream and lake documentation

We traced all visible supraglacial streams using the WV1 image from August 2009 (~0.5 m resolution) in QGIS. We interpolated stream paths between sites of positive stream identification using undercut ice cliffs. Many smaller streams on the Kennicott glacier are not visible in the WV1 imagery and are therefore not captured in the survey. Supraglacial lake areas were documented throughout the study area. Recently drained lakes were traced based on their high water lines.

4.3.4 Glacier surface relief and velocity

We calculated surface relief over a 10,000 m^2 window using TopoToolbox Matlab functions and a 5-m horizontal resolution DEM derived from two July 15, 2013 WV 1 stereo-pair images (Schwanghart and Kuhn, 2010). We calculated glacier surface velocities using two WV1 images from June 19 and July 15, 2013, using feature-tracking in the program Cosi-Corr (Leprince et al., 2007).

4.4 Theoretical Background

We now present a theoretical background for relief change on the glacier surface. The local rate of change of glacier surface relief, *R*, is

$$\frac{\partial R}{\partial t} = \frac{\partial z_{\max}}{\partial t} - \frac{\partial z_{\min}}{\partial t}. \tag{4.2}$$

The rate of change of elevation of the glacier surface, $z = z_{bed} + H$, is dependent on the time rate of change in ice thickness $\frac{\partial H}{\partial t} = \dot{b} - \frac{\partial Q}{\partial x}$. If the area over which relief *R* is defined is small enough, changes in the gradient in ice discharge $\frac{\partial Q}{\partial x}$ and glacier bed elevation, z_{bed}, are small enough to be neglected and equation 4.2 becomes

$$\frac{\partial R}{\partial t} = \dot{b}(z_{\max}) - \dot{b}(z_{\min}), \tag{4.3}$$

where $\dot{b}(z_{\max})$ is the local surface mass balance at the location of maximum local elevation and $\dot{b}(z_{\min})$ is the local surface mass balance at the location of minimum local elevation in the area over which relief is calculated. The local difference in the melt rate controls glacier surface relief production. If $\dot{b}(z_{\max})$ decreases (e.g., from 2 m/yr of melt to 1 m/yr) relative to that at the elevation minimum, relief *R* will increase (and visa versa). Likewise, if the magnitude of $\dot{b}$ at z_{min} increases relative to $\dot{b}$ at z_{max}, *R* increases (and visa versa). $\frac{\partial R}{\partial t}$ in equation 4.3 is the rate of change of local relief not taking into account down-glacier advection. Taking the Lagrangian point of view, the total derivative of glacier surface relief becomes:

$$\frac{DR}{Dt} = \frac{\partial R}{\partial t} + \frac{\partial U_s R}{\partial x}, \tag{4.4}$$

where U_s is the local ice surface velocity and $\frac{\partial R}{\partial x} = \frac{\partial z_{\max}}{\partial x} - \frac{\partial z_{\min}}{\partial x}$. $\frac{\partial R}{\partial x}$ accounts how relief changes down glacier and ultimately reflects how processes that control glacier relief and the mean glacier slope vary down glacier. It is important to note that in general processes effecting relief further from the equilibrium line altitude, *ELA*, will have more time to effect relief because glacier surface speeds tend to decrease toward valley glacier termini.

Change in surface relief through time as an area element is advected down glacier is therefore dependent on the local melt rates (or surface changes due to glacier surface collapse) at the highest elevation and lowest elevation points within the area of interest and how those melt rates vary in space. The processes that perturb vertical melt rates on debris-covered glaciers are numerous and are vital for interpreting the pattern of relief change on a glacier (e.g., Reid and Brock, 2014; Benn and Evans, 2010; Boyd et al., 2004; Sakai et al., 2002; Iwata et al., 2000; Eyles, 1979). We now outline the processes that can lead to the generation, reduction, and maintenance of debris-covered glacier surface relief.

4.4.1 Debris-covered glacier surface processes contributing to relief production

We now discuss processes that lead to increases in glacier surface relief ($\frac{\partial R}{\partial t}$ is positive). Reid and Brock (2014) highlight three sets of processes that produce bare ice cliffs, which coincide with processes of relief production: they dubbed them *C-type* related to crevasse formation, *M-type* related to steep slopes on medial moraines or glacier margins, and *H-type* formed from the interaction of surface and englacial water with ice to steepen ice slopes. Expanding on the observations of Reid and Brock (2014), we have identified six processes (Fig. 4.3) that increase glacier surface relief within supraglacial debris cover: 1) the differential melt of crevasse walls ($\dot{b}(z_{\min})$ is larger in magnitude than $\dot{b}(z_{\max})$). By lowering the equator-ward

facing crevasse wall, local relief is generated (*C-type*); 2) the oversteepening of debris-covered slopes due to differential melt under debris of different thickness (($\dot{b}(z_{\max})$ is smaller in magnitude than $\dot{b}(z_{\min})$ (*M-type;* Purdie and Fitzharris, 1999; Drewry, 1972; Östrem, 1959); 3) the collapse of englacial tunnels ($\dot{b}(z_{\min})$ is larger in magnitude than $\dot{b}(z_{\max})$ (*H-type;* Kirkbride, 1993); 4) the steepening of slopes on the edge of supraglacial ponds by thermal erosion and collapse ($\dot{b}(z_{\min})$ is larger in magnitude than $\dot{b}(z_{\max})$ (Benn et al., 2001; Purdie and Fitzharris, 1999); 5) the steepening of debris-covered slopes due to vertical incision by adjacent supraglacial streams ($\dot{b}(z_{\min})$ is larger in magnitude than $\dot{b}(z_{\max})$ (*H-type*; Schomacker and Kjaer, 2008; Boyd et al., 2004); and 6) steepening of debris-covered slopes due to lateral incision by supraglacial streams ($\dot{b}(z_{\min})$ is larger in magnitude than $\dot{b}(z_{\max})$ (*H-type*; Gulley and Benn, 2007; Boyd et al., 2004). The processes outlined above have the potential to increase glacier surface relief. There are certainly exceptions where supraglacial streambed melt does not outpace nearby surface melt, in which case relief will not increase.

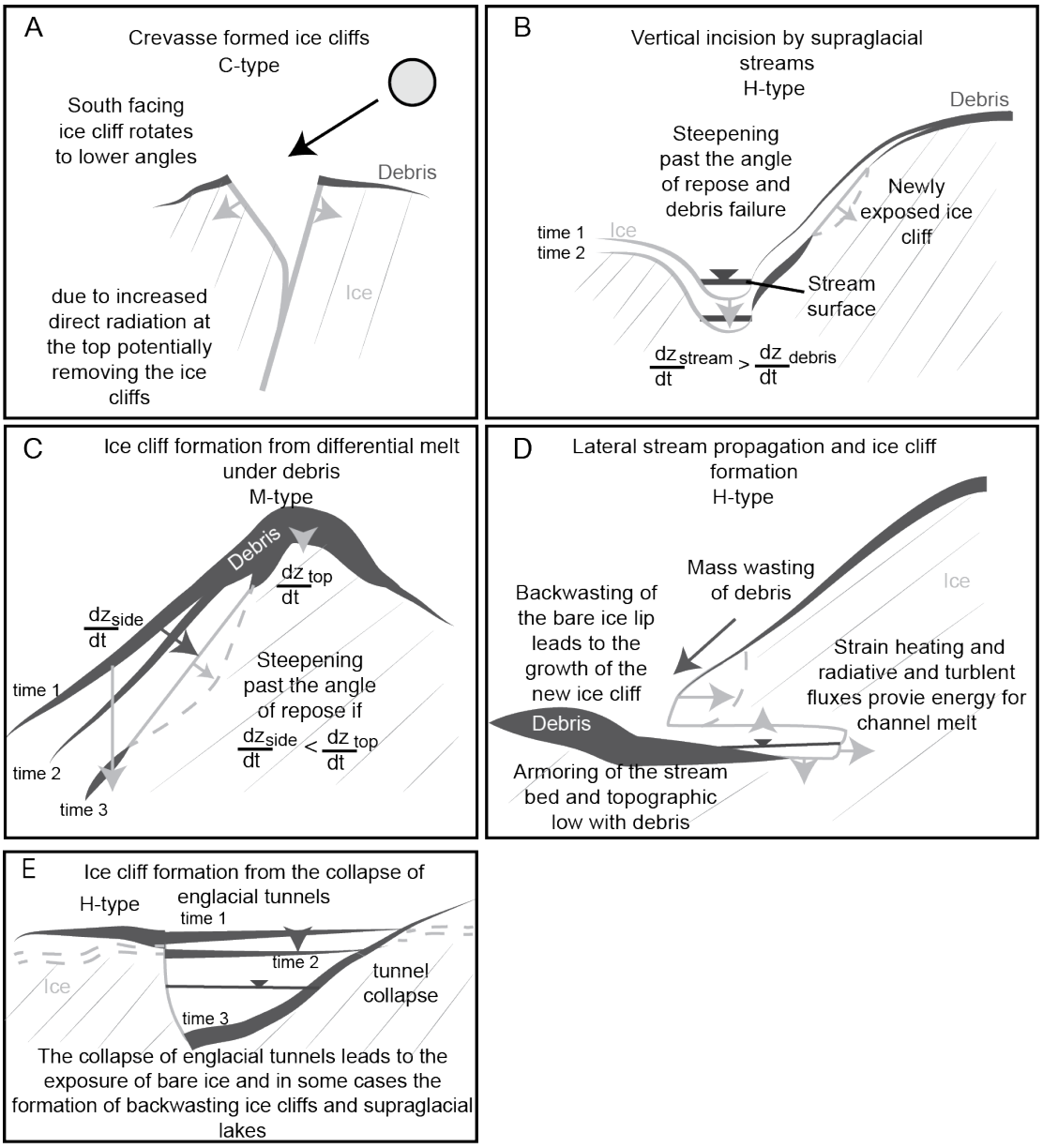

Figure 4.3 Ice cliff formation processes. A) Crevasse formed ice cliffs. B) Slope oversteepening caused by vertical supraglacial stream incision. C) Ice cliff formation from differential melt under debris. D) Ice cliff formation from lateral stream migration. E) Ice cliff formation by the collapse of englacial tunnels. F) Schematic showing the potential importance of surface relief in limiting the height of ice cliffs.

4.4.2 Debris-covered glacier surface processes contributing to relief reduction

The processes of relief reduction on debris-covered glaciers are the same processes that lead to the reduction of local slopes ($\frac{\partial R}{\partial t}$ is negative). We have identified four processes leading to the reduction of glacier surface relief: 1) the reduction of ice cliff slopes due to larger net radiation fluxes at the top of equatorward-facing ice cliffs due to differences in local shading ($\dot{b}(z_{\min})$ is larger than $\dot{b}(z_{\max})$ (defined as "layback", a process discussed by Sakai et al., 2002); 2) the burial of ice cliffs by accumulation of debris at the base of the ice cliff (as described by Reid and Brock (2014); Fig. 4.4C; 4.5D); 3) the backwasting of ice cliffs through local topography resulting in the removal of the topographic high and the ice cliff (Fig. 4.4A); and 4.4) the reduction of debris-covered slopes due to differential melt under debris of different thickness (thin debris on highs and thick debris in topographic lows, leading to a reduction in slope and the potential for topographic inversion). This relief-reducing effect lasts only until the highs are equal to the lows, at which point the differential melt under the debris again becomes a relief generating process. The effect of ice cliff layback and ice cliff burial are likely minor in changing the relief on >10,000 m^2 scales. These are local effects that remove ice cliffs from the supraglacial landscape but do little to change broader scale glacier surface relief. Increasing ice cliff backwasting rates not only increases the rate of topographic removal, but increases the chances that an ice cliff encounters an area of high debris thickness, which could result in ice cliff burial.

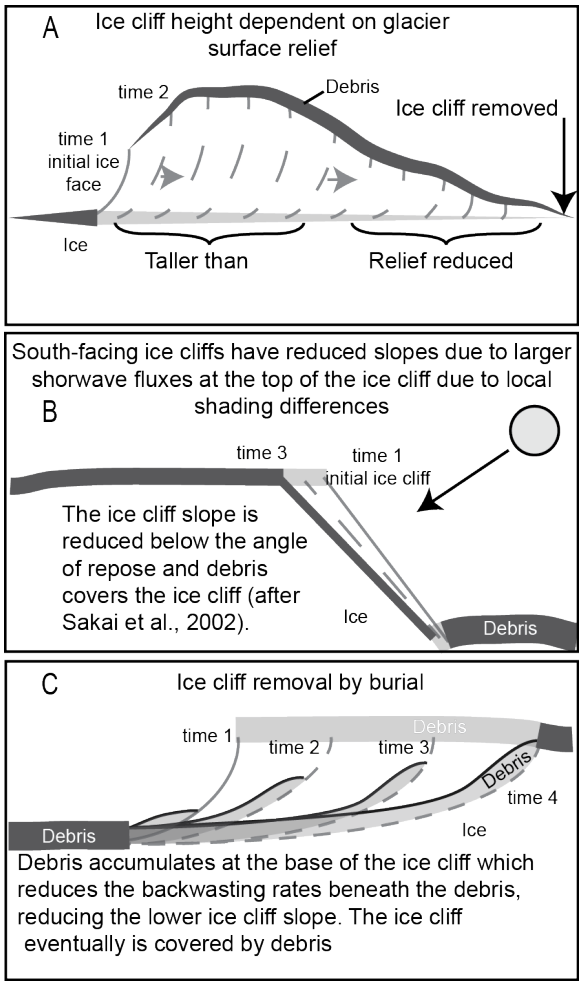

Figure 4.4 Ice cliff removal processes. (A) The dependence of ice cliff height on supraglacial topography. Ice cliffs that back waste through hills will remove the hill and be removed from the glacier surface. (B) For south-facing ice cliffs energy fluxes can be larger at the top of the ice cliff than at the bottom due to increased shading at the base of the ice cliff (Sakai et al. 2002). This can lead to the reduction of ice cliff dip below the angle of repose and the ice cliff can be buried by debris. (C) Debris can accumulate at the base of ice cliffs and gradually cover the ice cliff with debris, removing it from the glacier surface.

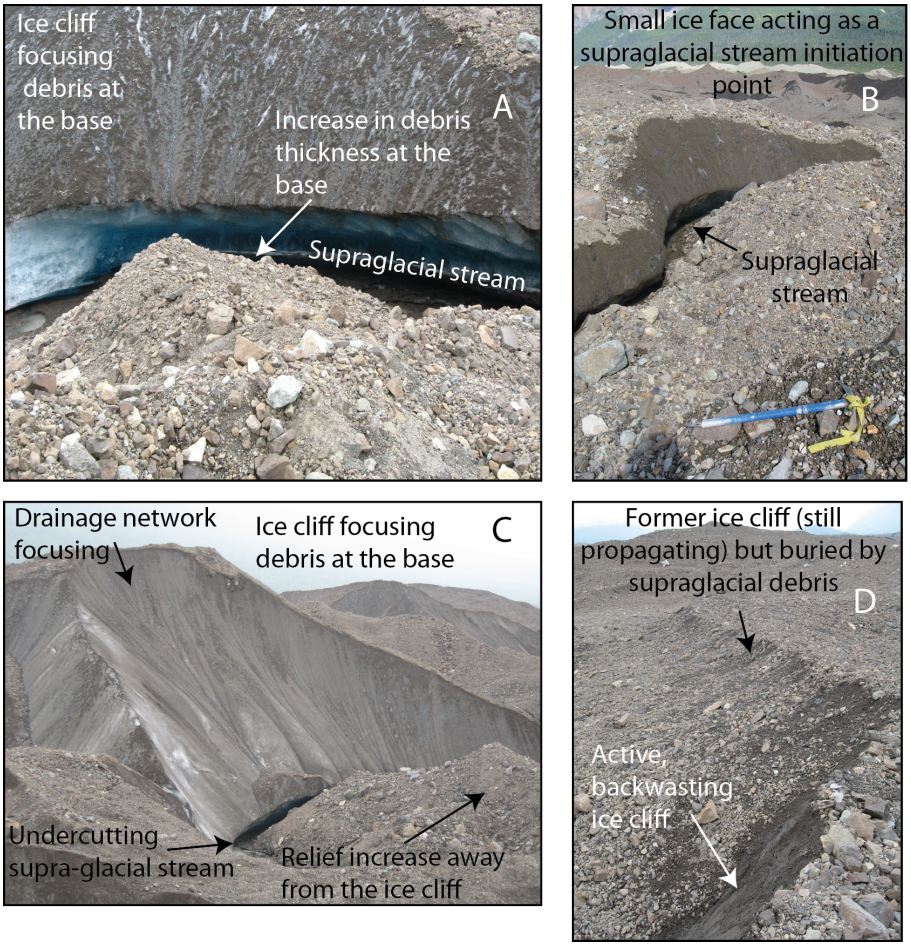

Figure 4.5 Photos of ice cliff processes. (A) An ~ 2m ice cliff showing the focusing effect of ice faces. (B) An ~ 1 m tall ice cliff which is acting as a supraglacial stream initiation point. Many small streams in the active portion of the glacier help form other small ice cliffs en route to larger inter-medial moraine streams. (C) A 20 m ice cliff undercut by a supraglacial stream. Debris is concentrated at the base of the ice cliff and surface relief increases away from the ice cliff. Notice the drainage network developed on the ice cliff. (D) An ice cliff being buried by debris in the "dead" ice portion of the glacier. Debris from the top of the ice cliff wastes to the base and then insulates a lower portion of the ice cliff until the entire cliff is covered with debris. The buried ice cliff retreated at 2 cm/day over a 48-day period.

4.4.3 Debris-covered glacier surface processes maintaining relief

Processes that tend to maintain supraglacial relief are also relevant for understanding the spatial variability of relief and ice cliffs. We have identified two processes that maintain glacier surface relief: First, supraglacial streams that undercut ice cliffs may prevent the destruction of ice cliffs by layback or by burial. The undercutting of ice cliffs often outpaces the sub-aerial retreat of the ice cliffs therefore limiting layback or ice cliff burial, which helps maintain glacier relief. Stream avulsion or a drastic change in stream discharge (potentially due to moulin development upstream) will remove this potential maintenance effect; Second, the larger the mean debris thickness in a particular area of the glacier, the more similar melt rates will become under variable debris thicknesses (e.g., Östrem, 1959). The melt rates become less variable in space, bringing the supraglacial landscape closer to steady state, where $\frac{\partial R}{\partial t} = 0$. Because debris cover tends to increase down glacier (e.g., Benn and Evans, 2010), rates of glacier surface relief production and reduction should generally decline toward the terminus.

4.4.4 Links between relief change and ice cliff concentration

While relief production is required to form ice cliffs, all relief production does not result in the formation of ice cliffs. Ice cliffs are produced only when local slopes pass a threshold slope that depends on the grain size and sorting of debris (Drewry, 1972). Many ice cliffs are ephemeral features that will be buried if their slope falls below the angle of repose. In order to model the long-term evolution of debris-covered glacier mass balance, we must explicitly track the formation and removal of ice cliffs (Reid and Brock, 2014; Sakai et al., 2002). As a first step toward a quantitative, process-based approach to ice cliff evolution, we present an equation for linear ice cliff concentration change in time. At a point on the glacier, the rate of change of linear ice cliff concentration (the total planview long-axis ice cliff length per area) is determined by the

rate of ice cliff length generation, change, and removal as well as the advection of ice cliffs down glacier:

$$\frac{\partial C}{\partial t} = \dot{L}_F + \dot{L}_C + \dot{L}_R - \frac{\partial C U_s}{\partial x}, \tag{4.5}$$

where C is the linear concentration of ice cliffs, $\dot{L}_F$ is the rate of ice cliff length from new ice cliffs in the domain per time ($\dot{L}$[=] m/m^2/yr), $\dot{L}_C$ is the rate of change of existing ice cliff length in the domain per time, $\dot{L}_R$ is the rate of change of ice cliff length from ice cliffs removed in the domain per time, and U_s is the local glacier surface speed. We use the Σ notation because we are summing the full population of ice cliffs created, removed or changed within the domain of interest. The $\Sigma(L_{change})$term captures the processes that modify the geometry of existing ice cliffs. If we assume that the system is steady, $\frac{\partial C}{\partial t}$ is zero and the advection of ice cliff concentration down glacier must equal the rate of change of linear ice cliff concentration due to the creation, removal, or modification of ice cliffs with in the domain of interest.

4.5 Results

To guide our presentation of results, we define three general debris-surface process zones on the lower 7 km of the Kennicott Glacier. These zones are defined based on 1) the type of debris cover (e.g., *slope-limited*, *volume-limited* or *transport-limited* and partial or continuous debris covered areas); 2) changes in glacier surface slope; 3) the presence and character of supraglacial streams; and 4) the abundance of supraglacial lakes.

(1) ***The volume/transport-limited isolated medial moraine zone (also Zone 1)***

Above 650 m elevation, isolated medial moraines are present (Fig. 4.1) with parabolic cross-sections (e.g., Anderson, 2000; Fig. 4.6). Above 475 m elevation, medial moraines create local slopes, perpendicular to the flow direction, that are much steeper than the average down-

glacier ice slope (Fig. 4.1) and therefore control local routing of supraglacial streams. Surface water is directed toward swales between medial moraines where the largest supraglacial streams reside (Fig. 4.6). Streams in the isolated medial moraine zone display low sinuosity (Fig. 4.6). Few debris-covered, ice-cored topographic cones are present and are concentrated in the medial moraines toward the glacier margin. Debris cover is typically a single clast thick except for medial moraines near the ice margin.

(2) ***The slope-limited partially debris-covered active-ice zone (also Zone 2)***

Between 650 m and 475 m elevation, the medial moraines have coalesced but are still separated by sinuous supraglacial streams (Fig. 4.6C; 4.6D). Ice-cored debris cones are more abundant in this zone (Fig. 4.6B) and local ice surface slopes generally increase (Fig. 4.7C). A distinct line of moulins at about 500 m elevation, at the transition between the coalesced medial moraine zone and the "dead" ice zone, removes the major trunk streams from the glacier surface.

(3) ***The slope-limited partially debris-covered "dead" ice zone (also Zone 3)***

The reduction in mean ice surface slope below 475 m elevation (Fig. 4.7C) coincides with the loss of the original medial moraine parabolic form. Few supraglacial streams are present (Fig. 4.6; 4.8C). Supraglacial lakes are more abundant and are associated with most ice cliffs in this zone (Fig. 4.8C). Zone 3 is assumed to be inactive "dead" ice where surface velocities are negligible and the glacier is effectively wasting in place (Rickman and Rosenkrans, 1997). Through the results section, we link these zones to the debris thickness, surface relief, and linear ice cliff concentration.

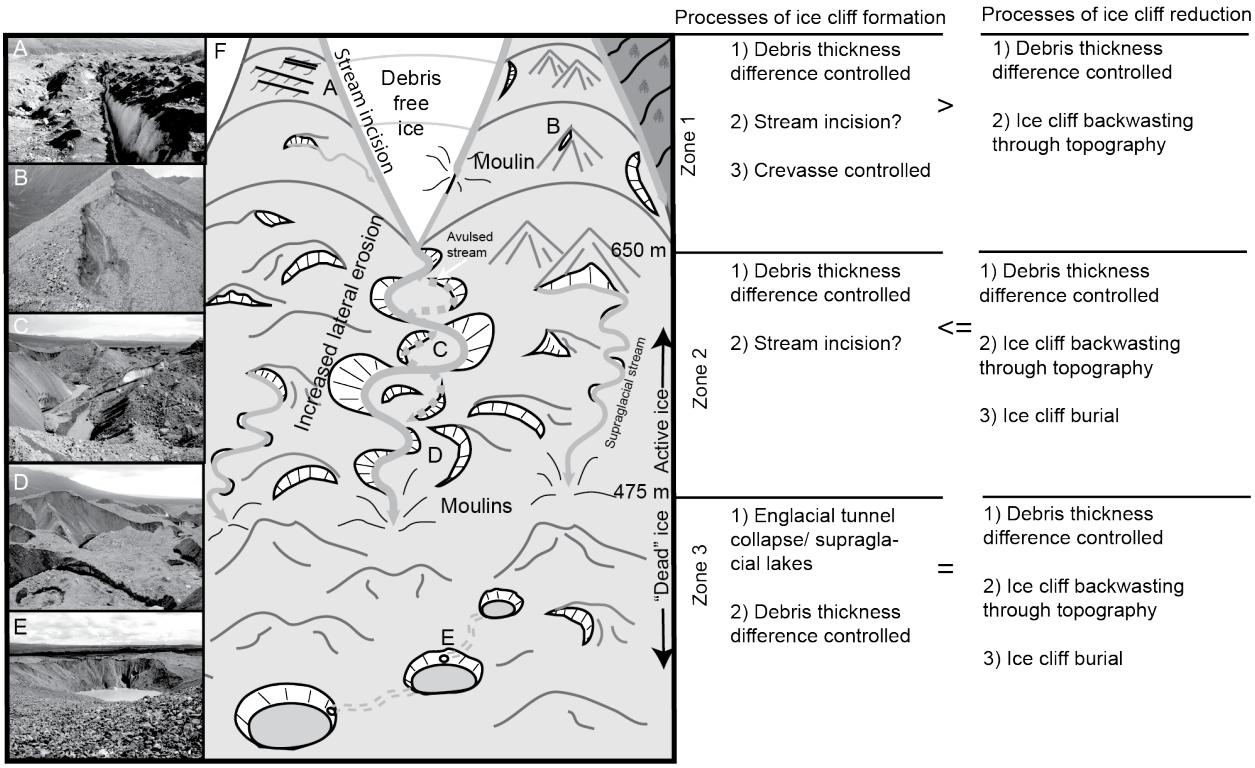

Figure 4.6 Distribution of ice cliffs related to supraglacial debris facies. Center) Schematic depicts a view up glacier from continuous debris-covered terminus into region of the glacier where debris occurs only on isolated medial moraines. Sites on the schematic are tied to photos: A) shows a small ice cliff formed from a crevasse; B) ice cliff formed from differential vertical melt, caused by differences in local debris thicknesses; C) sinuous supraglacial stream that has laterally eroded beneath several bare ice cliffs; D) similar to 3 but lower on the glacier where ice cliffs tend to be larger; E) ice cliffs associated with a supraglacial lake likely initiated by englacial tunnel collapse.

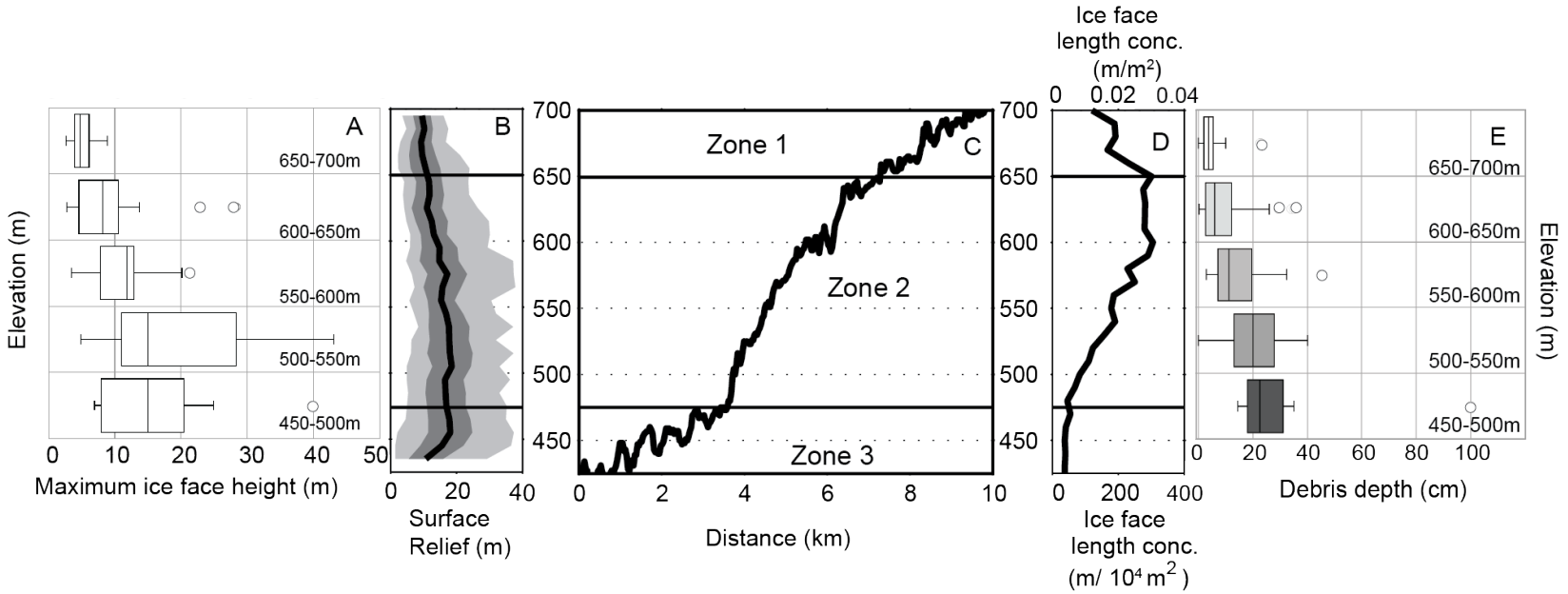

Figure 4.7 Plot comparing the Kennicott Glacier ice surface profile with several debris-related elevation profiles. A) Measured maximum ice cliff height. B) Glacier surface relief within a 50 m cell, measured in a swath down the center of the glacier. The black line is the mean relief, the dark grey shading shows the 1-sigma relief envelope and the light grey shading shows the range relief for each elevation band. C) Kennicott Glacier ice surface profile. D) Ice cliff length concentration per 100 m^2 with elevation. E) Supraglacial debris thickness.

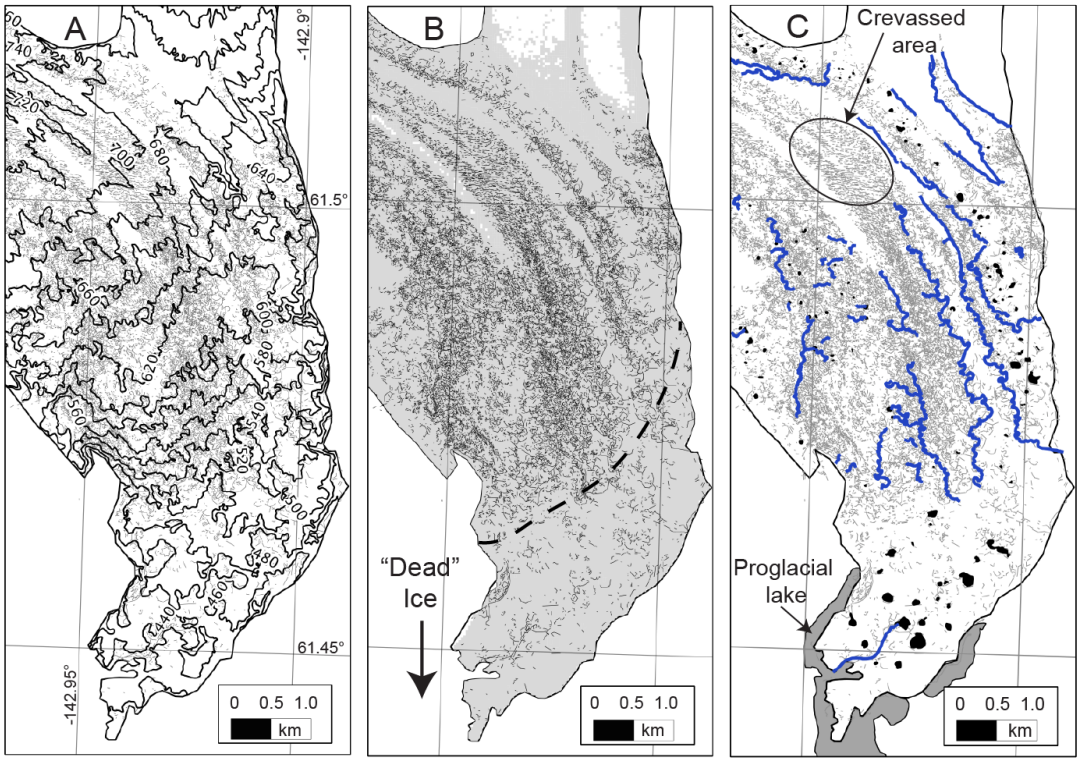

Figure 4.8 A) Map of the Kennicott Glacier terminal region with 20 m contours derived from a July 2013 Worldview 1 image. B) Map of the digitized ice cliffs in the terminal region of the glacier. Note the concentration of the ice cliffs into stripes associated with topographic lows, marking the boundary between medial moraines. Grey shading shows the areal extent of debris cover. We interpret the distinct change of slope at 475 m elevation (depicted by the dashed line) as the edge of the dead ice and the start of the active glacier margin. The chaotic surface topography with 20 m fluctuations below 475 m elevation is associated with broad debris-mantled hills and 100-200 m diameter supraglacial lakes. C) Map of ice cliffs with supraglacial streams (in blue) visible on the 2009 WV1 image and all supraglacial lakes visible in the same image (in black). Major streams are present between medial moraines and between coalesced medial moraines.

4.5.1 Debris thickness

Debris thickness increases down glacier. Linear regression of supraglacial debris thickness through the mean values of the binned debris thickness data (Fig. 4.9A) reveals a roughly 20 cm increase in debris thickness for every 100 m of elevation loss. Debris thickness in zone 1 is low and ranges from bare ice to 22 cm, with mean values of 5 cm. Zone 2 supports debris thicknesses that range from 1 to 44 cm, with mean values of 12 cm. Zone 3 supports debris thicknesses that range from 15 to 100 cm with a mean of 23 cm.

4.5.2 Sub-debris ablation

Sub-debris melt rates decreased non-linearly with debris thickness. Maximum melt rates were 7.7 cm/day (beneath 1 cm of debris) and minimum measured melt rates were 1 cm/ day (23 and 37 cm of debris) (Fig. 4.9B). The dependence of melt rate on debris thickness can be fit with either exponential [this is not shown on the figure] or power-law curves (Fig. 4.9B). For the exponential case the characteristic e-folding thickness scale is 10-11 cm. We ultimately chose the power-law fit in Figure 4.9B because it accommodates the asymptotic decay of melt rates towards zero as debris thickness increases. The humped relationship between melt rate and thin debris first shown by Östrem (1959), with maximum melt rates beneath very thin debris, was present in our data, but the variable melt rates beneath debris less than 3 cm thick prevents detailed analysis of this portion of the relationship (Fig. 4.9B).

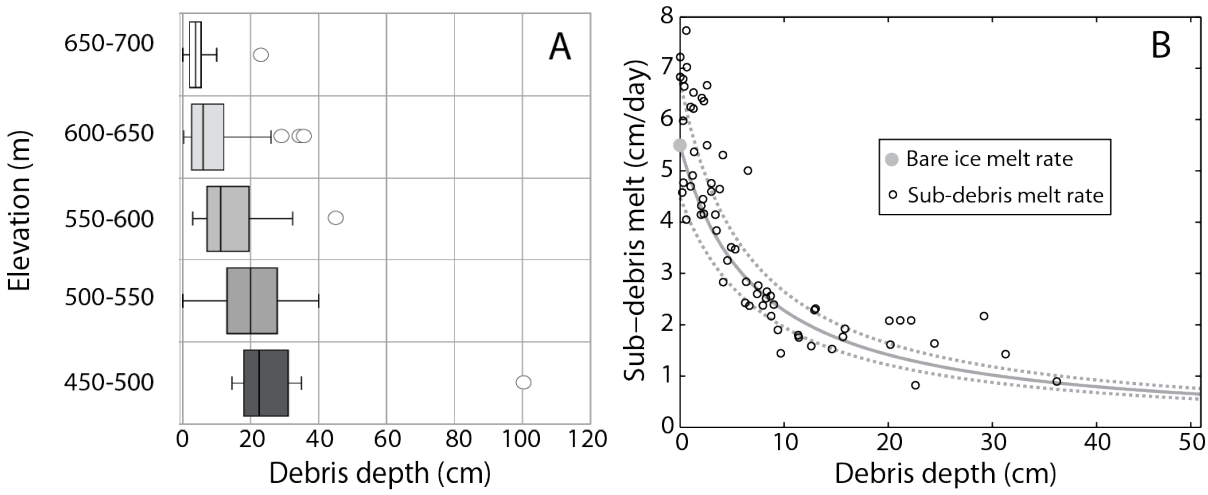

Figure 4.9 Debris thickness and sub-debris melt rate. A) Debris as a function of elevation in 500 m bins. B) Dependence of melt rate on debris thickness. Our best-fit line, defined by $m = (50 \pm 2.8)(h + (7.94 \pm 1.2))^{-(1.07 \pm .05)}$*, where m is melt rate in cm/day, and h is debris thickness in cm, both passes through the bare ice melt rate and asymptotes toward zero. The dashed lines represent the error bounds.*

4.5.3 Ice cliff backwasting and geometry

We documented ice cliff backwasting at 60 locations ranging from 430 to 700 m elevation (Fig. 4.1C). Retreat rate increases with decreasing elevation, from mean rates of 4 cm day^{-1} to 7 cm day^{-1} (Fig. 4.10A). Backwasting rates in zone 1 are half as large as backwasting rates in the lower portions of zone 2 and zone 3. Between 6.6 and 18.7% of the debris-covered terminus on the Kennicott glacier is bare ice in planview. The range of values is based on the uncertainty of average ice cliff dip and ice cliff geometry (40 to 50° and whether planview ice cliff area is better represented by triangles or rectangles). The average ice cliff slope on the upper 30 cm of ice cliff was 48°, ranged from 61° to 29°, with a standard deviation of 6° (for 120 measurements). The area of individual ice cliffs increases monotonically down glacier. Ice cliffs less than 100 m^2 are present in all elevation and orientation bins (Fig. 4.10B). West-facing ice cliffs tend to be larger in area and more variable in size than those with different orientations (Fig. 4.10D).

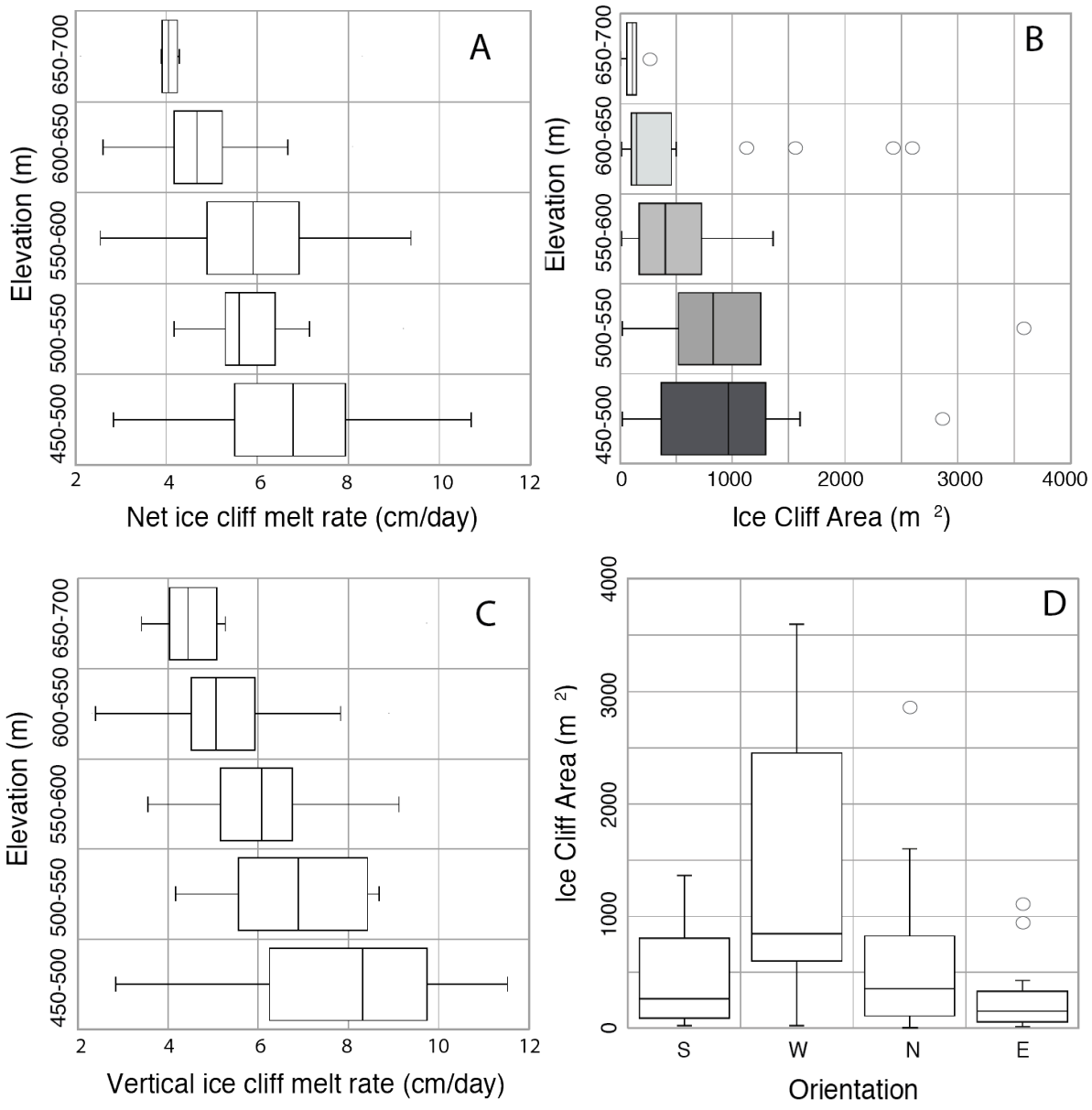

Figure 4.10 Ice cliff data. A) Net backwasting rate as a function of elevation in 500 m bins. B) Dependence of ice cliff area on elevation. C) Vertical ice cliff melt rate component. D) Ice cliff area with orientation for all measured ice cliffs.

4.5.4 Ice cliff spatial distribution

There are approximately 480 km (Fig. 4.5B) of ice cliffs in the study area. Ice cliff linear concentration (ice cliff length per unit area, averaged across 10m elevation bands) attains a maximum value at 650 m elevation, corresponding to the coalescence of the last separated medial moraines (Fig. 4.7D and 4.7C). Moving down glacier, ice cliff concentration declines beginning at 600 m elevation where mean debris thicknesses increase above 7.5 - 10 cm. Below 475 m, ice cliff concentrations are reduced even more and remain nearly uniform towards the terminus (Fig. 4.7D and 4.7E). The transition to near uniform ice cliff concentrations occurs close to the transition from zone 1 to zone 3. The number and total long-axis length of ice cliffs varies strongly with orientation, where north- and northwest-facing ice cliffs dominate the population (Fig. 4.11).

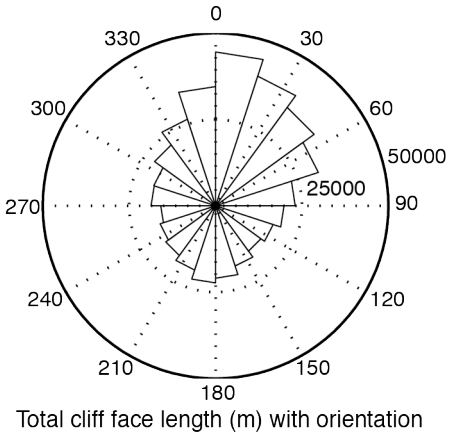

Figure 4.11 Rose diagram of total ice cliff length as a function of orientation derived from the full population of digitized ice cliffs. More ice cliffs face north and east.

4.5.5 Supraglacial streams and lakes

Supraglacial streams are most abundant in zone 2 with a linear concentration of 0.003 (m^{-1}). Zone 1 has a concentration of $1x10^{-3}$ m^{-1} whereas zone 3 has a concentration, with only one visible supraglacial stream, of $2x10^{-4}$ m^{-1}. Supraglacial streams are more sinuous in zone 2 than in zone 1. In zone 1 supraglacial streams have a mean sinuosity of 1.2 while the streams in zone 2 have a mean sinuosity of 1.7 (Fig. 4.12). Stream sinuosity varies more in zone 2 with a standard deviation of 0.54 compared to 0.23 for streams in zone 1. Supraglacial streams are absent in zone 3 except for one large stream connecting a supraglacial lake and proglacial lake (Fig. 4.8C).

The Kennicott glacier supports a small number of perched supraglacial lakes between 500 and 750 m elevation. The ice cliffs above these lakes account for only 2.4% of the total ice cliff area, and their backwasting rates do not differ significantly from retreat rates of lake-free ice cliffs. Supraglacial lakes are most abundant in zone 3, where they account for 3.5% of the glacier surface, whereas only 0.7% is lake in zone 2 and 0.2% in zone 1 (Fig. 4.8C). We use supraglacial lake areal concentration in each zone as an indicator of the effects of supraglacial streams and englacial tunnel collapse on relief production.

4.5.6 Glacier surface relief

Mean and maximum glacier surface relief increase through the isolated medial moraine zone into the *slope-limited* active ice (to ~600 m elevation; Fig. 4.7B). As relief increases between 700 and 600 m elevation, relief production outpaces relief reduction (Fig. 4.7B). This increase in relief coincides with mean debris thicknesses that are at or below 7.5 -10 cm, for which the largest changes of melt rate occur for a given change in debris thickness. Below ~600 m mean and maximum glacier surface relief are nearly uniform to the terminus. The 1 standard

deviation envelope of relief reveals that the highest relief elements in each elevation band increase down-glacier.

Measured ice cliff maximum height, ice cliff area and glacier surface relief follow similar patterns (Fig. 4.7A and 4.7B). The variability of ice cliff area and height also increase down glacier, as does glacier surface relief.

4.5.7 Glacier surface velocity

Glacier surface velocity monotonically drops toward the terminus with ice velocities becoming indistinguishable from noise below 540 m elevation (Fig. 4.13). The areas in which the surface speeds are below 0.05 m d^{-1} are considered 'dead' ice, supporting the contention of Rickman and Rosenkrans (1997).

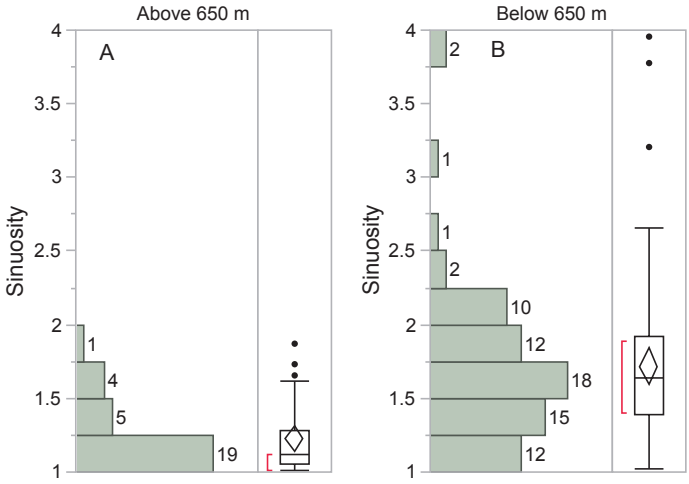

Figure 4.12 Supraglacial stream sinuosity derived from WV1 imagery. (A) Histogram and outlier box plot of stream sinuosities for streams above 650 m elevation. The red bracket shows the densest region of the data. The diamond contains the mean and the upper and lower 95% of the mean. (B) Histogram and outlier box plot of stream sinuosities for streams above 650 m elevation.

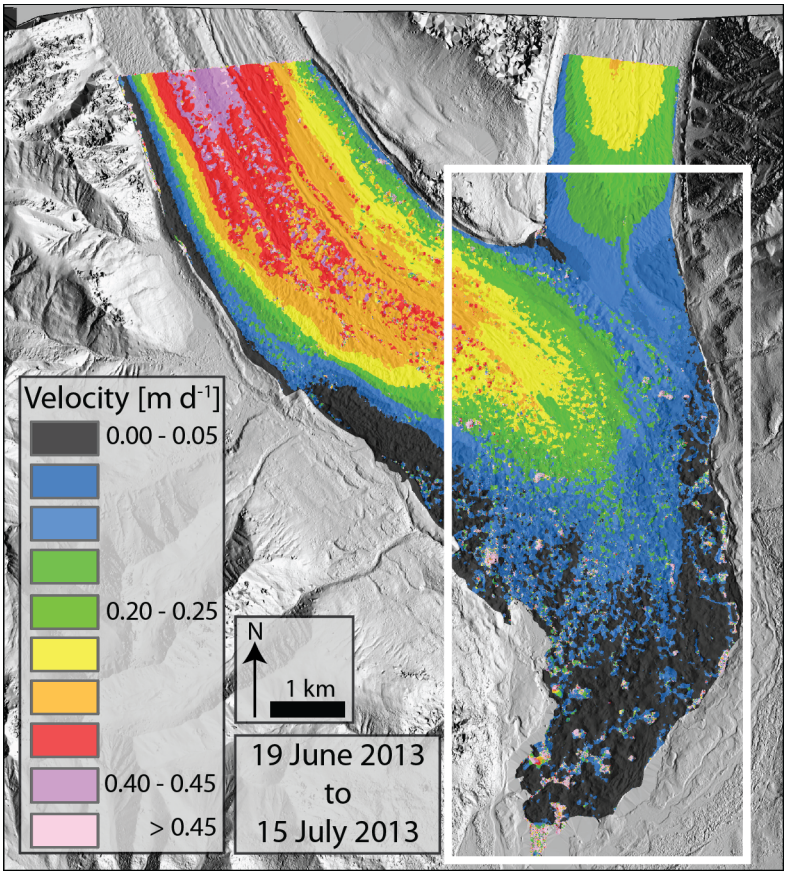

Figure 4.13 Glacier surface velocity map derived from 2013 WV1 imagery for the lower portion of the Kennicott Glacier. The white rectangle shows the extent of the panels in Figures 4.1 and 4.8. We consider the area if the glacier with surface velocities below 0.05 m d^{-1} to be inactive, or "dead" ice.

4.6 Discussion

4.6.1 Ice cliff melt rates and geometry

Net ice cliff melt rates increase down glacier nearly monotonically. This is likely caused by a combination of warmer air temperatures associated with the near-surface temperature lapse rate and the increase in debris cover at lower elevations, which leads to increased longwave fluxes from nearby the debris covered surfaces.

Between 6.6 and 18.7% of the debris-covered terminus of the Kennicott glacier is bare ice in planview. In contrast, the comparable metric on the Koxkar glacier in the Tien Shan Mountains is just 1.13% (Han et al., 2012), on the Lirung glacier in the Nepal Himalayas is 2% (Sakai et al., 2000), and on the Miage glacier, Mount Blanc massif, Italy, is 1.3% (Reid and Brock, 2014).

Individual ice cliff area and maximum ice cliff height monotonically increase down glacier, similar to glacier surface relief (Fig. 4.1C; 4.7A; 4.7B; 4.10B). This is not unexpected: ice cliff height and area should correlate with relief because ice cliffs cannot exceed glacier surface relief elements (Fig. 4.4A). Because higher relief hills can support small nascent ice cliffs and tall ice cliffs, variability in both ice cliff height and area increase toward lower elevations (Fig. 4.10B; 4.7A).

Nearly twice as many ice cliffs face pole-ward than equator-ward in the study area (Fig. 4.11). This is similar to the observations of Sakai et al. (2002) for glaciers in the Himalaya. Ice cliffs on debris-mantled glaciers may be preferentially oriented away from the strongest direct solar radiation fluxes. Sakai et al. (2002) hypothesized that shading at the base of south facing ice cliffs leads to reductions in ice cliff slope potentially below the angle of repose.

4.6.2 Supraglacial streams and lakes

Large supraglacial streams visible on WV1 imagery are more sinuous in zone 2 than in either zone 1 or 3. Supraglacial streams tend to transport more debris when in *slope-limited* partial debris-cover settings than in *volume-limited* debris-cover settings because there is both more debris available for transport and often times steeper slopes to move debris into the streams (Boyd et al., 2004). When streambed debris thicknesses exceed a few millimeters (or up to 1 cm for extreme parameters; see Isenko et al. (2005)) lateral channel wall melt rates outpace vertical rates. Even thin sediment at the streambed leads to undercutting of nearby debris-covered slopes (Fig. 4.5A). The tendency of supraglacial streams to meander and therefore incise laterally within zone 2 leads to the exposure of ice at the toes of the debris-covered slopes (Fig. 4.3D; 4.5A; 4.5C; 4.8C). This exposed ice can then propagate up the debris-covered slope, increasing relief while also forming new ice faces (Figs. 4.3D and 4.6).

Entrained sediment is preferentially deposited where basal shear stresses in the channels are low. Sediment is therefore more likely to be deposited on the inside of bends in supraglacial stream channels. This, in addition to the super-elevation of the water surface on the outside of the bend, causes increased lateral melt on the outer channel wall relative to the inner channel wall, potentially explaining the increased sinuosity of streams passing through zone 2 (Fig. 4.8C).

Increased concentrations of ice cliffs in the active portion of the glacier coincide with former medial moraine boundaries that localize supraglacial streams (Fig. 4.8). The lateral undercutting of ice cliffs may cause the crescent planview shape of ice cliffs seen on the Kennicott Glacier, where the crescent shape is set by the meander wavelength of the undercutting supraglacial stream.

The lack of supraglacial streams in zone 3 is likely related to both the reduction of sub-debris melt (and thus reduced water discharges) and the reduction of average glacier surface

slope. Reduced sub-debris melt rates will limit water available to form streams just as a reduction in glacier slope will allow the high glacier surface relief to reduce local drainage basin size. If streams do not have large enough discharges to transport the debris delivered to the channel, supraglacial water will be forced to flow interstitially within the coarse debris.

Supraglacial lakes are most abundant in zone 3 (Fig. 4.8C). The increase in the number and size of supraglacial lakes in this zone coincides with the dead ice portion of the glacier (e.g., Kirkbride and Warren (1999); Sakai et al., 2000; Benn et al., 2001; Röhl (2008).

4.6.3 Glacier surface relief

Relief increases down glacier from 700 m elevation to 575 m elevation. Relief generation processes therefore outpace relief destruction processes ($\frac{\partial R}{\partial t}$ is therefore positive) in this portion of the glacier (Fig. 4.7B). Both mean and maximum surface relief increase and are highly variable in this zone. Supraglacial ponds (and the inferred englacial tunnel collapses that lead to pond formation) cover a tiny fraction of this portion of the glacier and are therefore are not the primary driver of relief production. Supraglacial streams may play an important role in increasing surface relief in this zone, but further data are needed to determine the connection between stream erosion and relief production in regions with thin (<15 cm) debris cover. We hypothesize that the sub-debris melt pattern is the primary control on relief generation here. Debris cover is also the thinnest (mean <15 cm). The debris thickness-melt rate curve (Fig. 4.9B), suggests that variable, thin debris cover should produce greater sub-debris melt differences, which in turn lead to the greatest relief generation. Crevasses likely play a localized role in relief production in this portion of the glacier as well (Fig. 4.8C). Backwasting through topographic elements and the temporary relief-reducing effects of topographic inversion appear to be negligible in this portion of the glacier.

Relief is nearly uniform between 575 m and 475 m elevation ($\frac{\partial R}{\partial t} = 0$) either because relief generation balances relief destruction and/or both relief generation and destruction have been reduced to negligible values. We hypothesize that debris-cover plays the primary role in maintaining glacier surface relief in this portion of the glacier. Mean debris cover increases from 15 to 23 cm and becomes less variable in this zone. Thicker debris cover leads to smaller sub-debris melt rate variability and the increased likelihood that thick debris covers will preserve the topography. Crevasses are not present in this portion of the glacier and therefore play no role in the production of relief. Supraglacial ponds are increasingly abundant down glacier but their effect in increasing glacier surface relief is not apparent. Supraglacial streams may play an important role in producing glacier surface relief between 575 m and 500 m but their effects do not increase net glacier surface relief in this region.

4.6.4 Ice cliff spatial distribution

The linear concentration of ice cliffs (C) increases in zone 1 (700 m to 650 m elevation) is uniform (650 m to 600 m) and then decreases (600 m to 475 m) in zone 2 and is uniform in zone 3. C and R increase down glacier in zone 1, implying that relief and ice cliff producing processes are more effective than relief-reducing processes (Fig. 4.7). The maximum measured difference in sub-debris melt rates in zone 1, 7 cm/day, is the highest differential in the study area. Zone 1 therefore has the largest potential to increase R on the glacier from differential melt under debris (Fig. 4.9). We hypothesize that the rapid increase in R in this region with thin debris leads to the rapid increase in linear ice cliff concentration in zone 1. Ice cliff removal processes are likely less effective in zone 1 than lower on the glacier. Because debris is thin in zone 1, ice cliff removal by burial is small compared to lower on the glacier. The effect of ice cliff removal by backwasting through the topography is reduced in this zone because backwasting rates are

nearly two-fold lower than in zones 2 and 3. In zone 1, ice cliff production due to 1) debris thickness variations are the highest in the study area; 2) supraglacial streams is uncertain; and 3) supraglacial lake formation is minimal due to low areal concentrations. In zone 1, ice cliff removal due to 1) burial of ice cliff backwasting is the lowest in the study area; and 2) ice cliff backwasting rates are the lowest in the study area.

Ice cliff concentration *C* is uniform from 650 to 600 m but decreases from 600 m to 475 m elevation (Fig. 4.7D). As the mean debris thickness increases down glacier, *C* declines. Mean debris thicknesses at elevations between 650 and 600 m are below 10 cm, where variations in debris thickness produce large changes in sub-debris melt relative to the thicker debris covers down glacier (Fig. 4.9). From 600 m to 475 m mean debris thickness doubles from 10 cm to 20 cm, at which point variation in debris thickness generate much smaller variation in sub-debris melt rate, leading to a reduction in ice cliff formation rates. Supraglacial lake concentrations increase in zone 2 but are still too small and few in number control ice cliff concentration (Fig. 4.8C). Supraglacial streams visible in the WV1 imagery increase in both concentration and sinuosity in zone 2 but only coincide with local increases of ice cliff concentrations in the topographic valleys formed between the previously separated medial moraines (Fig. 4.8C). Smaller supraglacial streams, not visible from the WV1 imagery, may influence ice cliff concentrations between the major trunk streams. Ice cliff removal rates may increase down glacier. Thickening debris will lead to increased burial of ice faces. Furthermore, ice cliff backwasting rates increase nearly two-fold from the highest elevations in the study area to the lowest. Backwasting of ice cliffs through local topography will be more effective at lower elevations, potentially reducing the linear ice cliff concentration (Fig. 4.10A). In zone 2, 1) ice cliff production due to debris thickness variations is reduced relative to zone 1; 2) ice cliff

production by supraglacial streams may increase in this zone relative to zone 1 due to increased linear concentrations and stream sinuosities; and 3) production by supraglacial lakes is minimal due to low areal concentrations. In zone 2, ice cliff removal is increased relative to zone 1 due to 1) increased rates of burial of ice cliff by thick debris; and 2) higher rates of ice cliff backwasting (2 cm/ day higher than in zone 1).

Ice cliff concentration is nearly uniform below 475 m (Fig. 4.7D). The ice cliff concentration in the dead ice portion of the glacier (0.005 m/m^2 or 50 m/ 10^4 m^2) is four-fold lower than the average within the study area. Debris thicknesses at elevations below 500 m vary from 15 cm to 100 cm (Fig. 4.7E). Sub-debris melt rates in zone 3 beneath thick debris vary by a maximum of 2 cm/day. Relief production is greatly reduced in zone 3, leading to reduced ice cliff formation rates and to less melt available for local supraglacial streams. Thick debris in zone 3 also prevents the transport of debris by nascent streams, promoting the flow of meltwater underneath or within the debris. The creation of local basins by englacial tunnel collapse also reduces drainage basin areas; supraglacial streams are therefore limited in their contributing areas and hence in their discharges and flow speeds in this elevation band. Streams therefore play a minor role in zone 3; only one supraglacial stream was visible in the WV1 imagery (Fig. 4.8C). Supraglacial lake area concentrations increase by a factor of 5 from zone 2 to zone 3, and appear to control the formation and maintenance of ice cliffs in zone 3. Ice cliff backwasting self-removal rates are likely large, as backwasting rates are highest here (Fig. 4.10A). Because of the thick debris, ice cliffs in zone 3 are more likely to be buried. In summary, as ice moves into zone 3, 1) ice cliff production rate decreases due to high debris thickness, and low concentrations of supraglacial streams, but increases due to a 5-fold increase in supraglacial lakes, whereas 2) ice

cliff removal rate increases due to burial of ice cliff by thick debris, and high ice cliff backwasting rates.

Based on the discussion above, we suggest that mean debris thicknesses provide the primary control on ice cliff distribution on the Kennicott Glacier. Supraglacial debris thickness controls relief production through the debris thickness-melt rate relationship (Fig. 4.9). Debris thickness also modulates most processes that remove ice cliffs from the glacier. Rates of ice cliff backwasting are affected by the longwave radiation emitted from the glacier surface (Sakai et al., 2002); the thicker the debris, the higher the debris surface temperature, the more energy is available for ice cliff retreat and the potential burial and removal of topographic elements. If debris thickness is the primary control on the formation and removal of ice cliffs, it also plays a role in setting supraglacial stream discharge, potentially supraglacial stream sinuosity, and the degree to which supraglacial streams incise.

4.6.5 Links between debris thickness, relief, ice cliffs, and supraglacial streams

Melt rates under thin debris are higher than melt rates under thick debris, and therefore produce more surface water for supraglacial streams. Melt rates under thin debris are also more sensitive to inevitable local variations in debris thickness, therefore increasing relief production, debris failure events at the debris-ice plane, and ice cliff generation. Higher concentrations of ice cliffs, and associated high ice melt rates increase melt water production at the surface. Higher discharge supraglacial streams are more likely to erode both laterally and vertically due to increased strain heating potential. Ice cliffs on the Kennicott glacier act as initiation points for supraglacial streams away from the trunk streams between coalesced medial moraines (Fig. 4.5B). The small streams created by ice cliffs incise and meander, producing new ice cliff nucleation sites.

Ice cliffs also increase local variability in debris thickness. Many ice cliffs are crescent shaped in planview (this shape is more common when the ice cliff is undercut by a supraglacial stream) and support surface water drainage networks on the ice cliff surface (Fig 4.5A; 4.5B). Both the crescent ice cliff shape and the surface drainage networks help funnel supraglacial debris undermined from the top of ice cliffs into thicker debris accumulations at the base of ice cliffs (Fig 5A; 5B). Increasing debris concentrations in topographic lows can lead to the inversion of glacier surface topography. Thicker debris at the base of the ice cliff suppresses melt relative to the thinner debris at the top of the ice cliff. The debris thickness-ice cliff-supraglacial stream feedback may help account for the large concentration of ice cliffs on the Kennicott glacier.

4.6.6 Estimates of vertical melt due to ice cliff backwasting and sub-debris melt

Our data show a distinct distribution of ice cliffs on the Kennicott Glacier that affects the broad elevational pattern of melt (summer mass balance), and may therefore influence the glacier's dynamic response to climate change. Here we use all of our measurements to estimate the contribution of both ice cliffs and sub-debris melt to the surface mass balance of the Kennicott Glacier. The area-averaged surface mass balance of a *slope-limited* area of partial debris cover is

$$\dot{b} = \frac{(\overline{A}_{subdebris} Area_{subdebris} + \overline{A}_{iceface} \overline{h} \cos(\overline{\alpha}) \sum L)}{Area_{total}}, \qquad (4.6)$$

where $\overline{A}_{subdebris}$ is the average sub-debris ablation rate, $Area_{subdebris}$ is the total planview area of the debris covered portions of the area of interest, $\overline{A}_{iceface}$ is the average ice cliff ablation rate perpendicular to the ice cliff surface, $\overline{h}$ is the mean height of the ice cliffs in the area, $\overline{\alpha}$ is the average ice cliff slope defined at the top of the ice cliff, L is the long-axis length of ice cliffs in

the area, $Area_{Total}$ is the total area of interest. Mass loss due to ice cliff backwasting depends on the average ice cliff ablation rate, the geometry of the average ice cliff, and the number of ice cliffs in a given area. We find that ice cliffs most likely contribute 30% of melt in the study area but can locally account for up to 50% of the melt (Fig. 4.14).

Using a Monte Carlo method with 10,000 simulations we assess the uncertainty in the estimated contribution of ice cliffs to melt. We varied the mean ice cliff slope (between 35-50°), ice cliff area (whether the ice cliffs are best represented as triangular or rectangular in plan view; uncertainty factor allowed to vary in a uniform distribution between 1 and 0.5, 0.75 for the most likely case), ice cliff net melt rate with elevation (uniform distribution between ±1 cm/day for each elevation band), ice cliff height with elevation (uniform distribution between ±5 m), and the curve fit for the debris thickness-melt rate (using the bounds of the power-law curves in Fig. 4.9). We use a range of ice cliff slope values from 35-50° because the slope at the top of ice cliffs was commonly steeper than the slope at the foot of the ice cliff. We found that for one standard deviation bounds, 20-40% of the volume lost in the study area could be accounted for by ice cliff backwasting (Fig. 4.14); for two standard deviations, the rage increases to 10-50%.

The most likely 30% fraction of volume loss from ice cliffs on the Kennicott Glacier is large compared to that reported in other studies. Sakai et al. (2002) estimated that ice cliff retreat contributed 20% of the net ablation on the Lirung Glacier, Nepal; Reid and Brock (2014) estimated that 7.4% of the ablation of the debris-covered portion of the Miage Glacier, Italy, was due to ice cliff backwasting. Similarly, Han et al. (2010) report that 7.3% percent of total ablation from the debris covered area of Koxkar Glacier, China, was attributable to ice cliff retreat. Our ice cliff backwasting rates are similar to those reported in other studies (this study: 3-11 cm d^{-1}; Sakai et al., 2002: 7-11 cm d^{-1}; Reid and Brock, 2014: 6.1-7.5 cm d^{-1}; Han et al., 2010:

3-10 cm d^{-1}). The large contribution from ice cliff backwasting on the Kennicott Glacier must therefore result from the large concentration of ice cliffs. Differences in ice cliff height between the glaciers may also effect the contribution of ice cliff backwasting to net melt, but little ice cliff height data exist for comparison.

Sub-debris melt rates, decline rapidly as elevation drops, reflecting the near linear increase in debris thickness combined with the nonlinear decay of sub-debris melt with debris thickness (Fig. 4.9). Spatially averaged, vertical ice loss due to ice cliff backwasting (Fig. 4.14) increases from 700 m to 600 m elevation, maintains a maximum between 600 m and 540 m, and then declines towards the terminus. This profile results from the product of ice cliff concentration, ice cliff height, and ice cliff backwasting rates, which all vary with elevation. The maximum vertical melt due to ice cliff backwasting occurs just down-glacier from the ice cliff concentration maximum: here ice cliff concentrations are near their maximum values and ice cliff height and backwasting rates have increased relative to their values up glacier.

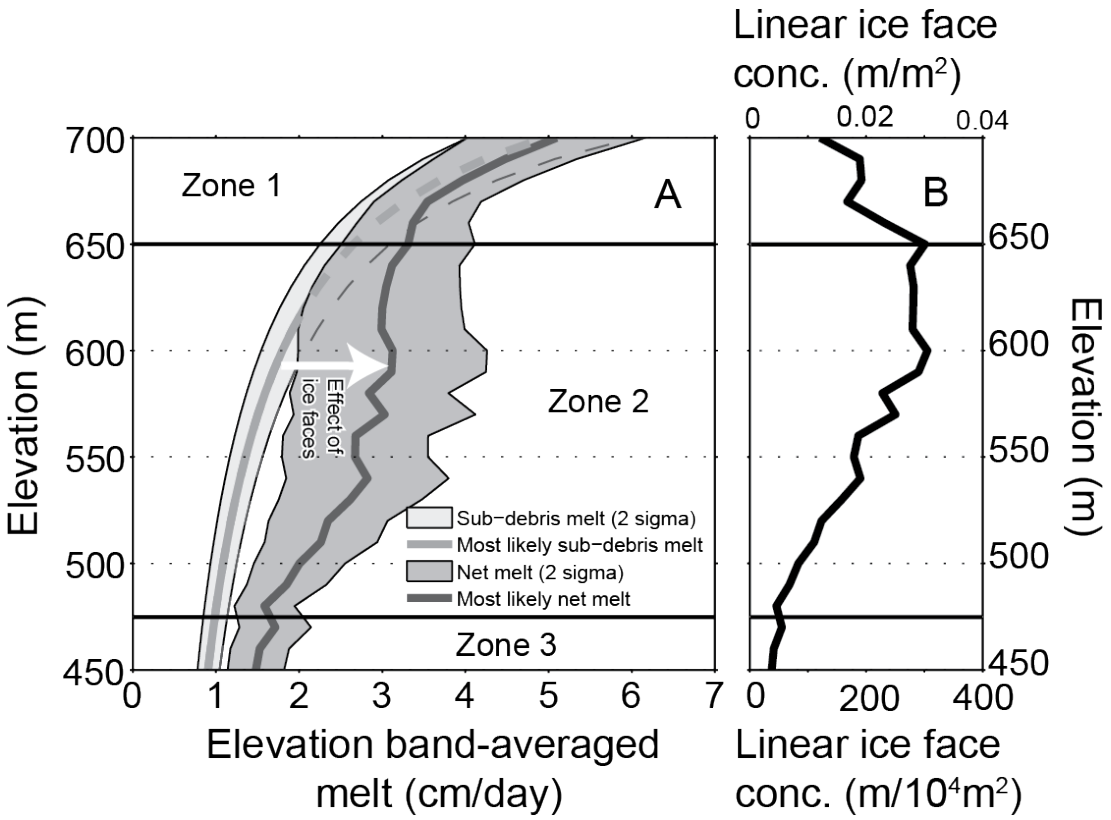

Figure 4.14 A) Calculated net elevation band-averaged melt and sub-debris melt band-average over the study period. The combined effect of increasing ice cliff retreat rates and ice cliff area at lower elevations leads to a peak in ice cliff loss below the peak in ice cliff concentration. B) The linear ice face concentration through the study area.

4.7 Implications

We outlined and described the processes leading to relief/ice cliff generation, maintenance, and removal, and attempted to constrain how these processes vary through the *slope-limited* debris-covered portion of the Kennicott glacier. While many of these processes are difficult to quantify without extensive in-situ documentation, we collected a wide range of in-situ and remotely sensed data to constrain the possible importance these processes in space. Based on these process indicators, it appears that supraglacial debris thickness is the most likely, primary control of patterns of glacier surface relief and ice cliff concentrations. The rate of supraglacial debris thickening down glacier may therefore exert primary control on ice cliff concentration on debris-covered glaciers. If debris thickness increases slowly (high surface velocity and low englacial debris concentration), and is locally variable, ice cliff concentration and relief will increase rapidly. If debris thickness increases rapidly down glacier and is relatively uniform, the positive feedbacks between relief production, ice cliff generation, and supraglacial stream formation will likely be suppressed. When debris cover is thick and mean ice surface slopes are low (as in zone 3), ice cliff generation will be controlled by the collapse of englacial conduits, as is assumed on the lower reaches of both Khumbu region glaciers and the Tasman Glacier (Sakai et al., 2000; Kirkbride, 1993).

The relatively uniform relief below 575 m on the Kennicott Glacier suggests that thick debris-cover maintains glacier relief due to the reduction of sub-debris melt variability under thicker debris covers. Further documentation of glacier surface relief and debris thickness on other debris-covered glaciers is needed to determine whether this hypothesized cause-effect relationship is more generally relevant on debris-covered glaciers. Further field studies are

required to document the physical relationship between debris cover, supraglacial streams and their discharge and sinuosity.

While we equate differences in local melt rates to differences in relief production, we have not explicitly accounted for the role of local debris transport leading to topographic inversion. Numerical models that capture the co-evolution of supraglacial debris thickness fields and glacier surface relief would aid in exploration of this geomorphic system.

Finally, if we assume that relative mass loss from sub-debris melt and ice cliff backwasting remains the same throughout the melt season, the pattern of melt in Figure 4.14 should reflect the pattern of full melt-season mass balance. Debris thicknesses typically increase down glacier on most debris-covered glaciers (e.g., Kellerer-Pirklbauer, 2008). The estimated average melt rate is roughly double what one would calculate given sub-debris melt alone in the largest region of the terminus, zone 2. This will enhance significantly the rate at which the debris-covered tongue thins, and should alter the evolution of mean glacier surface slope, the combination of which governs the ice speed.

4.8 Conclusions

We collected a wide range of in-situ and remotely sensed data that led to a number of conclusions, which we summarize below.

- **Glacier surface speed:** Based on the correlation of WV1 image pairs we determined that the lower 3 km of the Kennicott Glacier is dead ice.
- **Supraglacial debris thickness:** Debris thickness appears to be the primary control on glacier surface relief and ice cliff concentration. Thin mean debris thicknesses (on the Kennicott less than 10 cm) lead to the largest relief and ice cliff concentration increases. The thicker the

mean debris thickness the slower relief production and relief decay, leading the maintenance of glacier surface relief

- **Ice Cliffs:** Ice cliffs increase or maintain concentrations where mean and maximum glacier surface relief is increasing. Ice cliffs tend to decrease in concentration the thicker the debris cover (outside of *volume* and *transport-limited* partial debris-cover zones). Ice cliff removal by burial is more likely at lower elevations where backwasting rates and mean debris thicknesses are high. Ice cliff removal by backwasting through relief elements depends on backwasting rates and the width of relief elements. Ice cliffs increase supraglacial debris thickness variability by focusing debris down drainage networks on ice cliff surfaces, which leads to increased relief production and the potential to from more ice cliffs. Ice cliffs (for a population of ~32,000) preferentially cliff north and northeast throughout the study area. Supraglacial relief limits ice cliff area. Ice cliffs smaller than 500 m^2 are present throughout the study area, but larger ice cliffs preferentially occur where relief is high.
- **Supraglacial Streams:** Streams on the Kennicott Glacier become more sinuous within the debris-covered portion. There is a positive feedback between ice cliff formation and supraglacial streams: More cliffs lead to increase surface water and higher discharge in supraglacial streams which leads to more ice cliff formation
- **Supraglacial lakes:** Supraglacial lakes and tunnel conduit collapse appear to dominate ice cliff spatial distribution in the "dead" ice portion of the Kennicott Glacier (thick debris and low mean surface slopes).
- **Melt rate estimates:** In the debris-covered portion of the Kennicott Glacier, approximately 30% of the area-averaged melt is attributable to ice cliff backwasting. This contribution

largely reflects the high concentration of ice cliffs, which is likely the result of the thin debris mantle at the upper end of the debris-covered portion of the glacier.

High concentrations of ice cliffs on debris-portions of glaciers alter the mass balance profile, acting to mute the insulating effects of the debris cover. The response of debris-covered glaciers to climate change therefore cannot be properly anticipated without consideration of the role of ice cliffs and the processes that control their distribution on debris-covered glaciers.

4.9 Acknowledgements

L.S.A. acknowledges support from a 2011 Murie Science and Learning Center Fellowship and NSF DGE-1144083 (GRFP). R.S.A. acknowledges support of NSF EAR-1239281 (Boulder Creek CZO) and NSF EAR-1123855. We thank Craig Anderson, Emily Longano, and Oren Leibson for field support. We thank Per Jenssen, Susan Fison, Ben Hudson, Patrick Tomco (UA-A), Rommel Zulueta (UA-A), the Wrangell-St. Elias Interpretive Rangers, the Wrangell Mountains Center and Ted Scambos (NSIDC) for logistical support and the gracious loan of equipment. We thank Lucy Tyrell for facilitating outreach efforts. We also thank Joshua Scott, Wrangell - St Elias National Park and the Polar Geospatial Center for access to satellite imagery. We thank Regina Hock for a thoughtful discussion. L.S.A thanks the organizers and participants of the 2010 Glaciological Summer School held in McCarthy, AK, which inspired this work.

4.10 References Cited

Anderson, R.S., 2000, A model of ablation-dominated medial moraines and the generation of debris-mantled glacier snouts: Journal of Glaciology, v. 46, no. 154, 459–469, (doi: 10.3189/172756500781833025).

Anderson S.P., Walder J.S., Anderson R.S., Krall E.R., Cunico M., Fountain A.G. and Trabant D.C., 2003, Integrated hydrologic and hydrochemical observations of Hidden Creek Lake

jökulhlaups, Kennicott Glacier, Alaska: Journal of Geophysical Research, v. 108, no. F1, 6003 (doi: 10.1029/2002JF000004)

Bartholomaus T.C., Anderson, R.S. and Anderson S.P., 2008, Response of glacier basal motion to transient water storage: Nature Geoscience, v. 1, no.1, 33–37 (doi: 10.1038/ngeo.2007.52)

Bartholomaus T.C., Anderson, R.S. and Anderson S.P., 2011, Growth and collapse of the distributed subglacial hydrologic system of Kennicott Glacier, Alaska, USA, and its effects on basal motion: Journal of Glaciology, v. 57, no. 206, 985–1002 (doi: 10.3189/002214311798843269)

Benn D.I., Bolch T., Hands K., Gulley J., Luckman A., Nicholson L.I., Quincey D., Thompson S., Toumi R. and Wiseman S., 2012, Response of debris-covered glaciers in the Mount Everest region to recent warming, and implications for outburst flood hazards: Earth-Science Reviews, v. 114, no. 1-2, 156–174, (doi: 10.1016/j.earscirev.2012.03.008).

Benn, D. I., and Evans, D.J.A., 1998, Glaciers and glaciation: London. Edward Arnold. 734 p.

Benn D.I., Wiseman S. and Hands K.A., 2001, Growth and drainage of supraglacial lakes on debris-mantled Ngozumpa Glacier, Khumbu Himal, Nepal: Journal of Glaciology, v. 47, no. 159, 626–638.

Boyd, B., Goetz, S.L. and Ham, N.R., 2004, Supraglacial stream incision into debris-covered ice, Matanuska Glacier, AK: in Geological Society of America Abstract, v. 36, no. 3, p. 11.

Das I., Hock R., Berthier, E. and Lingle, C.S., 2014, 21st century increase in glacier mass loss in the Wrangell Mountains, Alaska from airborne laser altimetry and satellite stereo-imagery: Journal of Glaciology, v. 20, 283-293.

Drewry, D.J., 1972, A quantitative assessment of dirt-cone dynamics: Journal of Glaciology, v. 11, no. 63, 431–446.

Eyles, N., 1979, Facies of supraglacial sedimentation on Icelandic and Alpine temperate glaciers: Canadian Journal of Earth Science, v. 17, no. 7, 1341–1361.

Eyles, N. and Rogerson, R.J., 1978, A framework for the investigation of medial moraine formation: Austerdalsbreen, Norway, and Berendon Glacier, British Columbia, Canada: Journal of Glaciology, v. 20, 99–113.

Gulley J. and Benn D.I., 2007, Structural control of englacial drainage systems in Himalayan debris-covered glaciers: Journal of Glaciology, v. 53, no. 182, 399–412.

Han, H., Wang, J., Wei, J. and Liu, S., 2010, Backwasting rate on debris-covered Koxkar glacier, Tuomuer mountain, China: Journal of Glaciology, v. 56, no. 196, 287–296 (doi: 10.3189/002214310791968430).

Isenko, E., Naruse, R. and Mavlyudov, B., 2005, Water temperature in englacial and supraglacial channels: Change along the flow and contribution to ice melting on the channel wall: Cold Regions Science and Technology, v. 42, no. 1, 53–62 (doi: 10.1016/j.coldregions.2004.12.003).

Iwata, S., Aoki, T., Kadota, T., Seko, K. and Yamaguchi, S., 2000, Morphological evolution of the debris cover on the Khumbu Glacier, Nepal, between 1978 and 1995, in Debris-Covered Glaciers: Proceedings of an international workshop at the University of Washington, Seattle, IAHS Publication, p. 3–11.

Kellerer-Pirklbauer, A., 2008, The Supraglacial Debris System at the Pasterze Glacier, Austria: Spatial Distribution, Characteristics and Transport of Debris. Z. Geomorphol., v. 52, no. 1, 3–25, (doi: 10.1127/0372-8854/2008/0052S1-0003).

Kirkbride, M.P., 1993, The temporal significance of transitions from melting to calving termini at glaciers in the central Southern Alps of New Zealand. The Holocene, v. 3, no. 3, 232–240, (doi: 10.1177/095968369300300305).

Kirkbride, M.P., 2011, Debris-covered glaciers, In Singh VP, Singh P and Haritashya UK eds. Encyclopedia of snow, ice and glaciers. Springer, Dordrecht, 190–191.

Kirkbride, M.P. and Warren, C.R., 1999, Tasman Glacier, New Zealand: 20th-century thinning and predicted calving retreat. Global and Planetary Change, **22**(1-4), 11–28, (doi: 10.1016/S0921-8181(99)00021-1).

Korn, D.L., 2010, Glacier and climate fluctuations in South-Central Alaska as observed through the PTAA model (MS thesis, University of Colorado-Boulder).

Leprince, S., Barbot. S., Ayoub, F. and Avouac, J-P., 2007, Automatic and precise orthorectification, coregistration, and subpixel correlation of satellite images, application to ground deformation measurements. Geoscience and Remote Sensing, IEEE Transactions on, v. 45, no. 6, 1529–1558.

Östrem G., 1959, Ice Melting under a Thin Layer of Moraine, and the Existence of Ice Cores in Moraines Ridges. Geografiska Annaler, v. 41, no. 4, 228–230.

Purdie, J. and Fitzharris, B., 1999, Processes and rates of ice loss at the terminus of Tasman Glacier, New Zealand. Global and Planetary Change, v. 22, 79–91.

Reid, T.D. and Brock, B.W., 2014, Assessing ice-cliff backwasting and its contribution to total ablation of debris-covered Miage glacier, Mont Blanc massif, Italy: Journal of Glaciology, v. 60, no. 219, 3–13 (doi: 10.3189/2014JoG13J045).

Rickman, R.L. and Rosenkrans, D.S., 1997, Hydrologic conditions and hazards in the Kennicott River Basin, Wrangell-St. Elias National Park and Preserve, Alaska. USGS Water-Resources Investigations Report, v. 53.

Rohl, K., 2008, Characteristics and evolution of supraglacial ponds on debris-covered Tasman Glacier, New Zealand: Journal of Glaciology, v. 54, no. 188, 867–880.

Sakai, A., Nakawo, M. and Fukita, K., 2002, Distribution characteristics and energy balance of ice cliffs on debris-covered glaciers, Nepal Himalaya. Arct. Antarct. and Alp. Res., v. 34, no. 1, 12–19.

Sakai, A., Nishimura, K., Kadota, T. and Takeuchi, N., 2009, Onset of calving at supraglacial lakes on debris-covered glaciers of the Nepal Himalaya: Journal of Glaciology, v. 55, no. 193, 909–917 (doi: 10.3189/002214309790152555).

Sakai, A., Takeuchi, N., Fujita, K. and Nakawo, M., 2000, Role of supraglacial ponds in the ablation process of a debris-covered glacier in the Nepal Himalayas, In Nakawo, N., Fountain, A. and Raymond, C. eds. Debris-covered glaciers, IAHS Publication, p. 264, 53–61.

Schomacker, A. and Kjaer, K.H., 2008, Quantification of dead-ice melting in ice-cored moraines at the high-Arctic glacier Holmströmbreen, Svalbard. Boreas, v. 37, no. 2, 211–225, (doi: 10.1111/j.1502-3885.2007.00014.x).

Schwanghart, W. and Kuhn, N.J., 2010, TopoToolbox: A set of Matlab functions for topographic analysis: Environmental Modeling and Software, v. 25, no. 6, 770–781 (doi: 10.1016/j.envsoft.2009.12.002)

Zhang, Y., Fujita, K., Liu, S., Liu, Q. and Nuimura, T., 2011, Distribution of debris thickness and its effect on ice melt at Hailuogou glacier, southeastern Tibetan Plateau, using in situ surveys and ASTER imagery: Journal of Glaciology, v. 57, no. 206, 1147–1157 (doi: 10.3189/002214311798843331)

Chapter 5 Bibliography

Anderson, B.M., 2004, The response of "Ka Roimata o Hine Hukatere" Franz Josef Glacier to climate change [Ph.D. Thesis]: Christchurch, University of Canterbury, 106 p.

Anderson, B.M., Lawson, W., Owens, I., and Goodsell, B., 2006, Past and future mass balance of "Ka Roimata o Hine Hukatere" Franz Josef Glacier, New Zealand: Journal of Glaciology, v. 52, no. 179, p. 597–607, doi: 10.3189/172756506781828449.

Anderson, R.S., 2000, A model of ablation-dominated medial moraines and the generation of debris-mantled glacier snouts: Journal of Glaciology, v. 46, no. 154, 459–469, (doi: 10.3189/172756500781833025).

Anderson S.P., Walder J.S., Anderson R.S., Krall E.R., Cunico M., Fountain A.G. and Trabant D.C., 2003, Integrated hydrologic and hydrochemical observations of Hidden Creek Lake jökulhlaups, Kennicott Glacier, Alaska: Journal of Geophysical Research, v. 108, no. F1, 6003 (doi: 10.1029/2002JF000004)

Anslow, F.S., Hostetler, S., Bidlake, W.R., and Clark, P.U., 2008, Distributed energy balance modeling of South Cascade Glacier, Washington and assessment of model uncertainty: Journal of Geophysical Research, v. 113, no. F2, p. F02019, doi: 10.1029/2007JF000850.

Arendt, A., and Sharp, M., 1999, Energy balance measurements on a Canadian high arctic glacier and their implications for mass balance modelling: IAHS Publication, 165-172.

Arsenault, A.M. and Meigs A.J., 2005, Contribution of deep-seated bedrock landslides to erosion of a glaciated basin in southern Alaska: Earth Surface Processes and Landforms, v. 30, no. 9, 1111–1125, (doi: 10.1002/esp.1265).

Ballantyne C.K., 1994, The Periglaciation of Great Britain: CUP Archive.

Bartholomaus T.C., Anderson, R.S. and Anderson S.P., 2008, Response of glacier basal motion to transient water storage: Nature Geoscience, v. 1, no.1, 33–37 (doi: 10.1038/ngeo.2007.52)

Bartholomaus T.C., Anderson, R.S. and Anderson S.P., 2011, Growth and collapse of the distributed subglacial hydrologic system of Kennicott Glacier, Alaska, USA, and its effects on basal motion: Journal of Glaciology, v. 57, no. 206, 985–1002 (doi: 10.3189/002214311798843269)

Benediktsson, Í.Ö., Möller, P., Ingólfsson, Ó., Van der Meer, J.J.M., Kjær, K.H., and Krüger, J., 2008, Instantaneous end moraine and sediment wedge formation during the 1890 glacier surge of Brúarjökull, Iceland: Quaternary Science Reviews, v. 27, no. 3-4, p. 209–234, doi: 10.1016/j.quascirev.2007.10.007.

Benediktsson, Í.Ö., Schomacker, A., Lokrantz, H., and Ingólfsson, Ó., 2010, The 1890 surge end

moraine at Eyjabakkajökull, Iceland: a re-assessment of a classic glaciotectonic locality: Quaternary Science Reviews, v. 29, no. 3-4, p. 484–506, doi: 10.1016/j.quascirev.2009.10.004.

Benn D.I., Bolch T., Hands K., Gulley J., Luckman A., Nicholson L.I., Quincey D., Thompson S., Toumi R. and Wiseman S., 2012, Response of debris-covered glaciers in the Mount Everest region to recent warming, and implications for outburst flood hazards: Earth-Science Reviews, v. 114, no. 1-2, 156–174, (doi: 10.1016/j.earscirev.2012.03.008).

Benn, D. I., and Evans, D.J.A., 1998, Glaciers and glaciation: London. Edward Arnold. 734 p.

Benn, D.I. and Evans, D.J.A., 2010, Glaciers and Glaciation: Hodder Education, London.

Benn, D.I., and Lukas, S., 2006, Younger Dryas glacial landsystems in North West Scotland: an assessment of modern analogues and palaeoclimatic implications: Quaternary Science Reviews, v. 25, no. 17-18, p. 2390–2408, doi: 10.1016/j.quascirev.2006.02.015.

Benn, D.I. and Owen, L.A., 2002, Himalayan glacial sedimentary environments: a framework for reconstructing and dating the former extent of glaciers in high mountains: Quaternary International, v. 98, p. 3–25, (doi: 10.1016/S1040-6182(02)00048-4).

Benn D.I., Wiseman S. and Hands K.A., 2001, Growth and drainage of supraglacial lakes on debris-mantled Ngozumpa Glacier, Khumbu Himal, Nepal: Journal of Glaciology, v. 47, no. 159, 626–638.

Bennett, M., Huddart, D., Hambrey, M.J., and Ghienne, J.F., 1996, Moraine development at the high-arctic valley glacier Pedersenbreen, Svalbard: Geografiska Annaler. Series A, v. 78, no. 4, p. 209–222.

Bennett, M., Huddart, D., Waller, R., Cassidy, N., Tomio, a, Zukowskyj, P., Midgley, N., Cook, S., Gonzalez, S., and Glasser, N., 2004, Sedimentary and tectonic architecture of a large push moraine: a case study from Hagafellsjökull-Eystri, Iceland: Sedimentary Geology, v.172, no. 3-4, p. 269–292, doi: 10.1016/j.sedgeo.2004.10.002.

Bennett, M.R., 2001, The morphology, structural evolution and significance of push moraines: Earth-Science Reviews, v. 53, no. 3-4, p. 197–236, doi: 10.1016/S0012-8252(00)00039-8.

Bennett, M.R., Huddart, D., and McCormick, T., 2000, An integrated approach to the study of glaciolacustrine landforms and sediments: a case study from Hagavatnet, Iceland: Quaternary Science Reviews, v. 19, no. 7, p. 633–665, doi: 10.1016/S0277-3791(99)00013-X.

Benson, L., Madole, R., Landis, G., and Gosse, J., 2005, New data for Late Pleistocene Pinedale alpine glaciation from southwestern Colorado: Quaternary Science Reviews, v. 24, no. 1-2, p. 49–65, doi: 10.1016/j.quascirev.2004.07.018.

Bøggild, C., Reeh, N., and Oerter, H., 1994, Modelling ablation and mass-balance sensitivity to

climate change of Storstrømmen, northeast Greenland: Global and Planetary Change, v. 9, p. 79–90.

Bolch T., Buchroithner M., Pieczonka T. and Kunert A., 2008, Planimetric and volumetric glacier changes in the Khumbu Himal, Nepal, since 1962 using Corona, Landsat TM and ASTER data: Journal of Glaciology, v. 54, no. 187, 592–600, (doi: 10.3189/002214308786570782).

Boulton G. and Eyles N., 1979, Sedimentation by valley glaciers: a model and genetic classification: In Moraines and Varves (C. Schluchter, Ed.): Balkema, Rotterdam.

Boulton, G., 1986, Push-moraines and glacier-contact fans in marine and terrestrial environments: Sedimentology, v. 33, p. 677–698.

Boulton, G.S., Van Der Meer, J.J.M., Beets, D.J., Hart, J.K., and Ruegg, G.H.J., 1999, The sedimentary and structural evolution of a recent push moraine complex : Holmstrombreen , Spitsbergen: Quaternary Science Reviews, v. 18, p. 339–371.

Boulton, G.S., Van Der Meer, J.J.M., Hart, J., Beets, D., Ruegg, G.H.J., Van Der Waterer, Jarvis, J., 1996, Till and moraine emplacement in a deforming bed surge— An example from a marine environment: Quaternary Science Reviews, v. 15, no. 95, p. 961–987.

Box, J., and Rinke, A., 2003, Evaluation of Greenland ice sheet surface climate in the HIRHAM regional climate model using automatic weather station data: Journal of Climate, v. 16, p.1302–1319.

Boyd, B., Goetz, S.L. and Ham, N.R., 2004, Supraglacial stream incision into debris-covered ice, Matanuska Glacier, AK: in Geological Society of America Abstract, v. 36, no. 3, p. 11.

Bozhinskiy, A.N., Krass, M.S. and Popovnin V.V., 1986, Role of debris cover in the thermal physics of glaciers: Journal of Glaciology, v. 32, no. 111, 255–266.

Braithwaite, R.J., 1981, On glacier energy balance, ablation, and air temperature: Journal of Glaciology, v. 27, p. 381–391.

Braithwaite, R.J., and Zhang, Y., 2000, Sensitivity of mass balance of five Swiss glaciers to temperature changes assessed by tuning a degree-day model: Journal of Glaciology, v. 46, no. 152, p. 7–14.

Braun, M., and Hock, R., 2004, Spatially distributed surface energy balance and ablation modelling on the ice cap of King George Island (Antarctica): Global and Planetary Change, v. 42, no. 1-4, p. 45–58, doi: 10.1016/j.gloplacha.2003.11.010.

Brock, B.W., Mihalcea, C., Kirkbride, M.P., Diolaiuti, G., Cutler, M.E.J., and Smiraglia, C., 2010, Meteorology and surface energy fluxes in the 2005–2007 ablation seasons at the Miage debris-covered glacier, Mont Blanc Massif, Italian Alps: Journal of Geophysical Research, v. 115, no. D9, p. D09106, doi: 10.1029/2009JD013224.

Brook, M.S., and Paine, S., 2012, Ablation of Ice-Cored Moraine in a Humid, Maritime Climate: Fox Glacier, New Zealand: Geografiska Annaler: Series A, Physical Geography, v. 94, no. 3, p. 339–349, doi: 10.1111/j.1468-0459.2011.00442.x.

Brugger, K.A., 2007, Cosmogenic ^{10}Be and ^{36}Cl ages from Late Pleistocene terminal moraine complexes in the Taylor River drainage basin, central Colorado, USA: Quaternary Science Reviews, v. 26, no. 3-4, p. 494–499, doi: 10.1016/j.quascirev.2006.09.006.

Brugger, K.A., 2010, Climate in the Southern Sawatch Range and Elk Mountains, Colorado, U.S.A., during the Last Glacial Maximum: Inferences using a simple degree-day model: Arctic, Antarctic, and Alpine Research, v. 42, no. 2, p. 164–178, doi: 10.1657/1938-4246- 42.2.164.

Budd W.F. and Jenssen D., 1975, Numerical modelling of glacier systems. IAHS Publ., v. 104**,** 257–291.

Burke, E.E., and Roe, G.H., 2013, The absence of memory in the climatic forcing of glaciers: Climate Dynamics, p. 1–12, doi:10.1007/s00382-013-1758-0.

Burki, V., Larsen, E., Fredin, O., and Margreth, A., 2009, The formation of sawtooth moraine ridges in Bødalen, western Norway: Geomorphology, v. 105, no. 3-4, p. 182–192, doi: 10.1016/j.geomorph.2008.06.016.

Buttstadt, M., Moller, M., Iturraspe, R., and Schneider, C., 2009, Mass balance evolution of Martial Este Glacier , Tierra del Fuego (Argentina) for the period 1960 – 2099: Advances in Geosciences, v. 22, p. 117–124.

Clark, P.U., Dyke, A.S., Shakun, J.D., Carlson, A.E., Clark, J., Wohlfarth, B., Mitrovica, J.X., Hostetler, S.W., and McCabe, A.M., 2009, The Last Glacial Maximum: Science, v. 325, no. 5941, p. 710–714, doi:10.1126/science.1172873.

Conway H. and Rasmussen L.A., 2000 Summer temperature profiles within supraglacial debris on Khunibu Glacier, Nepal, in Debris-covered Glaciers: Proceedings of an International Workshop Held at the University of Washington in Seattle, Washington, USA, 13-15 September 2000, p. 89.

Cuffey K.M. and Paterson W.S., 2010, The physics of glaciers: Elsevier, Oxford, UK.

Das I., Hock R., Berthier E. and Lingle C.S., 2014, 21st century increase in glacier mass loss in the Wrangell Mountains, Alaska from airborne laser altimetry and satellite stereo-imagery: Journal of Glaciology, v. 20, 283-293.

Denby, B., and Greuell, W., 2000, The use of bulk and profile methods for determining surface heat fluxes in the presence of glacier winds: Journal of Glaciology, v. 46, no. 154, p. 445– 452, doi: 10.3189/172756500781833124.

Drewry, D.J., 1972, A quantitative assessment of dirt-cone dynamics: Journal of Glaciology, v. 11, no. 63, 431–446.

Eyles, N., 1979, Facies of supraglacial sedimentation on Icelandic and Alpine temperate glaciers: Canadian Journal of Earth Science, v. 17, no. 7, 1341–1361.

Eyles, N. and Rogerson, R.J., 1978, A framework for the investigation of medial moraine formation: Austerdalsbreen, Norway, and Berendon Glacier, British Columbia, Canada: Journal of Glaciology, v. 20, 99–113.

Gardner, A.S., Sharp, M.J., Koerner, R.M., Labine, C., Boon, S., Marshall, S.J., Burgess, D.O., and Lewis, D., 2009, Near-surface temperature lapse rates over Arctic glaciers and their implications for temperature downscaling: Journal of Climate, v. 22, no. 16, p. 4281–4298, doi: 10.1175/2009JCLI2845.1.

Gibbons, A.B., Megeath, J.D., and Pierce, K.L., 1984, Probability of moraine survival in a succession of glacial advances: Geology, v. 12, p. 327–330, doi:10.1130/0091-7613, 1984)12<327:POMSIA>2.0.CO;2.

Glasser, N.F., and Hambrey, M.J., 2002, Sedimentary facies and landform genesis at a temperate outlet glacier: Soler Glacier, North Patagonian Icefield: Sedimentology, v. 49, no. 1, p. 43– 64, doi: 10.1046/j.1365-3091.2002.00431.x.

Glasser, N.F., Jansson, K., Mitchell, W. a., and Harrison, S., 2006, The geomorphology and sedimentology of the "Témpanos" moraine at Laguna San Rafael, Chile: Journal of Quaternary Science, v. 21, no. 6, p. 629–643, doi: 10.1002/jqs.1002.

Gosse, J.C., Klein, J., Lawn, B., Middleton, R., and Evenson, E.B., 1995, Beryllium-10 dating of the duration and retreat of the last Pinedale glacial sequence: Science (New York, N.Y.), v. 268, no. 5215, p. 1329–33, doi: 10.1126/science.268.5215.1329.

Grabiec, M., Budzik, T., and G!owacki, P., 2012, Modeling and hindcasting of the mass balance of Werenskioldbreen (Southern Svalbard): Arctic, Antarctic, and Alpine Research, v. 44, no. 2, p. 164–179.

Greuell, W., and Smeets, P., 2001, Variations with elevation in the surface energy balance on the Pasterze (Austria): Journal of Geophysical Research, v. 106, no. D23, p. 31717–31727.

Gulley J. and Benn D.I., 2007, Structural control of englacial drainage systems in Himalayan debris-covered glaciers: Journal of Glaciology, v. 53, no. 182, 399–412.

Gümundsson, S., Björnsson, H., Palsson, F., and Haraldsson, H.H., 2003, Physical energy balance and degree-day models of summer ablation on Langjökull ice cap, SW-Iceland: National Power Company of Iceland.

Hambrey, M.J., and Huddart, D., 1995, Englacial and proglacial glaciotectonic processes at the snout of a thermally complex glacier in Svalbard: Journal of Quaternary Science, v. 10, p. 313–326.

Han, H., Wang, J., Wei, J. and Liu, S., 2010, Backwasting rate on debris-covered Koxkar glacier, Tuomuer mountain, China: Journal of Glaciology, v. 56, no. 196, 287–296 (doi: 10.3189/002214310791968430).

Hanna, E., Huybrechts, P., Janssens, I., Cappelen, J., Steffen, K., and Stephens, A., 2005, Runoff and mass balance of the Greenland ice sheet: 1958–2003: Journal of Geophysical Research, v. 110, no. D13, p. D13108, doi: 10.1029/2004JD005641.

Hart, J.K., 1996, Proglacial glaciotectonic deformation associated with glaciolacustrine sedimentation, Lake Pukaki, New Zealand: Journal of Quaternary Science, v. 11, no. 2, p. 149–160, doi: 10.1002/(SICI)1099-1417, 199603/04)11:2<149::AID-JQS227>3.0.CO;2-2.

Hart, J.K., and Watts, R.J., 1997, A comparison of the styles of deformation associated with two recent push moraines, South Van Keulenfjorden, Svalbard: Earth Surface Processes and Landforms, v. 22, no. 12, p. 1089–1107, doi: 10.1002/(SICI)1096-9837, 199712)22:12<1089::AID-ESP804>3.0.CO;2-8.

He, X., Du, J., Ji, Y., Zhang, N., Li, Z., Wang, S. and Theakstone, W.H., 2010, Characteristics of DDF at Baishui Glacier No. 1 region in Yulong Snow Mountain: Journal of Earth Science, v. 21, no. 2, p. 148–156, doi: 10.1007/s12583-010-0013-4.

Heimsath, A.M. and McGlynn, R., 2008, Quantifying periglacial erosion in the Nepal high Himalaya. Geomorphology, v. 97, no. 1-2, 5–23, (doi: 10.1016/j.geomorph.2007.02.046).

Hock, R., 2003, Temperature index melt modelling in mountain areas: Journal of Hydrology, v. 282, no. 1-4, p. 104–115, doi: 10.1016/S0022-1694(03)00257-9.

Hock, R., and Holmgren, B., 2005, A distributed surface energy-balance model for complex topography and its application to Storglaciären, Sweden: Journal of Glaciology, v. 51, no. 172, p. 25–36.

Hodgkins, R., Carr, S., Pálsson, F., Gu"mundsson, S., and Björnsson, H., 2013, Modelling variable glacier lapse rates using ERA-Interim reanalysis climatology: an evaluation at Vestari- Hagafellsjökull, Langjökull, Iceland: International Journal of Climatology, v. 33, no. 2, p. 410–421, doi: 10.1002/joc.3440.

Howat, I.M., Tulaczyk, S., Rhodes, P., Israel, K., and Snyder, M., 2006, A precipitation-dominated, mid-latitude glacier system: Mount Shasta, California: Climate Dynamics, v. 28, no. 1, p. 85–98, doi: 10.1007/s00382-006-0178-9.

Humlum, O., 2000, The geomorphic significance of rock glaciers : estimates of rock glacier debris volumes and headwall recession rates in West Greenland. Geomorphology, v. 35, 41-67.

Humlum, O., 2005, Holocene permafrost aggradation in Svalbard. Geological Society, London, Special Publications, v. 242, no. 1, 119–129, (doi: 10.1144/GSL.SP.2005.242.01.11).

Humlum, O., 1985, Genesis of an imbricate push moraine, Höfdabrekkujökull, Iceland: The Journal of Geology, v. 93, p. 185–195.

Isenko, E., Naruse, R. and Mavlyudov, B., 2005, Water temperature in englacial and supraglacial channels: Change along the flow and contribution to ice melting on the channel wall: Cold Regions Science and Technology, v. 42, no. 1, 53–62 (doi: 10.1016/j.coldregions.2004.12.003).

Iwata, S., Aoki, T., Kadota, T., Seko, K. and Yamaguchi, S., 2000, Morphological evolution of the debris cover on the Khumbu Glacier, Nepal, between 1978 and 1995, in Debris-Covered Glaciers: Proceedings of an international workshop at the University of Washington, Seattle, IAHS Publication, p. 3–11.

Jóhannesson, T., Raymond, C.F., and Waddington, E.D., 1989, Time-scale for adjustment of glaciers to changes in mass balance: Journal of Glaciology, v. 35, no. 121, p. 355–369.

Johnson, M.D., and Gillam, M.L., 1995, Composition and construction of late Pleistocene end moraines, Durango, Colorado: Geological Society of America Bulletin, v. 107, no. 10, p. 1241–1253, doi:10.1130/0016-7606, 1995)107<1241:CACOLP>2.3.CO;2.

Johnson, M.D., and Gillam, M.L., 1995, Composition and construction of late Pleistocene end moraines, Durango, Colorado: GSA Bulletin, v. 107, no. 10, p. 1241–1253.

Johnson, P.G, 1972, A possible advanced hypsithermal position of the Donjek Glacier: Arctic, v. 25, n. 4, p. 302-305.

Johnson, P.G., 1971, Ice cored moraine formation and degradation, Donjek Glacier, Yukon Territory, Canada: Geografiska Annaler: Series A, Physical Geography, v. 53, no. 3/4, p. 198–202.

Karlén, W., 1973, Holocene glacier and climatic variations, Kebnekaise mountains ,Swedish Lapland: Geografiska Annaler., Series A, v. 55, no. A, p. 29–63.

Kayastha, R.B., Ageta, Y., Nakawo, M., Fujita, K., Sakai, A., and Matsuda, Y., 2003, Positive degree-day factors for ice ablation on four glaciers in the Nepalese Himalayas and Qinghai- Tibetan Plateau: Bulletin of glaciological research, v. 20,p. 7-14.

Kellerer-Pirklbauer, A., 2008, The Supraglacial Debris System at the Pasterze Glacier, Austria: Spatial Distribution, Characteristics and Transport of Debris. Z. Geomorphol., v. 52, no. 1, 3–25, (doi: 10.1127/0372-8854/2008/0052S1-0003).

Kessler, M.A., Anderson, R.S. and Stock, G.M., 2006, Modeling topographic and climatic control of east-west asymmetry in Sierra Nevada glacier length during the Last Glacial Maximum: Journal of Geophysical Research, v. 111, no. F2, F02002, (doi: 10.1029/2005JF000365).

Kirkbride, M.P., 1993, The temporal significance of transitions from melting to calving termini at glaciers in the central Southern Alps of New Zealand. The Holocene, v. 3, no. 3, 232–240, (doi: 10.1177/095968369300300305).

Kirkbride, M.P., 1995, Ice Flow Vectors on the Debris-Mantled Tasman Glacier, 1957-1986: Geografiska Annaler, Series A: Physical Geography, v. 77, no. 3, 147–157.

Kirkbride, M.P., 1995, Relationships between temperature and ablation on the Tasman Glacier, Mount Cook National Park, New Zealand Relationships between temperature and ablation on the Tasman Glacier , Mount Cook National Park , N: New Zealand Journal of Geology and Geophysics, v. 38, p. 17–27.

Kirkbride, M.P., 2011, Debris-covered glaciers, In Singh VP, Singh P and Haritashya UK eds. Encyclopedia of snow, ice and glaciers. Springer, Dordrecht, 190–191.

Kirkbride, M.P. and Warren, C.R., 1999, Tasman Glacier, New Zealand: 20th-century thinning and predicted calving retreat. Global and Planetary Change, **22**(1-4), 11–28, (doi: 10.1016/S0921-8181(99)00021-1).

Konrad, S.K. and Humphrey, N.F., 2000, Steady-state flow model of debris-covered glaciers (rock glaciers). IAHS PUBLICATION, 255–266.

Konrad, S.K., Humphrey, N.F., Steig, E.J., Clark, D.H., Potter, N., and Pfeffer, W.T., 1999, Rock glacier dynamics and paleoclimatic implications. Geology, v. 27, no. 12, 1131, (doi: 10.1130/0091-7613, 1999)027<1131:RGDAPI>2.3.CO;2).

Konya, K., Matsumoto, T., and Naruse, R., 2004, Surface heat balance and spatially distributed ablation modelling at Koryto Glacier, Kamchatka peninsula, Russia: Geografiska Annaler: Series A, v. 86, no. 4, p. 337–348.

Korn, D.L., 2010, Glacier and climate fluctuations in South-Central Alaska as observed through the PTAA model (MS thesis, University of Colorado-Boulder).

Krüger, J., 1993, Moraine-ridge formation along a stationary ice front in Iceland: Boreas, v. 22, no. 2, p. 101–109.

Krüger, J., 1995, Origin, chronology and climatological significance of annual-moraine ridges at Myrdalsjökull, Iceland: The Holocene, v. 5, no. 4, p. 420–427.

Krüger, J., and Kjær, K.H., 2000, De-icing progression of ice-cored moraines in a humid, subpolar climate, Kötlujökull, Iceland: The Holocene, v. 10, no. 6, p. 737–747, doi: 10.1191/09596830094980.

Krüger, J., Kjær, K.H., Van Der Meer, J.J.M., 2002, From push moraine to single-crested dump moraine during a sustained glacier advance: Norwegian Journal of Geography, no. 4, p. 37– 41.

Laabs, B.J.C., Marchetti, D.W., Munroe, J.S., Refsnider, K.A., Gosse, J.C., Lips, E.W., Becker, R.A., Mickelson, D.M., and Singer, B.S., 2011, Chronology of latest Pleistocene mountain glaciation in the western Wasatch Mountains, Utah, U.S.A.: Quaternary Research, v. 76, no. 2, p. 272–284, doi: 10.1016/j.yqres.2011.06.016.

Laabs, B.J.C., Plummer, M.A., and Mickelson, D.M., 2006, Climate during the last glacial maximum in the Wasatch and southern Uinta Mountains inferred from glacier modeling: Geomorphology, v. 75, no. 3-4, p. 300–317, doi: 10.1016/j.geomorph.2005.07.026.

Laumann, T., and Reeh, N., 1993, Sensitivity to climate change of the mass balance of glaciers in southern Norway: Journal of Glaciology, v. 39, no. 133.

Leprince, S., Barbot. S., Ayoub, F. and Avouac, J-P., 2007, Automatic and precise orthorectification, coregistration, and subpixel correlation of satellite images, application to ground deformation measurements. Geoscience and Remote Sensing, IEEE Transactions on, v. 45, no. 6, 1529–1558.

Letréguilly, A., and Reynaud, L., 1989, Spatial patterns of mass-balance fluctuations of North American glaciers: Journal of Glaciology, v. 35, no. 120, p. 163–168.

Li, J., Liu, S., Zhang, Y., and Shangguan, D., 2011, Surface energy balance of Keqicar Glacier, Tianshan Mountains , China , during ablation period: Sciences in Cold and Arid Regions, v. 3, no. 3, p. 197–205, doi: 10.3724/SP.J.1226.2011.00197.

Licciardi, J.M., Clark, P.U., Brook, E.J., Elmore, D., and Sharma, P., 2004, Variable responses of western U.S. glaciers during the last deglaciation: Geology, v. 32, no. 1, p. 81, doi: 10.1130/G19868.1.

Lliboutry, L., Arnao, B.M., and Schneider, B., 1977, Glaciological problems set by the control of dangerous lakes in Cordillera Blanca, Peru. III Study of moraines and mass balances at Safuna: Journal of Glaciology, v. 18, no. 79, p. 275–290.

Lukas, S., 2012, Processes of annual moraine formation at a temperate alpine valley glacier: insights into glacier dynamics and climatic controls: Boreas, v. 41, no. 3, p. 463–480, doi: 10.1111/j.1502-3885.2011.00241.x.

Lyså, A. and Lønne, I., 2001, Moraine development at a small high-arctic valley glacier: Rieperbreen, Svalbard: Journal of Quaternary Science, v. 16, no. 6, p. 519–529, doi: 10.1002/jqs.613.

MacDougall, A.H., and Flowers, G.E., 2011, Spatial and temporal transferability of a distributed energy-balance glacier melt model: Journal of Climate, v. 24, p. 1480–1498, doi: 10.1175/2010JCLI3821.1.

Mair, D., Burgess, D.O., and Sharp, M.J., 2005, Thirty-seven year mass balance of Devon Ice Cap, Nunavut, Canada, determined by shallow ice coring and melt modeling: Journal of Geophysical Research, v. 110, no. F1, p. F01011, doi: 10.1029/2003JF000099.

Marshall, S.J., Bjornsson, H., Flowers, G.E. and Clarke, G.K.C., 2005, Simulation of Vatnajökull ice cap dynamics: Journal of Geophysical Research, v.110, no. F3, 126–135, (doi: 10.1029/2004JF000262).

Marshall, S., Sharp, M., Burgess, D.O., and Anslow, F.S., 2007, Near−surface temperature lapse rates on the Prince of Wales Icefield, Ellesmere Island, Canada: Implications for regional downscaling of temperature: International Journal of Climatology, v. 398, no. September2006, p. 385–398, doi: 10.1002/joc.

Marshall, S.J., and Sharp, M.J., 2009, Temperature and Melt Modeling on the Prince of Wales Ice Field, Canadian High Arctic: Journal of Climate, v. 22, no. 6, p. 1454–1468, doi: 10.1175/2008JCLI2560.1.

Meier, M.F., and Post, A.S., 1962, Recent variations in mass net budgets of glaciers in western North America, International Association of Hydrological Sciences Publication, No. 58, p. 63–77.

Messerli, B., 1968, Block gletscher im Weissmies und Aletsch und ihre photogrammetrische Kartierung. Die Alpen, v. 3, 139–152.

Mihalcea, C., Mayer, C., Diolaiuti, G., Lambrecht, A., Smiraglia, C., and Tartari, G., 2006, Ice ablation and meteorological conditions on the debris-covered area of Baltoro glacier, Karakoram, Pakistan: Annals of Glaciology, v. 43, no. 1894, p. 292–300.

Motyka, R.J., and Echelmeyer, K. a., 2003, Taku Glacier (Alaska, U.S.A.) on the move again: active deformation of proglacial sediments: Journal of Glaciology, v. 49, no. 164, p. 50–58, doi: 10.3189/172756503781830962.

Munroe, J.S., Laabs, B.J.C., Shakun, J.D., Singer, B.S., Mickelson, D.M., Refsnider, K. A., and Caffee, M.W., 2006, Latest Pleistocene advance of alpine glaciers in the southwestern Uinta Mountains, Utah, USA: Evidence for the influence of local moisture sources: Geology, v. 34, no. 10, p. 841, doi: 10.1130/G22681.1.

Naito, N., Nakawo, M., Kadota, T. and Raymond, C.F., 2000, Numerical simulation of recent shrinkage of Khumbu Glacier, Nepal Himalayas, in Debris-covered Glaciers: Proceedings of an International Workshop Held at the University of Washington in Seattle, Washington, USA, 13-15 September 2000, p. 245.

Nicholson, L. and Benn, D.I., 2006, Calculating ice melt beneath a debris layer using meteorological data: Journal of Glaciology, v. 57, no. 178, 463–470, (doi: 10.3189/172756506781828584).

Nussbaumer, S.U., and Zumbühl, H.J., 2011, The Little Ice Age history of the Glacier des Bossons (Mont Blanc massif, France): a new high-resolution glacier length curve based on historical documents: Climatic Change, v. 111, no. 2, p. 301–334, doi: 10.1007/s10584-011-0130-9.gsa 2013 schedule

Nussbaumer, S.U., Nesje, A., and Zumbuhl, H.J., 2011, Historical glacier fluctuations of Jostedalsbreen and Folgefonna (southern Norway) reassessed by new pictorial and written evidence: The Holocene, v. 21, no. 3, p. 455–471, doi: 10.1177/0959683610385728.

Nye, J., 1965, The frequency response of glaciers: Journal of Glaciology, v. 5, no. 41, 567–587.

O'Farrell, C.R., Heimsath, A.M., Lawson, D.E., Jorgensen, L.M., Evenson, E.B., Larson, G. and Denner, J., 2009, Quantifying periglacial erosion : insights on a glacial sediment budget, Matanuska Glacier, Alaska. Earth Surface Processes and Landforms. v. 34, 2008–2022, (doi: 10.1002/esp).

Oerlemans J., 1986, An Attempt to Simulate Historic Front Variations of Nigardsbreen, Norway. Theoretical and applied climatology, v. 37, 126–135.

Oerlemans, J., 2001, Glaciers and Climate Change: Lisse, NL, Swets and Zeitlinger, 160 p.

Oerlemans, J., Kuhn, M., Obleitner, F., Palsson, F., Smeets, C.J.P.P., Vugts, H.F., and Wolde, J.D.E., 1999, Glacio-meteorological investigations on Vatnajökull, Iceland, summer 1996: An overview: Boundary Layer Meteorology, v. 92, p. 3–26.

Oerlemans, J., and Vugts, H., 1993, A meteorological experiment in the melting zone of the Greenland ice sheet: Bulletin of the American Meteorological Society, v. 74, no. 3, p. 355–365, doi: 10.1175/1520-0477, 1993)074<0355:AMEITM>2.0.CO;2.

Östrem G., 1959, Ice Melting under a Thin Layer of Moraine, and the Existence of Ice Cores in Moraines Ridges. Geografiska Annaler, v. 41, no. 4, 228–230.

Owen, L.A. and Derbyshire E., 1989, The Karakoram Glacial Depositional System. Zeitschrift für Geomorphologie, Supplementary Issues, v. 46, 33–73.

Owen, L.A., Derbyshire, E. and Scott, C.H., 2003, Contemporary sediment production and transfer in high-altitude glaciers. Sedimentary Geology, v. 155, 13–36.

Pellicciotti, F., Brock, B., Strasser, U., Burlando, P., Funk, M., and Corripio, J., 2005, An enhanced temperature-index glacier melt model including the shortwave radiation balance: development and testing for Haut Glacier d'Arolla, Switzerland: Journal of Glaciology, v. 51, no. 175, p. 573–587, doi: 10.3189/172756505781829124.

Petersen, L., and Pellicciotti, F., 2011, Spatial and temporal variability of air temperature on a melting glacier: Atmospheric controls, extrapolation methods and their effect on melt modeling, Juncal Norte Glacier, Chile: Journal of Geophysical Research, v. 116, no. D23,

p. D23109, doi: 10.1029/2011JD015842.

Phillips, F., and Zreda, M., 1997, Cosmogenic ^{36}Cl and ^{10}Be ages of Quaternary glacial and fluvial deposits of the Wind River Range, Wyoming: GSA Bulletin, v. 109, no. 11, p. 1453– 1463.

Porter, S.C., and Swanson, T.W., 2008, ^{36}Cl dating of the classic Pleistocene glacial record in the northeastern Cascade Range, Washington: American Journal of Science, v. 308, no. 2, p. 130–166, doi: 10.2475/02.2008.02.

Purdie, J. and Fitzharris, B., 1999, Processes and rates of ice loss at the terminus of Tasman Glacier, New Zealand. Global and Planetary Change, v. 22, 79–91.

Quincey, D.J., Copland, L., Mayer, C., Bishop, M., Luckman, A. and Belo M., 2009a, Ice velocity and climate variations for Baltoro Glacier, Pakistan: Journal of Glaciology, v. 55, 194), 1061–1071.

Quincey, D.J., Luckman, A. and Benn, D., 2009b, Quantification of Everest region glacier velocities between 1992 and 2002, using satellite radar interferometry and feature tracking: Journal of Glaciology, v. 55, no. 192, 596–606, (doi: 10.3189/002214309789470987).

Rabassa, J., Rubulis, S., and Suárez, J., 1979, Rate of formation and sedimentology of (1976–1978) push-moraines, Frías Glacier, Mount Tronador (42 10’ S, 71 53’ W), Argentina: Moraines and Varves, 65-79.

Raper, S.C.B. and Braithwaite, R.J., 2006, Low sea level rise projections from mountain glaciers and icecaps under global warming: Nature, v. 439, no. 7074, 311–3, (doi: 10.1038/nature04448).

Reichert, B.K., Bengtsson, L., and Oerlemans, J., 2002, Recent glacier retreat exceeds internal variability: Journal of Climate, v. 15, no. 21, p. 3069–3081, doi:10.1175/1520-0442, 2002)015<3069:RGREIV>2.0.CO;2.

Reid, T.D. and Brock, B.W., 2014, Assessing ice-cliff backwasting and its contribution to total ablation of debris-covered Miage glacier, Mont Blanc massif, Italy: Journal of Glaciology, v. 60, no. 219, 3–13 (doi: 10.3189/2014JoG13J045).

Reid, T.D. and Brock, B.W., 2010, An energy-balance model for debris-covered glaciers including heat conduction through the debris layer: Journal of Glaciology, v. 56, no. 199, 903–916, (doi: 10.3189/002214310794457218).

Reinardy, B.T.I., Leighton, I., and Marx, P.J., 2013, Glacier thermal regime linked to processes of annual moraine formation at Midtdalsbreen, southern Norway: Boreas, no. 1971, p. n/a–n/a, doi: 10.1111/bor.12008.

Rickman, R.L. and Rosenkrans, D.S., 1997, Hydrologic conditions and hazards in the Kennicott River Basin, Wrangell-St. Elias National Park and Preserve, Alaska. USGS Water-Resources Investigations Report, v. 53.

Roe, G.H. and Baker, M.B., 2014, Glacier response to climate perturbations: an accurate linear geometric model: Journal of Glaciology, v. 60, no. 222, 670–684.

Roe, G.H., 2011, What do glaciers tell us about climate variability and climate change?: Journal of Glaciology, v. 57, no. 203, p. 567–578, doi:10.3189/002214311796905640.

Roe, G.H., and O'Neal, M.A., 2009, The response of glaciers to intrinsic climate variability: observations and models of late-Holocene variations in the Pacific Northwest: Journal of Glaciology, v. 55, p. 839–854, doi:10.3189/002214309790152438.

Rohl, K., 2008, Characteristics and evolution of supraglacial ponds on debris-covered Tasman Glacier, New Zealand: Journal of Glaciology, v. 54, no. 188, 867–880.

Sakai, A., Nakawo, M. and Fukita, K., 2002, Distribution characteristics and energy balance of ice cliffs on debris-covered glaciers, Nepal Himalaya. Arct. Antarct. and Alp. Res., v. 34, no. 1, 12–19.

Sakai, A., Nishimura, K., Kadota, T. and Takeuchi, N., 2009, Onset of calving at supraglacial lakes on debris-covered glaciers of the Nepal Himalaya: Journal of Glaciology, v. 55, no. 193, 909–917 (doi: 10.3189/002214309790152555).

Sakai, A., Takeuchi, N., Fujita, K. and Nakawo, M., 2000, Role of supraglacial ponds in the ablation process of a debris-covered glacier in the Nepal Himalayas, In Nakawo N, Fountain A and Raymond C eds. Debris-covered glaciers, IAHS Publication, p. 264, 53–61.

Schäfer, J.M., Denton, G.H., Barrell, D.J., Ivy-Ochs, S., Kubik, P.W., Andersen, B.G., Phillips, F.M., Lowell, T.V., and Schlüchter, C., 2006, Near-synchronous interhemispheric termination of the last glacial maximum in mid-latitudes: Science, v. 312, no. 5779, p. 1510–1513, doi:10.1126/science.1122872.

Scherler, D., Bookhagen, B. and Strecker, M.R., 2011a, Hillslope-glacier coupling: The interplay of topography and glacial dynamics in High Asia: Journal of Geophysical Research, v. 116, no. F2, F02019, (doi: 10.1029/2010JF001751).

Scherler, D., Bookhagen, B. and Strecker, M.R., 2011b, Spatially variable response of Himalayan glaciers to climate change affected by debris cover: Nature Geoscience, v. 4, no.3 , 156–159, (doi: 10.1038/ngeo1068).

Scherler, D., 2014, Climatic limits to headwall retreat in the Khumbu Himalaya, eastern Nepal: Geology, (September), (doi: 10.1130/G35975.1).

Schildgen, T.F., and Dethier D.P., 2000, Fire and ice: using isotopic dating techniques to interpret the geomorphic history of Middle Boulder Creek, Colorado: Geological Society

of America Abstracts with Programs, v. 32, no. 7, p.18.

Schneider, C., Kilian, R., and Glaser, M., 2007, Energy balance in the ablation zone during the summer season at the Gran Campo Nevado Ice Cap in the Southern Andes: Global and Planetary Change, v. 59, no. 1-4, p. 175–188, doi: 10.1016/j.gloplacha.2006.11.033.

Schomacker, A. and Kjaer, K.H., 2008, Quantification of dead-ice melting in ice-cored moraines at the high-Arctic glacier Holmströmbreen, Svalbard: Boreas, v. 37, no. 2, 211–225, (doi: 10.1111/j.1502-3885.2007.00014.x).

Schwanghart, W. and Kuhn, N.J., 2010, TopoToolbox: A set of Matlab functions for topographic analysis: Environmental Modeling and Software, v. 25, no. 6, 770–781 (doi: 10.1016/j.envsoft.2009.12.002).

Sharp, M., 1984, annual moraine ridges at Skalafellsjökull southeast Iceland: Journal of Glaciology, v. 30, no. 104, p. 82–93.

Six, D., Wagnon, P., Sicart, J.E., and Vincent, C., 2009, Meteorological controls on snow and ice ablation for two contrasting months on Glacier de Saint-Sorlin, France: Annals of Glaciology, v. 50, p. 66–72.

Smolarkiewicz, P.K., 1983, A simple positive definite advection scheme with small implicit diffusion: Monthly Weather Review, v. 111, no. 3, 479–486.

Steffen, K., and Box, J., 2001, Surface climatology of the Greenland ice sheet: Greenland Climate Network 1995–1999: Journal of Geophysical Research, v. 106, no. D24, p. 33951– 33964.

Strasser, U., Corripio, J., Pellicciotti, F., Burlando, P., Brock, B., and Funk, M., 2004, Spatial and temporal variability of meteorological variables at Haut Glacier d'Arolla (Switzerland) during the ablation season 2001: Measurements and simulations: Journal of Geophysical Research, v. 109, p. D03103, doi: 10.1029/2003JD003973.

Szafraniec, J., 2002, Influence of positive degree % days and sunshine duration on the surface ablation of Hansbreen, Spitsbergen glacier: Polish Polar Research, v. 23, no. 3, p. 227–240.

Thorarinsson, S., 1956, On the variations of Svinafellsjökull, Skaftafellsjökull and Kviarjökull in Oraefi: Jökull, v. 6, p. 1–15.

Vacco, D.A., Alley, R.B. and Pollard, D., 2010, Glacial advance and stagnation caused by rock avalanches: Earth and Planetary Science Letters, v. 294, no.1-2, 123–130, (doi: 10.1016/j.epsl.2010.03.019).

Van de Wal, R., 1992. Ice and climate. PhD Thesis, Utrecht University, 144 pp.

Van den Broeke, M.R., Smeets, C.J.P.P., and Van de Wal, R.S.W., 2011, The seasonal cycle and interannual variability of surface energy balance and melt in the ablation zone of the west

Greenland ice sheet: The Cryosphere, v. 5, no. 2, p. 377–390, doi: 10.5194/tc-5-377-2011.

Wagnon P, Vincent C, Arnaud Y, Berthier E, Vuillermoz E, Gruber S, Ménégoz M, Gilbert A, Dumont M, Shea JM, Stumm D and Pokhrel BK, , 2013) Seasonal and annual mass balances of Mera and Pokalde glaciers (Nepal Himalaya) since 2007: The Cryosphere, v.7, no. 6, 1769–1786, (doi: 10.5194/tc-7-1769-2013).

Ward, D.J., Anderson, R.S., Guido, Z.S., and Briner, J.P., 2009, Numerical modeling of cosmogenic deglaciation records, Front Range and San Juan mountains, Colorado: Journal of Geophysical Research, v. 114, no. F1, p. F01026, doi: 10.1029/2008JF001057.

Winkler, S., and Matthews, J. A., 2010, Observations on terminal moraine-ridge formation during recent advances of southern Norwegian glaciers: Geomorphology, v. 116, no. 1-2, p. 87–106, doi: 10.1016/j.geomorph.2009.10.011.

Worsley, P., and Alexander, M.J., 1976, Glacier and Environmental Changes. Neoglacial Data from the Outermost Moraine Ridges at Engabreen, Northern Norway: Geografiska Annaler. Series A, Physical Geography, v. 58, no. 1/2, p. 55, doi: 10.2307/520743.

Yong, Z., Shiyin, L., and Yongjian, D., 2007, Glacier meltwater and runoff modelling, Keqicar Baqi glacier, southwestern Tien Shan, China: Journal of Glaciology, v. 53, no. 180, p. 91–98, doi: 10.3189/172756507781833956.

Young, N.E., Briner, J.P., Leonard, E.M., Licciardi, J.M., and Lee, K., 2011, Assessing climatic and nonclimatic forcing of Pinedale glaciation and deglaciation in the western United States: Geology, v. 39, no. 2, p. 171–174, doi:10.1130/G31527.1.

Young, N.E., Briner, J.P., Leonard, E.M., Licciardi, J.M., and Lee, K., 2011, Assessing climatic and non-climatic forcing of Pinedale glaciation and deglaciation in the western United States: Geology, v. 39, no. 2, p. 171–174, doi: 10.1130/G31527.1.

Zhang, Y., Fujita, K., Liu, S., Liu, Q. and Nuimura, T., 2011, Distribution of debris thickness and its effect on ice melt at Hailuogou glacier, southeastern Tibetan Plateau, using in situ surveys and ASTER imagery: Journal of Glaciology, v. 57, no. 206, 1147–1157 (doi: 10.3189/002214311798843331).

Zhang, Y., Liu, S., and Ding, Y., 2006, Observed degree-day factors and their spatial variation on glaciers in western China: Annals of Glaciology, v. 43, no. 1, p. 301–306.

Zumbühl, H.J., Steiner, D., and Nussbaumer, S.U., 2008, 19th century glacier representations and fluctuations in the central and western European Alps: An interdisciplinary approach: Global and Planetary Change, v. 60, no. 1-2, p. 42–57, doi: